12-2022

Delineating Field Variation Using Apparent Electrical Conductivity in an Ozark Highlands Agroforestry System

Shane Reid Ylagan
University of Arkansas, Fayetteville

Delineating Field Variation Using Apparent Electrical Conductivity in an Ozark Highlands
Agroforestry System

A thesis submitted in partial fulfillment
of the requirements for the degree of
Master of Science in Crop, Soil, and Environmental Sciences

by

Shane Ylagan
University of Arkansas
Bachelor of Science in Environmental, Soil, and Water Sciences, 2020

December 2022
University of Arkansas

This thesis is approved for recommendation to the Graduate Council.

_____
Kristofor R. Brye, Ph.D.
Thesis Director

_____
Amanda J. Ashworth, Ph.D.
Committee Member

_____
Phillip R. Owens, Ph.D.
Committee Member

_____
Aurelie M. Poncet, Ph.D.
Committee Member

Abstract

Little to no work has been conducted assessing field variability using repeated electromagnetic induction (EMI) apparent electrical conductivity (EC_a) surveys in agroforestry (AF) systems within regions similar to the Ozark Highlands. The objectives of this thesis were to identify i) spatiotemporal EC_a variability; ii) EC_a-derived soil management zones (SMZs); iii) correlations among EMI-EC_a and *in-situ*, sentential-site soil properties; iv) whether fewer, EMI-EC_a surveys could be conducted to capture similar EC_a variance as mid-monthly EMI-EC_a surveys; v) correlations between EC_a and forage yield, tree growth, and terrain attributes based on plant (forage and tree) species, and fertility treatments, and EC_a-derived SMZs, and vi); and terrain attributes that have the largest contribution to EC_a variability at a 20-year-old, 4.25-ha, AF system in the Ozark Highlands of northwest Arkansas. Between August 2020 and July 2021, 12, mid-monthly EC_a surveys were conducted and soil-sensor-based volumetric water content and EC_a measurement were made and soil samples for gravimetric water content, EC, and pH were collected from various soil depths at fixed locations. Fourteen terrain attributes of the AF site were obtained. Tree diameter at breast height (DBH) and tree height (TH) measurements were made in December 2020 and March 2021, respectively, and total forage yield samples were collected seven times during Summer 2018 and 2019. The overall mean perpendicular geometry (PRP) and horizontal coplanar geometry (HCP) EC_a ranged between 1.8 to 18.0 and 3.1 to 25.8 mS m^{-1}, respectively, and the overall mean HCP EC_a was 67% greater than the mean PRP EC_a. Largest measured EC_a occurred within the local drainage way, which has mapped inclusions with aquic soil moisture regimes, or areas of potential groundwater movement, and smallest measured EC_a values occurred within areas with decreased effective soil depth and increased coarse fragments. A positive ($r^2 = 0.4$; $P < 0.05$) linear relationship occurred over time between

PRP EC_a standard deviation, with a negative linear relationship ($r^2 = 0.93$; $P < 0.05$) between HCP EC_a coefficient of variation across season (i.e., Summer to Spring). The K-means-clustering method was used to delineate three precision SMZs that were reflective of areas with similar EC_a and EC_a variability. Relationships between EC_a and tree properties were generally stronger within the whole-site, averaged across tree property and EC_a configuration ($| r | = 0.38$), than the SMZs, averaged across tree property, EC_a configuration, and SMZ ($| r | = 0.27$). The strength of the SMZs' terrain-attribute-PRP-EC_a relationships were 9 to 205% greater than that for the whole-site. Whole-site, multi-linear regressions showed that Slope Length and Steepness (LS)-Factor (10.5%), Mid-slope (9.4%), and Valley Depth (7.2%) were terrain attributes that had the greatest influence (i.e., largest percent of total sum of squares) on PRP EC_a variability, whereas Valley Depth (15.3%), Wetness Index (11.9%), and Mid-slope (11.2%) had the greatest influence on HCP EC_a variability. Results of this study show how EC_a varies and relates to soil, plant (i.e., DBH and TH and forage yield), and terrain attributes in AF systems with varying topography that could be used to influence AF management.

Acknowledgments

I would like to thank my Thesis Committee members, Dr. Kristofor R. Brye, Dr. Amanda J. Ashworth, Dr. Phillip R. Owens, and Dr. Aurelie M. Poncet for all their support and guidance throughout my graduate research. I would also like to thank Dr. Ashworth and Dr. Owens for supporting this research through funding provided by the Foundation for Food and Agriculture Research (Agreement 58-6022-9-002; Grant No. 0000000025).

I would like to sincerely thank Dr. Brye for his continuous support throughout my time at the University of Arkansas. Dr. Brye's teachings, guidance, and mentorship allowed me to find a passion for soil science and inspired me to pursue a career in soils. Dr. Brye's unceasing support, belief in his students, and pursuit for high quality research allowed for a dyslexic kid like me to see their true academic and literary potential.

I would also like to thank Dr. David Miller, Dr. Lisa Wood, Shelby Lebeau, Ryder Anderson, Taylor Adams, Harrison Smith, Machaela Morrison, Matt Janorski, and Chandler Arel for their support and conversation throughout my time in the CSES department.

I would like to sincerely thank my mother for always encouraging and supporting me throughout my undergraduate and graduate career. Without her, none of this would have been possible.

Dedication

I dedicate this thesis to my late father who I aspired to be, and to my mother who made me who I

am.

Table of Contents

Chapter 3

Chapter 3

Introduction

Crop yield variability due to spatially heterogeneous soil properties has been well recognized. As a result, several methods have been developed to map spatial variability and delineate management zones at the field-scale, including soil sampling (i.e., grid sampling), yield-monitor maps, and geophysical methods for proximal soil sensing [i.e., electromagnetic-induction (EMI)-based methods; Allered et al., 2016; Soil Science Division Staff, 2017]. However, soil sampling and yield-monitor maps are often expensive and labor-intensive, making grid sampling impractical for whole-farm-scale operations (Johnson et al., 2001, 2003). Because EMI-based methods are non-invasive, simple to implement, able to cover large areas quickly, and can accurately delineate spatial changes in belowground properties, EMI-based methods have become a common tool for landscape-scale and field-variability characterization in lieu of intensive soil sampling (Corwin & Lesch, 2005a,b).

Electromagnetic-induction-based methods are able to delineate spatial changes in belowground properties through proximally sensing soil apparent electrical conductivity (EC_a), which is the ability of a soil to conduct an electrical current (Corwin & Lesch, 2005a,b). The measurements collected from EMI-EC_a surveys have been used for digital soil mapping, remote sensing, optimizing soil sampling strategies, delineating crop and soil management zones, yield prediction, and many more applications and disciplines (Heil & Schmidhalter, 2017; Johnson et al., 2001). Additionally, EMI-EC_a surveys have been used to evaluate variations in a multitude of soil and plant properties within a variety of different land management systems and ecosystems across the world (Heil & Schmidhalter, 2017; Johnson et al., 2001). However, no work has been conducted that assesses the spatiotemporal variability of the EMI-EC_a, and the EMI-EC_a's relationships with soil, plant, and terrain attributes, of an agroforestry system within the Ozark Highlands.

References

Allered, B. J., Adamchuck, V. I., Viscarra Rossel, R. A., Doolittle, J., Freeland, R. S., Grote, K. R., & Corwin, D. L. (2016). Geophysical methods. *Encyclopedia of Soil Science*, 3, 1–8.

Corwin, D. L., & Lesch, S. M. (2005a). Apparent soil electrical conductivity measurements in agriculture. *Computers and Electronics in Agriculture*, 46, 11–43.

Corwin, D. L., & Lesch, S. M. (2005b). Characterizing soil spatial variability with apparent soil electrical conductivity – survey protocols. *Computers and Electronics in Agriculture*, 46, 103–133.

Heil, K., & Schmidhalter, U. (2017). The application of EM38: Determination of soil parameters, selection of soil sampling points and use in agriculture and archaeology. *Sensors*, 17, 1–44.

Johnson, C. K., Doran, J. W., Duke, H. R., Wienhold, B. J., Eskridge, K. M., & Shanahan, J. F. (2001). Field□scale electrical conductivity mapping for delineating soil condition. *Soil Science Society of America Journal*, 65, 1829–1837.

Johnson, C. K., Mortensen, D. A., Wienhold, B. J., Shanahan, J. F., & Doran, J. W. (2003). Site-specific management zones based on soil electrical conductivity in a semiarid cropping system. *Agronomy Journal*, 95, 303–315.

Soil Science Division Staff. (2017). Tools for proximal soil sensing. In C. Ditzler, K. Scheffe, & H. C. Monger (Eds.), *USDA Handbook 18: Soil survey manual* (pp. 355–394). Government Printing Office. Washington, DC.

Chapter 1

Literature Review

Soil Variability and Spatial Soil Mapping Methods

      Soils are innately heterogeneous, where they vary spatially and temporally (Corwin & Scudiero, 2019; Garcia-Tomillo et al., 2017). Spatial soil variability is a result of temporal, local, and regional differences in topography, climate, vegetation, and parent material (Garcia-Tomillo et al., 2017). However, soil property variations may also be attributed to management, including land use, crop type, tillage (frequency and intensity), and fertilizer sources (organic and inorganic) and rates (Garcia-Tomillo et al., 2017). Such variabilities often create challenges for agricultural producers, as variations in soil properties substantially affect water movement, solute transport, and plant–water–soil interactions, which, in turn, influence soil quality and crop yield (Corwin & Scudiero, 2019). Additionally, soil spatial variability also affects tillage and planting equipment performance, resulting in uneven stand establishment, which increases competition between plants, and further reduces yield. Accurate characterization of spatial variability of soils is not only essential for understanding field-scale processes across landscapes and within the soil, but also an essential component of soil quality (SQ) assessments, site-specific crop management, and non-point pollutant transport within the vadose zone (Corwin & Lesch, 2005b).

      Several methods are documented in literature to map spatial variability and delineate management zones in a field. However, little work has been conducted to assess the accuracy of these methods in different ecosystems and further research is required to develop standard guidelines, proven to work under field conditions, to help growers select the most accurate mapping and delineation method for their specific application and environment (Abdu et al., 2017; Garcia-Tomillo et al., 2017). Soil spatial variability is often characterized using soil sampling or a variety of different sensors, with each method having its advantages and limitations (Johnson et al., 2001). For instance, soil samples can be collected using different

sampling strategies (grid, random, stratified). They provide a direct measurement of soil properties in the sampling location and data are interpolated using different techniques to estimate soil properties across the study area (Garcia-Tomillo et al., 2017; Johnson et al., 2003). However, soil sampling is often expensive and labor-intensive, making grid sampling impractical for whole-farm-scale operations and identifying soil-landscape relationships (Johnson et al., 2001, 2003).

Geophysical methods for proximal soil sensing can help overcome the limitations of spatial characterization via soil sampling and be used as an alternative method for measuring spatial variability (Abdu et al., 2017). Proximal soil sensing methods are techniques which use different sensors to measure soil properties, where these sensors can operate in direct contact with, or near (< 2 m) the soil surface (Soil Science Division Staff, 2017; Viscarra Rossel et al., 2011). The data collected by proximal soil sensing methods do not provide a direct measurement of soil properties, but rather correlate to specific geophysical attributes. As a result, the collected data must be processed and interpreted to predict or infer spatial changes in soil physico-chemical properties; identify soil lithologic and stratigraphic boundaries; and describe soil patterns and characteristics (Soil Science Division Staff, 2017). The data processing step uses machine learning and various statistical techniques to identify contrasts within the study area. There are many different types of geophysical methods for proximal soil sensing [e.g., ground-penetrating radar (GPR), electrical resistivity (ER), electromagnetic induction (EMI), optical reflectance, gamma-ray spectrometry, time domain reflectometry]; however, EMI, ER, and GPR are most commonly used in soil and agricultural applications (Allered et al., 2016; Soil Science Division Staff, 2017).

Electromagnetic-induction-based Methods and Apparent Electrical Conductivity

Electromagnetic-induction-based methods are non-invasive and are the most frequently used proximal soil sensing (Serrano et al., 2014). Electromagnetic induction methods characterize a soil's bulk apparent electrical conductivity (EC_a), which is the ability of a soil to conduct an electrical current (Abdu et al., 2017; Garcia-Tomillo et al., 2017). There are three parallel pathways in which a soil can conduct an electrical current, including i) a soil-liquid pathway, where the current largely travels through the exchangeable cations associated with clay particles; ii) a liquid-phase pathway, where the current travels through the dissolved salts in the soil water of macropores; and iii) a solid pathway, where the current travels through the soil particles that come into direct, continuous contact with each other (Corwin & Scudiero, 2017). As a result of these pathways of conductance, in-field measured soil EC_a is the result of complex interactions of many soil properties, including soil salinity, base saturation (BS), bulk density (BD), clay content and mineralogy, soil water content (SWC), soil organic matter (SOM), cation exchange capacity (CEC), and soil temperature (Corwin & Scudiero, 2017).

The soil properties that affect measured EC_a can be grouped into three categories: the bulk soil, solid particles, and the soil solution (Friedman, 2005; Pedrera-Parrilla et al., 2014). The bulk-soil category includes soil properties that describe the volumetric portions of the soil's three phases (i.e., solid, liquid, and gas) and potential secondary structural arrangements, including aggregation, porosity, and SWC (Friedman, 2005; Pedrera-Parrilla et al., 2014). Soil properties in the solid-particle category are relatively temporally stable, including particle-size distribution, particle shape and orientation, wettability, and CEC (Friedman, 2005; Pedrera-Parrilla et al., 2014). The soil-solution category includes soil properties that are temporally variable and react rapidly with changes in environmental conditions and management, including cation

composition, ionic strength, sodium adsorption ratio (SAR), and soil temperature (Friedman, 2005; Pedrera-Parrilla et al., 2014).

Soil properties that affect EC_a also contribute to varying degrees when the soil is under different conditions. In saline soils, most variations in soil EC_a measurements can be attributed to the salt concentration, whereas, in non-saline soils, measured soil EC_a is reflects the combined effects of soil texture, SWC, BD, and CEC (Corwin & Lesch, 2005b). A saline soil is defined as a soil that has a saturated extract EC (EC_e) of > 400 mS m^{-1}, exchangeable sodium percentage (ESP) of < 15%, and a pH of < 8.5 (Weil & Brady, 2017). Additionally, a sodic soil is defined as a soil with an EC_e of < 400 mS m^{-1}, ESP > 15%, and a pH of > 8.5, while a saline-sodic soil has an EC_e of > 400 mS m^{-1}, ESP > 15%, and a pH of < 8.5 (Weil & Brady, 2017).

Electromagnetic induction methods characterize a soil's EC_a using a ground conductivity meter (GCM). When operated, a transmitter coil positioned at one side of the GCM produces eddy-current loops in the soil directly below the device, where the size of these loops is directly proportional to the EC of the soil that is within the vicinity of the loop (Serrano et al., 2014). Additionally, each current loop emitted by the GCM produces a secondary EM field, which is proportional to the current moving in the soil within the loop vicinity (Serrano et al., 2014). A proportion of the generated secondary EM field from each loop is received by the receiver coil of the GCM, and the combined quantity of these loops is increased and turned into a produced voltage that corresponds to depth-weighted soil EC_a (Serrano et al., 2014). Common EMI-based GCM are the EM31-MK2, EM34-3, and EM38-MK2, produced by Geonics Limited (Mississauga, ON, Canada), and the DUALEM-1S, DUALEM-1HS, DUALEM-2S, produced by Dualem Inc. (Milton, ON, Canada).

Areas of Application for EMI-based Spatial EC$_a$ Measurements

  Although EC$_a$ measurements are complex, obtaining EC$_a$ measurements via EMI-based methods has become a common tool for landscape-scale and field-variability characterization in lieu of intensive soil sampling for a multitude of reasons. Electromagnetic induction EC$_a$ surveys are simple of implement, capable of covering large areas in limited amounts of time because they are non-invasive, mobile, have an instant measurement, and can travel at relatively high speeds (Corwin & Lesch, 2005a,b). Additionally, EMI-EC$_a$ surveys are cost affordable, recognized for their reliability, and have the ability to help characterize a multitude of soil properties and processes (Corwin & Lesch, 2005a,b). However, because measured soil EC$_a$ represents a combination of specific soil properties, in-situ soil property measurements (i.e., soil sampling or soil sensor) are still required for ground-truthing/calibrating and correlating EMI-EC$_a$ variability with in-field soil property variability (Abdu et al., 2017; Corwin & Lesch, 2005b; Corwin & Scudiero, 2017).

  Lab-measured electrical conductivity (EC) has commonly been used to measure soil salinity (Abdu et al., 2017; Garcia-Tomillo et al., 2017). However, through calibrations and correlations, soil characteristics that can be derived from EMI-EC$_a$ surveys include salinity, nutrients, SWC, texture, depth to sand layers or claypans, BD, and many indirect properties and processes [i.e., OM, CEC, leaching, groundwater recharge, and soil drainage class, among others; Corwin & Lesch, 2005b]. Additionally, applications of EMI-EC$_a$ measurements include: digital soil mapping, remote sensing, precision agriculture (Heil & Schmidhalter, 2017; Johnson et al., 2001), and the collected data can be used to optimize soil sampling strategies, characterize soil texture boundaries, delineate crop management zones, predict yield (Heil & Schmidhalter,

2017), map depth to limiting layer (i.e., petrocalcic horizons and claypans), assess herbicide leaching potential, and identify site-specific septic-system failure locations (Abdu et al., 2017).

EMI-EC$_a$ Measurements and Terrain Attributes

Understanding the controlling factors (i.e., terrain and geologic attributes) of soil property development is also important when contextualizing and characterizing spatial EC$_a$ measurements (Kühn et al., 2009). For instance, the mobilization and transportation of sediments, colloids, and solutes from the surrounding landscape affect soil development and soil properties at all landscape positions (Kühn et al., 2009). Additionally, transport processes are governed by geology and terrain attributes (i.e., elevation, slope, aspect, flow accumulation, etc.) at the landscape rather than the field scale (Kühn et al., 2009). Thus, as a result of landscape terrain attributes influencing the soil properties that directly affect EC$_a$, landscape terrain attributes, in turn, indirectly affect the measured EC$_a$ (Kühn et al., 2009).

Relationships between terrain attributes and EMI-EC$_a$ have been evaluated and both have been used to create management zones or functional units and for predictive mapping, individually and/or in combination (Altdorff & Dietrich, 2014; Beucher et al., 2020; Jiang et al., 2021; Kitchen et al., 2003; Pedrera-Parrilla et al., 2014; Robinson et al., 2010; Singh et al., 2016; Taghizadeh-Mehrjardi et al., 2014). In order to assess the relationship between EC$_a$ and terrain attributes (i.e., elevation, slope, curvature), Kitchen et al. (2003) conducted an EC$_a$ survey on a 13-ha field in Boone County, Missouri that had been previously planted with corn (*Zea mays* L.) and soybean (*Glycine max* L.) over the previous three years, respectively. The two dominate soils mapped at the field were the Mexico (Aeric Vertic Epiaqualfs) and Adco (Vertic Albaqualfs) soil series and a Veris 3100 sensor system (Veris 3100 Division of Geoprobe

10

Systems, Salina, KS) was used to conduct the EC_a survey (Kitchen et al., 2003). The shallow EC_a (0-30 cm) had a positive relationship ($P \leq 0.01$) with slope and aspect ($r = 0.30$ and $r = 0.41$, respectively), while the deep EC_a (0-100 cm) had a positive relationship with elevation, slope, and aspect ($r = 0.37$, 0.12, and 0.26, respectively) and a negative relationship with curvature ($r = -0.18$; Kitchen et al., 2003). However, more information on additional terrain attributes that affect EC_a and their relationship within different agroecosystems and land management systems is necessary to further enhance spatial predictions of soil properties based on measured EC_a and to improve the EC_a-derived management zones in precision agriculture.

Application of EMI-based Spatial EC_a Measurements in Agroforestry

Although there has been significant research conducted using EMI-EC_a surveys (Corwin & Lesch, 2005a), little work has been conducted using EMI-EC_a surveys within agroforestry (AF) systems. Agroforestry is a conservation-oriented, land management practice which has continued to gain appeal and recognition by growers due to the many provided benefits of AF systems being documented in published literature. An AF system is defined as the intentional integration of agriculture/horticulture and forestry to benefit from the subsequent interactive effects that are produced from growing agricultural/horticultural crops and/or livestock alongside trees and/or shrubs (NAC, 2019). Additionally, although there are multiple types of AF systems (i.e., alley-cropping, silviculture, silvopasture, forest farming, windbreaks, and riparian forest buffer), common AF systems are alley-cropping and silvopastoral systems. In alley-cropping system, trees are planted in rows and agricultural crops are grown in the subsequent alleys, whereas in silvopastoral systems, trees and forages are integrated for livestock production. Both alley-cropping and silvopastoral systems provide growers with different, short- and long-term,

income sources due to the production of their main/original product (i.e., agricultural crops or livestock products), alongside the production of additional high-value crops (i.e., nuts and fruits) or other products (i.e., lumber and biofuel) on the same parcel of land, allowing producers to respond to variations in markets.

In addition to AF practices producing multiple products, AF practices have also displayed their ability to improve SQ, while also providing ecosystem services (Dollinger & Jose, 2018). Potential AF-provide ecosystem services include water quality (WQ) enhancement, increased biodiversity, reduced soil erosion (wind and water), elevated aesthetic value, carbon (C) sequestration, oxygen (O) production, and greenhouse gas mitigation (Jose, 2009). Additionally, silvopastoral systems benefit livestock by creating cooler environments (microclimates) in warmer months for livestock; and facilitating livestock protection from weather events (NAC, 2019). Other ecosystem services or benefits provided by AF systems include reduced particulate matter in the air from reduced wind velocity, and thus also reduced wind erosion, reduced noise pollution, and odor mitigation of concentrated livestock operations (Jose, 2009). Furthermore, SQ benefits from AF have include enhanced soil fertility (Dollinger & Jose, 2018), soil organic C (SOC) storage (Lorenz & Lal, 2014; Schoeneberger et al., 2012; Udawatta & Jose, 2012), soil structure (Gelaw et al., 2015), and conservation of biodiversity (Jose, 2009; Nair, 2011). However, the magnitude of the effects of AF systems varies by soil type, climate, and management system. Thus, further research is needed to identify the drivers of variability and quantify effect of AF systems on soil properties, SQ dynamics, and landscape-level processes in different ecosystems.

Although there has been little application of EMI-EC_a surveys in AF systems, Huth & Poulton (2007) developed techniques for the application of EMI-EC_a measurements in AF

systems for the monitoring of soil moisture variations. Huth & Poulton (2007) used EMI-EC$_a$ surveys to generate data to assess whether their developed linear calibration equation could be used to successfully estimate soil moisture changes when monitoring tree-crop competition. Huth & Poulton (2007) conducted their study at a farm near Warra, Queensland, Australia. At the farm, there were 7-year-old, Queensland western white gum (*Eucalyptus argophloia*), planted in a belt of 4 rows (~ 5 x 5 m spacing) alongside the border of a field used for cotton (*Gossypium hirsutum*), wheat (*Triticum aestivum*), and chickpea (*Cicer arietinum*) production. The soil at the site was characterized as a self-mulching Grey-Vertisols (Huth & Poulton, 2007). In order to study soil moisture extraction via the trees in cropped and fallow land within the same season, two adjacent cropping bays were selected. Two soil cores were extracted at 6 to 8 sampling locations at different times of the year from the top 1.5-m depth and separated into 0.15-m increments to assess soil properties (Huth & Poulton, 2007). Additionally, an EM38 was used to measure the EC$_v$ and EC$_h$ (vertical and horizontal dipole, respectively) at transects of 5-m intervals between 0 and 50 m away from the trees. The transects were replicated four times total in three adjacent fields (Huth & Poulton, 2007). The study took place over a 1.5-year period, where Huth & Poulton (2007) built a calibration dataset that consisted of paired values of both soil moisture and a weighted average of the EC$_v$ and EC$_h$. Huth & Poulton (2007) concluded that their calibrated EMI techniques were successful in describing the measured soil moisture and that the techniques enable greater flexibility when precise knowledge of the vertical distribution of soil moisture is less important than knowing its variability in time and space. Thus, the information generated by Huth & Poulton (2007) supports that EMI-based techniques can be an efficient and effective method for observing temporal soil moisture patterns in AF systems (Huth & Poulton, 2007).

Although potentially not considered an AF system, EMI-EC$_a$ surveys have also been applied within olive (*Olea europaea* L.) orchards. Pedrera-Parrilla et al. (2014) collected soil sample, soil pit, and EMI-EC$_a$ measurements on two occasions, 1-year apart, across an 8-ha olive orchard near Córdoba, Spain to establish areas of impaired olive tree development and determine the relationships between EMI-EC$_a$ and the soil properties that caused the spatial variability in the olive tree development. The olive orchard was established in 1993 at 240 trees ha^{-1} and was located on a Chromic Haploxerert (Pedrera-Parrilla et al., 2014). Additionally, Pedrera-Parrilla et al. (2014) used a DUALEM-21S (Dualem Inc., Milton, ON, Canada) to conduct the two EMI-EC$_a$ surveys. Through the EC$_a$ surveys, Pedrera-Parrilla et al. (2014) delineated three zones across the olive orchard based on EC$_a$ values, ranging between 0 and 27.5, 27.5 and 57.5, and > 57.5 mS m^{-1}, and determined that the spatial pattern of the measured EC$_a$ correlated to the spatial pattern of canopy coverage. The zone with the lowest EC$_a$ range (0–27.5 mS m^{-1}) displayed optimal tree growth (45 % canopy coverage) and was likely the result of sufficient drainage conditions, as the zone possessed substantially less average clay contents than the other zones (Pedrera-Parrilla et al., 2014). Furthermore, the zone with the intermediate EC$_a$ range (27.5–57.5 mS m^{-1}) displayed deficient tree development (12 % canopy coverage) and was likely the result of poor drainage conditions, as the zone was located along the drainage pathway and possessed the greatest clay, coarse fragments, OM, and SWC (Pedrera-Parrilla et al., 2014). Through the results of their study, Pedrera-Parrilla et al. (2014) concluded that, not only did EMI-EC$_a$ surveys distinguished slight soil property variations and yielded practical knowledge on delimiting areas with constrained tree development, but also that their procedure could be used as a pre-examination technique before establishing tree plantations.

Although EC_a surveys have not been applied within silvopastoral AF systems, EC_a surveys have been applied in pastoral production systems. Cicore et al. (2019) collected biomass accumulation samples and conducted an EC_a survey at a 5.75-ha paddock in the Buenos Aires Province of Argentina to assess whether EC_a surveys can delimit areas of varying yield potential in tall fescue [*Lolium arundinaceum* (Schreb.) Darbysh] during contrasting growing seasons and at different nitrogen (N) fertilization rates (0 and 250 kg N ha^{-1}) for site-specific management. Cicore et al. (2019) conducted the EC_a survey with a Veris 3100 sensor system and then collected biomass accumulation samples in the spring and fall for two consecutive years. Additionally, the mapped soils at the AF site were the Chelforo (Vertic Natraqualfs), Monsalvo (Vertic Argiudoll), and Juncalito series (Glossic Natraqualf; Cicore et al., 2019). Although EC_a-derived management zones were not able to be delineated during the fall, Cicore et al. (2019) determined that tall fescue production in the Argentinean Pampas can still be managed by EC_a-derived management zones, as a correlation between the EC_a and tall fescue forage yield during the spring growing period was observed.

Application of Agroforestry in the Ozark Highlands

Major Land Resource Area 116A - Ozark Highlands

A region with unique features that could benefit greatly from the application of conservative land management practices, like AF systems, is the Ozark Highlands. The Ozark Highlands (36–38° N, 91–95° W), Major Land Resource Area (MLRA) 116A, spans 85,110 km^2 across southern Missouri, northern Arkansas, and northeast Oklahoma (Brion et al., 2011; NRCS, 2006). The Ozark Highlands resides within the Springfield-Salem Plateaus Section of the Ozark Plateaus Province of the Interior Highlands, and acts as a transitional zone between the

more arid Great Plains to west and north and the more humid forestlands to the south and east (Brion et al., 2011; Brye & West, 2005; NRCS, 2006). The annual air temperature in the Ozark Highlands ranges from ~ 12 to 16°C and the majority of the Ozark Highlands has an annual precipitation range of 96.5 to 114.5 cm (NRCS, 2006). Landscapes within the Ozark Highlands range from gentle, prairie-like, rolling upland hills to greatly divided, steep-sloped wooded hills and narrow gravel valleys, and possess well-developed karst topography (i.e., sinkholes, caves, dry valleys, box valleys, and large springs; NRCS, 2006). Furthermore, oak (Quercus spp.)-hickory (Carya spp.) forests, with inclusions of tallgrass prairies, originally dominated the Ozark Highlands (Brion et al., 2011). However, the majority of the Ozark Highlands' native tallgrass prairies have been converted to hay meadows and pastures. Additionally, livestock grazing (i.e., beef cattle and horses) and poultry production are becoming increasingly more dominant in the Ozark Highlands (Brion et al., 2011).

Sedimentary rock makes up a large portion of the bedrock in the Ozark Highlands. Sedimentary rock types in the Ozark Highlands include Lower Mississippian-age dolostone and limestone, Ordovician-age dolostone and sandstone, and Pennsylvanian-age shale and sandstone (NRCS, 2006). The elevation within the Ozark Highlands ranges between ~ 90 and ~ 490 m above sea level and relief in the Ozark Highlands usually varies between ~ 60 and 245 m (NRCS, 2006). Generally, the majority of the soils in the Ozark Highlands MLRA are Alfisols or Ultisols. These soils are formed in materials that have been weathered from cherty limestone. Physical and chemical weathering have resulted in the cherty limestone disintegrating into its least soluble components of chert and clay (NRCS, 2006). The combination of overland flow and gravitational creep have resulted in the alteration of the cherty material in the upper portion of some soils in the area. Furthermore, a majority of the northern and eastern regions of the Ozark

Highlands are partially covered with a minor layer of loess deposits (NRCS, 2006). On average, the soils in the Ozark Highlands range between medium- to fine-textured, shallow to very deep profiles and are moderately well to excessively drained. Additionally, the soils in the Ozark Highlands generally have mixed or siliceous mineralogy, a soil temperature regime of mesic or borderline thermic, and have a soil moisture regime of udic (NRCS, 2006).

Conservation Issues Due to Ozark Highlands Features

The combined effects of the Ozark Highlands' unique features subject MLRA 116A to numerous potential conservation issues. The Ozark Highlands' soil properties (i.e., cherty and shallow), topography, climate, underlying karst geology, rapid urbanization, and predominant animal agriculture cause WQ, both surface- and groundwater, to be of particular concern as a result of elevated potential for WQ degradation via nutrient-rich runoff to surface water bodies and nutrient-rich leaching to shallow and/or easily accessed groundwater sources. Many of the soils in the Ozark Highlands, which overlie dolomitic bedrock and limestone, exist on steep slopes and are shallow to bedrock and stony. This unique combination of topography, soil properties, and geology results in the Ozark Highlands having an increased potential for rapid transmission of rainfall, thus any potential pollutants present at the soil surface, down slope as runoff and into surface waters. Additionally, if any rainfall and/or surface flow are able to infiltrate and potentially pollutant-carrying leachate be rapidly transmitted through the soil and into groundwater.

The physical landscape attributes that cause the Ozark Highlands to be at an increased potential for WQ degradation are compounded by the dominant form of agriculture in the Ozark Highlands, which is animal production (i.e., poultry production and pastoral livestock systems;

Brion et al., 2011; Brye & West, 2005). In 2019, the livestock inventory of Arkansas alone

totaled over 1.7 million head of cattle [i.e., beef and milk cows and calves (*Bos taurus*)], 1.1

billion head of chickens [i.e., broilers; (*Gallus gallus domesticus*)], and 30 million head of turkey

(*Meleagris gallopavo domesticus*; NASS, 2019), much of which are located in northwest

Arkansas (NWA). Consequently, large quantities of animal manure and poultry litter (PL) are

also produced. The combination of NWA producing large quantities of PL, PL being an excellent

fertilizer, and there being economic limitations of transporting the manure has resulted in

extensive annual applications of PL to pastures in the surrounding region for multiple decades

(Brion et al., 2011; Pirani et al., 2006). Additionally, PL application rates are primarily based off

the plant-N requirement, which has consequently caused an accumulation of phosphorus (P) in

pasture soils (Brion et al., 2011). Furthermore, due PL being applied to perennial pastures and P

accumulating near the soil surface, precipitated and sediment-bound P are often lost in runoff

causing an increased potential of surface WQ degradation. Thus, PL-applied pastures have been

determined to be a major contributor to non-point pollution source (i.e., excess P input) to NWA

surface water bodies (Brion et al., 2011).

The manner in which livestock (i.e., cattle) are managed on pastures also has a major

effect on WQ. For instance, cattle, with unrestricted stream access, frequently graze the

vegetation in the riparian-aquatic zone to a greater extent than upland-terrestrial areas and reduce

the stability of stream banks (BWA, 2012; Brion et al., 2011). Riparian buffers promote the

removal of pollutants in runoff and help support the stability of stream banks (BWA, 2012). The

degradation of riparian vegetation and stream bank stability, in turn, increases stream

bank/channel erosion and reduces how effective the riparian zone is at reducing soil erosion and

runoff velocity, volume, erosivity, and sediment and nutrient loads (BWA, 2012; Brion et al., 2011).

     An example of a reservoir watershed in the Ozark Highlands being affected by non-point pollution is the Beaver Lake Watershed. Beaver Lake is located at the very southwestern edge of the Ozark Highlands in NWA, where the largest tributary to Beaver Lake is the upper portion of the White River. Within the Beaver Lake Watershed, it is estimated that ~ 25% of the riparian buffers are impacted (< 30% vegetation), which has contributed to stream bank/channel erosion to become the largest sediment and P contributor to Beaver Lake, followed by pasture/agriculture (BWA, 2012). Phosphorus is of particular concern regarding the health of aquatic ecosystems because P is often the most limiting nutrient in aquatic systems. Thus, relatively small increases in P in surface waters can lead to surface water degradation via eutrophication. Eutrophication, in turn, feeds algal blooms followed by the creation of hypoxic zones, which are detrimental to aquatic organisms. Additionally, cattle also have the potential to overgraze forages, resulting in a barer soil surface, and cause soil compaction if not managed properly. Increased compaction and decreased surface cover further result in the potential of increased soil erosion and agricultural runoff into surface water bodies (Brion et al., 2011).

     The annual application of PL to pastures can also have negative effects on groundwater sources. Increased nitrate-N (NO_3-N) levels have been reported in vadose zone water as a direct result of PL applications (Adams et al., 1994). Elevated levels of NO_3-N in the vadose zone are of particular concern due to there being many shallow, cherty soils throughout the Ozark Highlands, which overlie karst bedrock, where, with adequate soil wetness, could result in the rapid transmission of NO_3-N into the groundwater supply. Background groundwater NO_3-N concentrations from pristine sampling sites in NWA have been measured at < 1.0 mg NO_3-N L^{-1}

(Peterson et al., 2002). However, certain springs during baseflow have been measured to range between 3.6 and 13.0 mg NO_3-N L^{-1} and 2.7 to 16.7 mg NO_3-N L^{-1} during storm events. The primary culprit of the elevated NO_3-N in springs has shown to be PL applications to pastures (Peterson et al., 2002). Although the water is not used for drinking purposes, it is worth mentioning that the upper concentration ranges during base- and storm-flow exceed the maximum NO_3-N concentration of 10 mg NO_3-N L^{-1} for drinking water (USEPA, 2009).

Unique Opportunity for Agroforestry in the Ozark Highlands

As result of the Ozark Highlands unique landscape attributes (i.e., topography and shallow, cherty soils overlying karst limestone geology), any agricultural activities (i.e., poultry production and pastoral livestock systems) must be carefully managed and the conservation of soil and water resources must be top priorities (Brion et al., 2011). Thus, the Ozark Highlands' distinctive features and need for conservative land management practices provide a particularly suitable ecosystems for the implementation of AF systems (i.e., riparian forest buffers and silvopastoral systems) to be particularly advantageous and multi-beneficial.

In addition to providing growers with supplementary and diversified income and ecosystem services, the conversion to and/or implementation of AF systems (i.e., silvopastoral systems) in the Ozark Highlands may also help reduce the potential for WQ degradation by limiting the amount of non-point source pollution (i.e., nutrient and sediment pollution) entering surface water bodies (Blanco & Lal, 2008). Silvopastoral systems have the potential to limit non-point source pollution from reduced soil erosion and sediment and nutrient transport in surface flow and runoff due to: reduced rain drop impact from tree canopy and leaf litter cover; reduced runoff volume and velocity; reduced soil erodibility due to increased SOM which improves soil

20

structure and increase porosity and infiltration; and increasing on-site sediment and nutrient deposition from reduced slope length and steepness from tree trunk interception of surface flow (Blanco & Lal, 2008). Additionally, trees in a silvopastoral systems can potentially reduce nutrient movement to groundwater sources in the Ozark Highlands by taking up excess nutrients (i.e., PL applications) from close to the surface and from below the root zone of forage/agronomic crops (Jose, 2009). Furthermore, the nutrient use efficiency (NUE) is increased in silvopastoral systems from the nutrients taken up in the trees, which are eventually returned to the soil from tree leaf litter decay and root turnover (Jose, 2009). Trees in AF systems also have a longer growing-season than most agronomic crops and forage species, thus improving NUE in AF systems from nutrient capture before, during, and after the cropping season (Jose, 2009).

Nair et al. (2007) conducted a study to compare the impacts of a pastoral system and varying silvopastoral systems on surface- and groundwater quality. The study was conducted in Ona, Florida, where, in December 1991, Florida slash pines (*Pinus elliotti*) were planted in a double-tree row formation at a tree density of 1120 trees ha^{-1} on a range with Pensacola bahiagrass (*Paspalum notatum*) and a native range made up of mostly wiregrass (*Aristida stricta*), creeping bluestem (*Schizachyrium stoloniferum*), and saw palmetto (*Serenoa repens;* Nair et al., 2007). The double-row planted trees were 2.4 m apart, with 1.2 m spacing among trees in a row, and 12.2-m wide alley between double-tree rows (Nair et al., 2007). In 1994, the pine-bahiagrass silvopasture was sown to Florida carpon desmodium (*Desmodium heterocarpum*) and Shaw vigna (*Vigna pakeri*) in 2001 (Nair et al., 2007). In 2002, the tree-less pasture was sown to Florida carpon desmodium and Shaw vigna (Nair et al., 2007). For all configurations, both legumes were sown at 5 kg ha^{-1} (Nair et al., 2007). Soils for all pasture

configurations were mapped as a Myakka fine sand (sandy, siliceous, hyperthermic Aeric Alaquod; Nair et al., 2007).

Cattle began grazing the native silvopasture every March and September after 1993 (Nair et al., 2007). In 2002 and 2003, the pine-bahiagrass silvopasture was split into 8-ha halves, where one half was not thinned and had a tree density of 494 trees ha^{-1} and one half was thinned to 309 trees ha^{-1} (Nair et al., 2007). Ten soil profile locations were randomly selected and sampled from each of the four pasture configurations and separated into six different depth increments (0-5-, 5-15-, 15-30-, 30-50, 50-75-, and 75-100-cm; Nair et al., 2007). Soil samples were then analyzed for water-soluble P (WSP), NO_3–N, and ammonium–N (NH_4–N), and P saturation ratio (PSR; Nair et al., 2007). The tree-less pasture had a greater WSP concentration (9.1 mg kg^{-1} in the 0-5 cm depth and 0.2 mg kg^{-1} at 1.0 m) than that of all silvopastures (2.5 mg kg^{-1} in the 0-5 cm depth and 0.1 mg kg^{-1} at 1.0 m; Nair et al., 2007). The tree-less pasture had a greater NO_3–N (2.4 mg kg^{-1}) and NH_4–N (9.8 mg kg^{-1}) concentration in the top 5 cm than that of all silvopastures (1.0 NO_3–N mg kg^{-1} and 6.5 NH_4–N mg kg^{-1} at 0-5 cm; Nair et al., 2007). Soils under all silvopasture configurations had greater soil P storage capacity (1,494 kg P ha^{-1}) than that of the tree-less pasture (270 kg P ha^{-1}; Nair et al., 2007).

The results of Nair et al. (2007) further suggests that silvopastoral systems increase nutrient retention within the system, thus reducing the potential for nutrient transport to surface water sources compared to a tree-less pasture system. Thus, the unique features of the Ozark Highlands (i.e., topography and shallow, cherty soils overlying karst limestone geology, poultry production, and pastoral livestock systems; Brion et al., 2011), which cause MLRA 116A to be at an increased potential for conservation issues (i.e., surface and groundwater quality degradation), makes the implementation and research of AF systems, specifically silvopastoral

systems, to be particularly advantageous, multi-beneficial, and intriguing due to the many

potential ecosystem services and benefits that silvopastoral systems offer [i.e., producer

economic and livestock benefits and ecosystem services (i.e., WQ and SQ enhancement and

reduced soil erosion and runoff)].

Justification

Although EMI-EC$_a$ surveys have been used for landscape-scale and field-variability

characterization within many different land management systems and ecosystems across the

world, EMI-EC$_a$ surveys have been minimally applied in AF systems. As a consequence, little to

no work has been conducted using repeated EMI-EC$_a$ surveys to create EC$_a$-derived soil

management zones (SMZs) and explore the spatiotemporal relationship between EMI-EC$_a$ and

soil property, tree growth, forage yield, and terrain attributes in AF systems, let alone AF

systems within regions that have similar features to the Ozark Highlands. Additionally, no

research has been conducted evaluating the necessary number of EMI-EC$_a$ surveys to capture the

full amount of spatiotemporal EC$_a$ variance within 1 year at an AF system.

Objectives and Hypotheses

As a result of the lack of information on EMI-EC$_a$ surveys in AF systems, the goals of

this study were to assess the spatiotemporal variability of measured EMI-EC$_a$, evaluate the

relationship between EMI-EC$_a$ and other variables, and provide soil data for precision soil

management for a 20-year-old AF system within the Ozark Highlands of northwest Arkansas.

Two sets of research objectives were established to accomplish the goals for this study.

The first set of objectives of this study were to i) use monthly EMI-EC$_a$ surveys to assess the

spatiotemporal pixel variation of the measured EC_a, ii) use k-means to identify clusters of similarly behaving populations for precision soil management, iii) identify correlations between EMI-EC_a data and in-situ, soil-sensor-measured volumetric water content (VWC) and EC_a measurements at two depths (15 and 75 cm and 15 and 50 cm, respectively) and benchtop-measured soil sample EC, gravimetric water content (GWC), and pH in two depth intervals (0-15 and 45-55 cm), and iv) determine whether fewer, evenly spaced, strategically selected EMI-EC_a surveys could have been conducted in one year to capture similar overall EC_a variance as the 12 mid-monthly EMI-EC_a surveys. It was hypothesized that i) there would be a significant change in the mean EC_a and EC_a variability [i.e., standard deviation (SD) and coefficient of variation (CV)] across time (i.e., survey dates and weather season) and that there would be significant difference between the EC_a mean, SD, and CV of surveys that were conducted in different weather seasons and in the tree growing/non-growing season, ii) monthly EMI-EC_a surveys can be grouped into similar functional populations and be delineated into zones for precision soil management, iii) monthly EMI-EC_a survey data are correlated with soil-sensor-based VWC and EC_a and soil-sample-based EC, GWC, and pH, and iv) fewer surveys than monthly could be conducted in a 1-year period to capture the same amount of overall EC_a variance as the 12 mid-monthly EMI-EC_a surveys conducted.

The second set of objectives were to: i) identify correlations between EMI-EC_a and total forage yield and tree growth data [tree height (TH) and diameter at breast height (DBH)] within the whole site and three EC_a-derived SMZs, ii) identify correlations between EC_a and total forage yield and tree growth data within forage/tree species and fertility treatment combinations, within the whole site and three EC_a-derived SMZs, and iii) identify correlations between EMI-EC_a and terrain attribute data at a 20-year AF system within the Ozark Highlands. It was hypothesized

that EMI-EC$_a$ data are correlated with total forage yield, tree growth, and terrain attribute data and that correlations between EMI-EC$_a$ and total forage yield and tree growth data can be improved with EC$_a$-derived SMZs.

References

Abdu, H., Robinson, D. A., Boettinger, J., & Jones, S. B. (2017). Electromagnetic induction mapping at varied soil moisture reveals field-scale soil textural patterns and gravel lenses. *Frontiers of Agricultural Science and Engineering*, 4, 135–145.

Adams, P. L., Daniel, T. C., Nichols, D. J., Pote, D. H., Scott, H. D., & Edwards, D. R. (1994). Poultry litter and manure contributions to nitrate leaching through the vadose zone. *Soil Science Society of America Journal*, 58, 1206–1211.

Allered, B. J., Adamchuck, V. I., Viscarra Rossel, R. A., Doolittle, J., Freeland, R. S., Grote, K. R., & Corwin, D. L. (2016). Geophysical methods. *Encyclopedia of Soil Science*, 3, 1–8.

Altdorff, D., & Dietrich, P. (2014). Delineation of areas with different temporal behavior of soil properties at a landslide affected Alpine hillside using time-lapse electromagnetic data. *Environmental Earth Sciences*, 72, 1357–1366.

Beaver Watershed Alliance (BWA). (2012). Beaver Lake Watershed Protection Strategy. Retrieved from https://www.beaverwatershedalliance.org/pdf/Beaver-Lake-Watershed-Protection-Strategy.pdf (accessed 8 Jul. 2022).

Beucher, A., Koganti, T., Iversen, B. V., & Greve, M. H. (2020). Mapping of Peat Thickness Using a Multi-Receiver Electromagnetic Induction Instrument. *Remote Sensing*, 12, 1–21.

Blanco, H., & Lal, R. (2008). Chapter 10: Agroforestry. In H. Blanco & R. Lal (Eds.), *Principles of soil conservation and management* (pp. 259–281). Springer. New York City, NY.

Brion, G., Brye, K. R., Haggard, B., West, C. P., & Brahana, J. (2011). Land☐use effects on water quality of a first☐order stream in the Ozark Highlands, mid☐southern United States. *River Research and Applications*, 27, 772–790.

Brye, K. R., & West, C. P. (2005). Grassland management effects on soil surface properties in the Ozark Highlands. *Soil Science*, 170, 63–73.

Cicore, P. L., Franco, M. C., Peralta, N. R., Marques da Silva, J. R., & Costa, J. L. (2019). Relationship between soil apparent electrical conductivity and forage yield in temperate pastures according to nitrogen availability and growing season. *Crop and Pasture Science*, 70, 908–916.

Corwin, D. L., & Lesch, S. M. (2005a). Apparent soil electrical conductivity measurements in agriculture. *Computers and Electronics in Agriculture*, 46, 11–43.

Corwin, D. L., & Lesch, S. M. (2005b). Characterizing soil spatial variability with apparent soil electrical conductivity – survey protocols. *Computers and Electronics in Agriculture*, 46, 103–133.

Corwin, D. L., & Scudiero, E. (2017). Field-scale apparent soil electrical conductivity. In S. Logsdon (Ed.), *Methods of soil analysis. Volume 1* (pp. 1–29). Soil Science Society of America. Madison, WI.

Corwin, D. L., & Scudiero, E. (2019). Mapping soil spatial variability with apparent soil electrical conductivity (ECa) directed soil sampling. *Soil Science Society of America Journal*, 83, 3–4.

Dollinger, J., & Jose, S. (2018). Agroforestry for soil health. *Agroforestry Systems*, 92, 213–219.

Friedman, S. P. (2005). Soil properties influencing apparent electrical conductivity: A review. *Computers and Electronics in Agriculture*, 46, 45–70.

Garcia-Tomillo, A., Miras-Avalos, J., Dafonte-Dafonte, J., & Paz-Gonzalez, A. (2017). Mapping soil texture using geostatistical interpolation combined with electromagnetic induction measurements. *Soil Science*, 182, 278–284.

Gelaw, A. M., Singh, B. R., & Lal, R. (2015). Soil quality indices for evaluating smallholder agricultural land uses in northern Ethiopia. *Sustainability*, 7, 2322–2337.

Heil, K., & Schmidhalter, U. (2017). The application of EM38: Determination of soil parameters, selection of soil sampling points and use in agriculture and archaeology. *Sensors*, 17, 1–44.

Huth, N. I., & Poulton, P. L. (2007). An electromagnetic induction method for monitoring variation in soil moisture in agroforestry systems. *Australian Journal of Soil Research*, 45, 63–72.

Jiang, Z.-D., Owens, P. R., Ashworth, A. J., Ponce, B. F., Thomas, A. L., & Sauer, T. (2021). Evaluating tree growth factors into species-specific functional soil maps for improved agroforestry system efficiency. *Agroforestry Systems*, 96, 479–490.

Johnson, C. K., Doran, J. W., Duke, H. R., Wienhold, B. J., Eskridge, K. M., & Shanahan, J. F. (2001). Field□scale electrical conductivity mapping for delineating soil condition. *Soil Science Society of America Journal*, 65, 1829–1837.

Johnson, C. K., Mortensen, D. A., Wienhold, B. J., Shanahan, J. F., & Doran, J. W. (2003). Site-specific management zones based on soil electrical conductivity in a semiarid cropping system. *Agronomy Journal*, 95, 303–315.

Jose, S. (2009). Agroforestry for ecosystem services and environmental benefits: An overview. *Agroforestry Systems*, 76, 1–10.

Kitchen, N. R., Drummond, S. T., Lund, E. D., Sudduth, K. A., & Buchleiter, G. W. (2003). Soil electrical conductivity and topography related to yield for three contrasting soil–crop systems. *Agronomy Journal*, 95, 483–495.

Kühn, J., Brenning, A., Wehrhan, M., Koszinski, S., & Sommer, M. (2009). Interpretation of electrical conductivity patterns by soil properties and geological maps for precision agriculture. *Precision Agriculture*, 10, 490–507.

Lorenz, K., & Lal, R. (2014). Soil organic carbon sequestration in agroforestry systems. A review. *Agronomy of Sustainable Development*, 34, 443–454.

Nair, P. K. R. (2011). Agroforestry systems and environmental quality: Introduction. *Journal of Environmental Quality*, 40, 784–790.

Nair, V. D., Nair, P. K. R., Kalmbacher, R. S., & Ezenwa, I. V. (2007). Reducing nutrient loss from farms through silvopastoral practices in coarse-textured soils of Florida, USA. *Ecological Engineering*, 29, 192–199.

National Agricultural Statistics Service (NASS). (2019). 2019 State Agricultural Overview – Arkansas. Retrieved from https://www.nass.usda.gov/Quick_Stats/Ag_Overview/stateOverview.php?state=ARKANSAS (accessed 8 Jul. 2022).

National Agroforestry Center (NAC). (2019). Agroforestry Practices. Retrieved from https://www.fs.usda.gov/nac/practices/index.shtml (accessed 8 Jul. 2022).

Natural Resources Conservation Service (NRCS). (2006). Land resource regions and major land resource areas of the United States, the Caribbean, and the Pacific Basin. In *USDA Handbook 296* (pp. 373–375). Government Printing Office. Washington, DC.

Pedrera-Parrilla, A., Martínez, G., Espejo-Pérez, A. J., Gómez, J. A., Giráldez, J. V., & Vanderlinden, K. (2014). Mapping impaired olive tree development using electromagnetic induction surveys. *Plant and Soil*, 384, 381–400.

Peterson, E. W., Davis, R. K., Brahana, J. V., & Orndorff, H. A. (2002). Movement of nitrate through regolith covered karst terrane, northwest Arkansas. *Journal of Hydrology*, 256, 35–47.

Pirani, A. L., Brye, K. R., Daniel, T. C., Haggard, B. E., Gbur, E. E., & Mattice, J. D. (2006). Soluble metal leaching from a poultry litter-amended Udult under pasture vegetation. *Vadose Zone Journal*, 5, 1017–1034.

Robinson, D. A., Lebron, I., & Querejeta, J. I. (2010). Determining soil-tree-grass relationships in a California oak savanna using eco-geophysics. *Vadose Zone Journal*, 9, 528–536.

Schoeneberger, M., Bentrup, G., Gooijer, H., Soolanayakanahally, R., Sauer, T., Brandle, J., Zhou, X., & Current, D. (2012). Branching out: Agroforestry as a climate change mitigation and adaptation tool for agriculture. *Journal of Soil and Water Conservation*, 67, 128–136.

Serrano, J., Shahidian, S., & Silva, J. (2014). Spatial and temporal patterns of apparent electrical conductivity: DUALEM vs. Veris sensors for monitoring soil properties. *Sensors*, 14, 1–19.

Singh, G., Williard, K., & Schoonover, J. (2016). Spatial relation of apparent soil electrical conductivity with crop yields and soil properties at different topographic positions in a small agricultural watershed. *Agronomy*, 6, 57.

Soil Science Division Staff. (2017). Tools for proximal soil sensing. In C. Ditzler, K. Scheffe, & H. C. Monger (Eds.), *USDA Handbook 18: Soil survey manual* (pp. 355–394). Government Printing Office. Washington, DC.

Taghizadeh-Mehrjardi, R., Minasny, B., Sarmadian, F., & Malone, B. P. (2014). Digital mapping of soil salinity in Ardakan region, central Iran. *Geoderma*, 213, 15–28.

Udawatta, R. P., & Jose, S. (2012). Agroforestry strategies to sequester carbon in temperate North America. *Agroforestry Systems*, 86, 225–242.

United States Environmental Protection Agency (USEPA) (2009). Ground water and drinking water – national primary drinking water regulations. Retrieved from https://www.epa.gov/ground-water-and-drinking-water/national-primary-drinking-water-regulations (accessed 8 Jul. 2022).

Viscarra Rossel, R. A., Adamchuk, V. I., Sudduth, K. A., McKenzie, N. J., & Lobsey, C. (2011). Proximal soil sensing: An effective approach for soil measurements in space and time. In D. L. Sparks (Ed.), *Advances in agronomy. Volume 113* (pp. 237–282). Academic Press. Burlington, MA.

Weil, R. W., & Brady, N. C. (2017). Soil of dry regions: Alkalinity, salinity, and sodicity. In D. Fox (Ed.), *The nature and properties of soils* (15th ed., pp. 420–463). Pearson Education, Inc. New York City, NY.

Chapter 2

Using Apparent Electrical Conductivity to Delineate Field Variation in an Agroforestry

System in the Ozark Highlands

Abstract

Minimal work has been conducted using repeated electromagnetic induction (EMI) apparent electrical conductivity (EC_a) surveys in agroforestry (AF) systems within regions similar to the Ozark Highlands of northwest Arkansas. Using remotely sensed field data may provide a non-destructive option to identify areas with similar properties and expected soil and plant responses that could serve as soil management zones (SMZs). Objectives of this study were to i) use EMI-EC_a surveys to assess the spatiotemporal pixel variation of measured EC_a; ii) identify clusters of similarly behaving populations for precision soil management; iii) identify correlations among EMI-EC_a data and *in-situ* volumetric water content (VWC), and EC_a measurements and sentential site soil-sample electrical conductivity (EC), gravimetric water content (GWC), and pH; and iv) determine whether fewer, EMI-EC_a surveys could be conducted to capture the same amount of EC_a variance as the 12 mid-monthly EMI-EC_a surveys. Between August 2020 and July 2021, 12 mid-monthly EC_a surveys were conducted at a 4.25-ha AF site in Fayetteville, AR. During each EC_a survey, soil-sensor-based VWC, soil temperature, and EC_a measurements were collected at two soil depths (15-, 15-, and 15-cm, respectively, and 75-, 75-, and 50-cm, respectively) and soil-sample-based GWC, EC, and pH measurements were collected from two soil depth intervals (0-15- and 45-55-cm) at fixed locations. Potential pedogenic and surface management effects were observed for the universally kriged EC_a data. The overall mean perpendicular geometry (PRP) and horizontal coplanar geometry (HCP) EC_a ranged between 1.8 to 18.0 and 3.1 to 25.8 mS m^{-1}, respectively, and the overall mean HCP EC_a was 67% greater than the mean PRP EC_a. The largest measured EC_a values occurred within the local drainage way, which has mapped inclusions with aquic soil moisture regimes, or areas of potential groundwater movement, and the smallest measured EC_a values occurred within areas with

31

decreased effective soil depth and increased coarse fragments. A positive ($r^2 = 0.4$; $P < 0.05$)

linear relationship occurred over time between PRP EC_a standard deviation (SD), with a negative

linear relationship ($r^2 = 0.93$; $P < 0.05$) between HCP EC_a coefficient of variation (CV) across

weather seasons (i.e., Summer to Spring). The PRP and HCP EC_a mean, SD, and CV were

unaffected by weather or tree growing-season. K-means clustering delineated three precision

SMZs that were reflective of areas with similar EC_a and EC_a variability. The variance of the 12

HCP EC_a surveys did not differ from that of the four and two HCP EC_a surveys conducted in the

middle of the four annual weather seasons and in the middle of the Winter and Summer seasons

specifically, respectively. Results of this study provided valuable information on the

spatiotemporal variability of EMI-EC_a, how EC_a correlates with soil properties and EC_a-derived

SMZs in an AF system with varying topography in the Ozark Highlands.

Introduction

Soils are innately heterogeneous, where they vary spatially and temporally [1,2]. Such variabilities often create challenges for agricultural producers, as variations in soil properties substantially affect water movement, solute transport, and plant–water–soil interactions, which, in turn, influence soil quality and crop yield [1]. Additionally, soil spatial variability also affects tillage and planting equipment performance, resulting in uneven stand establishment, which increases competition between plants and further reduces yield. Accurate characterization of spatial variability of soils is not only essential for understanding field-scale processes across landscapes and within the soil, but also an essential component of soil quality (SQ) assessments, site-specific crop management, and non-point pollutant transport within the vadose zone [3].

Several methods are available to map spatial variability and delineate management zones in a field. Soil spatial variability is often characterized using soil sampling or a variety of different sensors, with each method having advantages and limitations [4]. For instance, soil samples can be collected using different sampling strategies (i.e., grid, random, stratified, and transect). Soil sampling provides direct measurement of soil properties in sampling locations, where the data can be interpolated using different techniques to estimate soil properties across the study area [2,5]. However, soil sampling is often expensive and labor-intensive, making grid sampling impractical for whole-farm-scale operations and identifying soil-landscape relationships 4,5].

Non-destructive, geophysical methods for proximal soil sensing can help overcome the limitations of spatial characterization via soil sampling and be used as an alternative method for quantifying spatial variability [6]. There are many different types of geophysical methods for proximal soil sensing, however, electromagnetic-induction (EMI)-based methods are the most

frequently used [7]. Electromagnetic induction sensors are non-invasive and characterize a soil's apparent electrical conductivity (EC_a), which is the ability of a soil to conduct an electrical current and is most commonly used to measure soil salinity [2,6]. Measured soil EC_a in the field is the result of complex interactions of soil salinity, base saturation (BS), bulk density (BD), clay content and mineralogy, soil water content (SWC), soil organic matter (SOM), cation exchange capacity (CEC), and soil temperature [8].

Using EMI-based methods to obtain spatial EC_a measurements in lieu of intensive soil sampling has become a common tool for landscape-scale and field-variability characterization for many reasons. Electromagnetic induction-based methods are simple to implement, capable of covering large surface areas in a limited amount of time (i.e., non-invasive, instant measurement, mobile, and relatively high-speed), affordable, reliable, and can accurately delineate spatial changes in belowground properties [3,9]. Soil characteristics derived from EMI-EC_a surveys include salinity, nutrients, SWC, texture, depth to sand layers or claypans, BD, and many indirect properties and processes [i.e., organic matter (OM), CEC, leaching, groundwater recharge, and soil drainage class, among others] [3]. Additionally, applications of EMI-based EC_a measurements include digital soil mapping, remote sensing, and precision agriculture [4,10], and the collected data can be used to optimize soil sampling strategies, characterize soil texture boundaries, delineate crop management zones, predict yield [10], map depth to limiting layer (i.e., petrocalcic horizons and claypans), assess herbicide leaching potential, and identify site-specific septic-system failure locations [6]. However, because measured soil EC_a represents a combination of specific soil properties, sampling is still required to verify (i.e., ground-truth) and calibrate the data collected within agricultural field for precision agriculture, land management, and environmental research applications [3,6,8].

Although there has been significant research conducted relating EMI-EC$_a$ surveys to a multitude of soil properties in different types of land management systems and ecosystems [9], little work has been conducted using EMI-EC$_a$ surveys to investigate soil property variations within agroforestry (AF) systems. Agroforestry is a conservation-oriented, land management practice that has continued to gain appeal and recognition by growers. An AF system is defined as the intentional integration of agriculture/horticulture and forestry to benefit from the subsequent interactive effects that are produced from growing agricultural/horticultural crops and/or livestock alongside trees and/or shrubs [11]. The benefits of AF practices include SQ enhancements, additional ecosystem services [12], and opportunities for short- and long-term income sources for the producer. There are numerous potential ecosystem services that AF systems provide, including water quality (WQ) enhancement, increased biodiversity, reduced soil erosion (wind and water), elevated aesthetic value, carbon (C) sequestration, oxygen (O) production, and mitigation of greenhouse gases [13]. Furthermore, SQ benefits from AF have included enhanced soil fertility [12], soil organic C (SOC) storage [14–16], soil structure [17], conservation of biodiversity, and production diversity [13,18]. However, the magnitude of the effects of AF systems varies by soil series, climate, and management system.

A region with unique features that could benefit greatly from the application of conservative land management practices, like AF systems, is the Ozark Highlands. The Ozark Highlands (36–38° N, 91–95° W), Major Land Resource Area (MLRA) 116A, spans 85,110 km^2 across southern Missouri, northern Arkansas, and northeast Oklahoma [19,20]. The annual air temperature in the Ozark Highlands ranges from ~ 12 to 16°C and the majority of the Ozark Highlands has an annual precipitation range of 96.5 to 114.5 cm [19,20]. Landscapes within the Ozark Highlands range from gentle, prairie-like, rolling upland hills to greatly divided, steep-

sloped wooded hills and narrow gravel valleys, and possess well-developed karst topography (i.e., sinkholes, caves, dry valleys, box valleys, and large springs) [19,20]. Furthermore, the majority of the soils are Alfisols or Ultisols and are formed from materials that have been weathered from cherty limestone, where physical and chemical weathering have resulted in the cherty limestone disintegrating into its least soluble components of chert and clay [20]. On average, the soils in the Ozark Highlands range between medium- to fine-textured, shallow to very deep profiles and are moderately well to excessively drained. Additionally, many of the soils in the Ozark Highlands, which overlie dolomitic bedrock and limestone, exist on steep slopes and are stony and shallow to bedrock.

The combination of the Ozark Highlands' topography, soil properties, and climate result in an increased potential for conservation issues, specifically surface and groundwater quality degradation [19,20]. For instance, the topography of the Ozark Highlands results in an increased potential for rapid transmission of rainfall, and thus any potential pollutants present at the soil surface, down slope as runoff and into surface waters. Additionally, if rainfall and/or surface flow are able to infiltrate the Ozark Highlands' shallow, cherty soils that overlie karst limestone geology, any potential pollutant-carrying leachate may be rapidly transmitted through the soil and into groundwater [21]. Thus, the unique combination of the Ozark Highlands' features (i.e., topography; shallow, cherty soils overlying karst limestone geology; and climate) suggests the implementation and research of AF systems within the Ozark Highlands would be particularly advantageous, multi-beneficial, and intriguing due to the many potential ecosystem services and benefits that AF systems offer (i.e., WQ and SQ enhancement and reduced soil erosion and runoff).

Justification, Objectives, and Hypotheses

Although EMI-EC$_a$ surveys have been applied to evaluate variations in a multitude of soil properties within many different land management systems and ecosystems across the world, EMI-EC$_a$ surveys have been minimally applied in AF systems to investigate soil property variations. Additionally, little to no work has been conducted to explore the spatiotemporal relationship between repeated EMI-EC$_a$ surveys and soil property variations in AF systems within regions that have similar features to the Ozark Highlands. As a result of this lack of information and to provide spatially resolved soil data for precision soil management, the objectives of this study were to i) use monthly EMI-EC$_a$ surveys to assess the spatiotemporal pixel variation of the measured EC$_a$ of a 20-year-old AF system within the Ozark Highlands; ii) use k-means to identify clusters of similarly behaving populations for precision soil management; iii) identify correlations between EMI-based EC$_a$ data and in-situ, soil-sensor-measured volumetric water content (VWC) and EC$_a$ measurements at two depths (15 and 75 cm and 15 and 50 cm, respectively) and benchtop-measured soil sample EC, gravimetric water content (GWC), and pH in two depth intervals (0-15 and 45-55 cm); and iv) determine whether fewer, evenly spaced, strategically selected EMI-EC$_a$ surveys could have been conducted in one year to capture the same amount of overall EC$_a$ variance as the 12 mid-monthly EMI-EC$_a$ surveys conducted. It was hypothesized that there would be a significant ($P < 0.05$) change in the mean EC$_a$ and EC$_a$ variability [i.e., standard deviation (SD) and coefficient of variation (CV)] across time (i.e., survey dates and weather season) and that there would be significant difference between the EC$_a$ mean, SD, and CV of surveys that were conducted in different weather seasons and in the tree growing/non-growing season at a 20-year AF system within the Ozark Highlands. Furthermore, it was hypothesized that monthly EMI-EC$_a$ surveys can be grouped into similar

functional populations and be made into zones for precision soil management. It was also hypothesized that monthly EMI-EC$_a$ survey data are correlated with soil-sensor-based VWC and EC$_a$ and soil-sample-based EC, GWC, and pH. Additionally, it was hypothesized that fewer surveys than monthly could have been conducted in a 1-year period to capture the same amount of overall EC$_a$ variance as the 12 mid-monthly EMI-EC$_a$ surveys conducted.

Materials and Methods

Site Description

Mapped Soils and Tree and Forage Establishment

This study was conducted on a 4.25-ha paddock at the University of Arkansas Milo J. Shult Agricultural Research and Extension Center (SAREC) in Fayetteville, AR (36.09°N, 94.19°W). The study site is located within the Ozark Highlands, Major Land Resource Area (MLRA) 116A [22]. The experimental area is mostly mapped as Captina silt loam (fine-silty, siliceous, active, mesic Typic Fragiudults) with some Pickwick silt loam (fine-silty, mixed, semiactive, thermic Typic Paleudults) and small areas containing Johnsburg silt loam (fine-silty, mixed, active, mesic Aquic Fragiudults), Cleora fine sandy loam (Coarse-loamy, mixed, active, thermic Fluventic Hapludolls), and Nixa cherty silt loam (loamy-skeletal, siliceous, active, mesic Glossic Fragiudults; Figure 1) [23]. The paddock also contains an inclusion that is dissimilar, lower in elevation, and consistently wetter than surrounding areas and is not captured in the soil mapping units across the site. The wetter location within the paddock was classified as fine, mixed, active, thermic Typic Endoaqualfs [24]. The study site has an annual minimum, maximum, and average air temperature of 8.7, 20.3, and 14.6°C, respectively, and receives an annual average (30-yr mean, 1981 to 2010) of 1156 mm of precipitation [25].

Before the AF site was established, the paddock was split into two paddocks by a north-south fence, which were poorly managed, covered in weeds, and only used for equipment storage. Additionally, the paddocks had small terraces from previous management and had a gully forming. Prior to the site's conversion to an AF system, the fences were removed, the gully was filled in, the soil was leveled, and the vegetation was killed. In 2000, sixteen rows of eastern black walnut (*Juglans nigra* L.), Northern red oak (*Quercus rubra* L.), and pecan (*Carya illinoinensis* Wangenh. K. Koch) were established and oriented east-west at 15-m spacing between rows (Figure 1). The study site was never ideal for growing eastern black walnut, where they grew adequately on the east end, but struggled to grow in the wet, middle portion and dry Nixa soil on the west end of the rows. As a result, the eastern black walnut trees were replaced in 2014 with rows that consisted of three different fast-growing species: American sycamore (*Plantanus occidentalis* L.) in the well-drained portion, cottonwood (*Populus deltoides* W. Bartram ex Marshall) in the poorly drained portion, and pitch/loblolly pine (*Pinus rigida x Pinus taeda*) in the drought-prone area of the field (Figure 1). Additionally, two forage-species treatments were established in the alleys between tree rows, including a cool-season species [orchardgrass (*Dactylis glomerata* L., var. Tekapo)] that was seeded in Fall 2015 at 17 kg pure live seed (PLS) ha^{-1} and a native warm-season mix [8:1:1 big bluestem (*Andropogon gerardii* Vitman), little bluestem (*Schizachyrium scoparium* {Michx. Nash} and indiangrass (*Sorghastrum nutans* L.)] seeded in spring 2016 at 10 kg PLS ha^{-1} (Figure 1). A Haybuster 107C no-till drill (DuraTech, Jamestown, ND) was used to plant the alleys. Cornerstone® Plus (N-[phosphonomethyl] glycine, Winfield Solutions, St. Paul, MN) was applied before establishment to rid the alleys of any existing vegetation at a 2.2 kg ha^{-1} rate [41% active ingredient (ai)] and

alleys were treated with Plateau[TM] (ammonium salt of imazapic) after establishment at a 0.28 kg ha^{-1} rate (23.6% ai).

Fertilizer Applications

Each spring between 2001 and 2007, except for 2005, 3.9 to 6.7 Mg poultry litter (PL) ha^{-1} were distributed via broadcast application over the eastern half of the AF site and 50 to 76 kg nitrogen (N) ha^{-1}, as ammonium nitrate (NH_4NO_3) fertilizer, were broadcast applied over the western half of the AF site [26]. In 2005, PL and NH_4NO_3 were applied at a rate of 8.9 Mg PL ha^{-1} and 123 kg N ha^{-1} in the spring and fall, respectively [26]. Starting in June 2004, additional fertilizer was surface-applied to the surrounding ground near each tree as an annual application of Osmocote (The Scotts Miracle-Grow Co., Marysville, OH), a slow-release fertilizer, that contained 5.6, 2.4, and 4.6 g of N, phosphorus (P), and potassium (K), respectively [26]. In 2005, both PL and NH_4NO_3 applications were made in the spring and fall in order to evaluate the impacts of nutrient source on soil physiochemical properties.

In March 2017 and 2018 and April 2019, orchardgrass and native grass treatments in the alleys between tree rows received 84 kg N ha^{-1} (4.94 Mg ha^{-1}, fresh weight basis) of locally sourced PL (Figure 1). The chemical composition of the 2017 PL application was 2.69, 0.7, and 1.12 % N, P, and K, respectively, and had a pH of 6.1. The 2018 PL had 1.98, 0.58, and 1.02 % N, P, and K, respectively, and had a pH of 6.2. The 2019 PL had 2.48, 0.69, and 0.94 N, P, and K, respectively, and had a pH of 5.2. Additionally, the site was grazed by heifers (*Bos taurus* L.) at a density of 1.9 animal units (AU) ha^{-1} from May to June 2017, 2.2 AU ha^{-1} from May to July 2018, and 2.42 AU ha^{-1} from May to July 2019 [24,27,28]. Additionally, N, in the form of urea (46-0-0), was applied at a rate of 67.3 kg N ha^{-1} or 146 kg urea ha^{-1} on 30 March 2020 and 31

March 2021. Urea was applied to all alleys with a fertilizer spreader attached to a 3-point hookup with a spreading width of 15.2 m.

In April 2016, all trees at the AF site were amended with three different fertilizers at varying rates and areas surrounding the tree. Pecan trees were fertilized with 2.3 kg of NH_4NO_3, 5.7 kg of a 13-13-13 fertilizer (Greenkeeper's Secret 13-13-13 Premium Fertilizer, T&M, Inc., Foristell, MO), and 0.27 kg of gypsum ($CaSO_4$) in a circular area around each tree with an 9.1-m diameter. Sycamore, cottonwood, and loblolly pine trees were fertilized with 0.2 kg of NH_4NO_3, 0.48 kg of a 13-13-13 fertilizer, and 0.1 kg of gypsum, where the fertilizers were spread within a rectangular area around the trees in 2.4-m wide strips and 2.3 m between adjacent trees. For the northern red oak fertilization, if there were other red oak trees that were 2.4 m away on both sides of a red oak tree, the red oak tree was fertilized with 0.52 kg of NH_4NO_3, 1.3 kg of a 13-13-13 fertilizer, and 0.27 kg of gypsum in a 2.4- x 6.1-m rectangular area around the tree. If there were no other red oak trees within 2.4 m of either side of a red oak tree, the red oak tree was fertilized with 1.0 kg of NH_4NO_3, 2.6 kg of a 13-13-13 fertilizer, and 0.54 kg of gypsum in a 4.9- x 6.1-m rectangular area around the tree. If there was a red oak tree that was 2.4 m away of a red oak tree on one side only, the red oak tree was fertilized with 0.79 kg of NH_4NO_3, 2.0 kg of a 13-13-13 fertilizer, and 0.4 kg of gypsum in a 3.7- x 6.1-m rectangular area around the tree and offset to the open side of the tree 1.2 m and 2.4 m.

In April 2017, pecan trees were fertilized with 2.3 kg of a 32-0-0 fertilizer, 5.7 kg of a 13-13-13 fertilizer, and 0.27 kg of gypsum in a circular area around each tree with an 9.1-m diameter. Red oak trees were fertilized with 1.0 kg of a 32-0-0 fertilizer, 2.6 kg of a 13-13-13 fertilizer, and 0.54 kg of gypsum in a 4.9 x 6.1 m rectangular area around the tree (i.e., 2.4 m to either side of the red oak tree in the row and 3.0 m to each side of tree into the adjacent alley). In

41

May 2017, sycamore, cottonwood, and loblolly pine trees were fertilized with 0.2 kg of a 32-0-0 fertilizer, 0.48 kg of a 13-13-13 fertilizer, and 0.1 kg of gypsum in a 2.3 x 2.4 m rectangular area around the tree (i.e., 1.1 m to either side of the red oak tree in the row and 1.2 m to each side of tree into the adjacent alley).

All tree fertilizer rates were the same in 2018, 2019, and 2020 for red oak, pecan, and loblolly pine trees. Pecan trees were fertilized in May 2018, April 2019, and June 2020 with 11.7 kg of a 13-13-13 fertilizer, 4.7 kg of NH_4NO_3, and 2.4 kg of gypsum in a circular area around each tree with a 10.7-m diameter. Red oak trees were fertilized in May 2018, April 2019, and June 2020 with 8.5 kg of a 13-13-13 fertilizer, 3.4 kg of NH_4NO_3, and 1.8 kg of gypsum in a circular area around each tree with a 9.1-m diameter. Loblolly pine trees were fertilized in May 2018, April 2019, and May 2020 with 0.72 kg of a 13-13-13 fertilizer, 0.29 kg of NH_4NO_3, and 0.15 kg of gypsum based on a 2.4-m wide strip and 2.3 m between trees. Additionally, sycamore and cottonwood trees were thinned in summer 2019, however, the fertilizer footprint per tree was increased, making the per-area rate the same for 2018, 2019, and 2020. Sycamore trees were fertilized in May 2018, June 2019, and May 2020. For the 2018 and 2019 fertilizer applications, sycamore trees were fertilized with 1.1 kg of a 13-13-13 fertilizer, 0.44 kg of NH_4NO_3, and 0.23 kg of gypsum based on a 3.7-m wide strip and 2.3 m between trees. For the 2020 sycamore fertilizer application, trees were fertilized with 2.1 kg of a 13-13-13 fertilizer, 0.87 kg of NH_4NO_3, and 0.45 kg of gypsum in a circular area around each tree with a 4.6-m diameter. Cottonwood trees were fertilized in May 2018, June 2019, and June 2020. For the 2018 and 2019 fertilizer applications, sycamore trees were fertilized with 1.4 kg of a 13-13-13 fertilizer, 0.55 kg of NH_4NO_3, and 0.29 kg of gypsum based on a 4.6 m wide strip and 2.3 m between trees. For the 2020 cottonwood fertilizer application, the trees were fertilized with 2.1 kg of a 13-13-13

fertilizer, 0.87 kg of NH_4NO_3, and 0.45 kg of gypsum in a circular area around each tree with a 4.6-m diameter. Furthermore, the loblolly pine trees were also fertilized in June 2021 with 0.5 kg of a 13-13-13 fertilizer in a circular area around each tree with a 2.0-m diameter. Additional site establishment and management details were reported in Adams et al. [29], Adhikari et al. [30], Amorim et al. [31], Ashworth et al. [24], Ashworth et al. [32], DeFauw et al. [33], Dold et al. [34], Gurmessa et al. [28], Jiang et al. [35], Kharel et al. [36], Niyigena et al. [27], O'Brien et al. [37], Sauer et al. [26], Thomas et al. [38], and Ylagan et al. [39].

Survey Equipment

Geospatial, EMI-based EC_a measurements were obtained using a DUALEM-1S sensor (DUAL☐geometry Electro☐Magnetic; Dualem Inc., Milton, ON, Canada) and a Trimble R2 global positioning system (GPS) unit (Trimble Inc., Westminster, CO). The DUALEM-1S is a non-invasive, geo-conductivity sensor that has a transmitter, which operates at 9 kHz, and has two receivers that have different orientations [6,40]. With a 1-m separation, both the transmitter and the receiver use vertical dipoles in the horizontal coplanar geometry. The perpendicular geometry also uses a vertical dipole transmitter and the receiver, located 1.1 m away, and utilizes a horizontal dipole [6,40]. The depths of exploration (DOE) for the horizontal coplanar geometry (HCP) and the perpendicular geometry (PRP) are roughly 1.6 and 0.5 m, where the DOE is defined as the depth to which an array accumulates 70% of its total sensitivity. Thus, the HCP measures the bulk EC_a of the 0 to 1.6-m depth and the PRP measures the bulk EC_a of the 0 to 0.5-m depth and the conductivity range for the DUALEM-1S is 3000 mS m^{-1} [6,40].

The DUALEM-1S is powered by a 12-V, direct current (DC), external power source [6,40]. In this study, a Can-Am Side-by-Side (Defender, BRP US, Inc., Sturtevant, WI) was used

to power and pull the DUALEM-1S on a sled during surveying (Figure 2). Measurements from the DUALEM-1S were transmitted serially through a 9-socket, DB-9 connector port, and were collected concurrently with the GPS data via a hand-held geoinformation system program (HGIS; HGIS version 10.90, StarPal Inc., Fort Collins, CO) on a Trimble Yuma 2 rugged tablet computer (Trimble Inc., Westminster, CO) [6,40].

Survey Procedures

In order to capture the spatial and temporal variability of EC_a measurements at the AF site, mid-month scans were conducted between August 2020 and July 2021. To minimize the effects of temperature drift on the DUALEM-1S signal during surveying, surveys were conducted in the early morning and the DUALEM-1S sensor was powered on 30 minutes prior each survey in order for the sensor to reach ambient temperature. For each survey, the DUALEM-1S was securely suspended on a sled, 12.7 cm above the sled bottom, and was pulled at a rate of 4.8 to 8.0 km hr^{-1}. The front of the DUALEM-1S was located 2.10 m behind the side-by-side and the center of the DUALEM-1S was located 4.15 m behind the Trimble R2 GPS unit. Each survey was conducted in a looping pattern over two alleys at a time until four parallel drive paths per alley, 2 to 5 m apart, had been achieved (Figure 3). During the survey period, unnecessary stops were avoided and the sensor was kept > 1 m away from any metal objects. After each survey, a calibration line was driven over all subsequent survey lines so that any drift that occurred in the DUALEM-1S's measurement during the survey period could be monitored and accounted for. The calibration line was conducted in a "V" shape, starting in the northwest corner, ending in the southwest corner of the AF site, with the midpoint being around the eastern edge of Row 8 or 9 (Figure 3).

Weather and Soil Property Collection

The local air temperature and precipitation of the University of Arkansas SAREC in Fayetteville, AR was recorded every 30 minutes on a micrometeorological weather station, using a tipping bucket gauge, located 1.67 km away (36.101002°N, 94.173728°W) to the northeast of the northeast corner of the AF site. The recorded air temperature was averaged per day to obtain the daily average air temperature (DAAT) and the recorded daily precipitation was totaled to obtain the total daily precipitation (TDP).

Soil VWC and soil temperature were recorded every 4 hours using 5TM soil moisture sensors (ECH2O 5TM Soil Moisture Sensor; METER Group, Pullman, WA) at the 15- and 75-cm soil depths from the soil surface and logged on a Decagon EM50 data logger (METER Group, Pullman, WA; Figure 1). Additionally, two EC sensors (Teros 12; METER Group, Pullman, WA) were installed on 26 January 2021 at the 15- and 50-cm depths at each of the three sampling locations and at a location in the southwest corner of the site (Figure 1), where *in-situ* soil EC was measured every 4 hours on a Decagon EM50 data logger. At the conclusion of the measurement period, VWC and soil temperature recorded between 1 August 2020 and 31 July 2021 and EC recorded between 26 January 2021 and 31 July 2021 were averaged for each day and expressed as daily means.

During each scan, soil samples were collected at three sentinel sites across the study area. The sentinel sites were located near the local summit, depression area, and a mid-slope area (Figure 1). At each sentinel site, soil samples were collected by auguring as deep as possible near each logger. During the auguring process, the removed soil was placed on its specific depth on the marked auger rug. Afterward, soil from the 0- to 15-and 45- to 55-cm depth intervals was

45

collected beginning on 20 November 2020 and 15 July 2020, respectively. The collected soil

samples were placed in a sealed, plastic-lined bag and then weighed in the laboratory. Afterward,

the samples were oven-dried in a forced-air oven at 70°C for 48 hours, re-weighed for moisture

content determinations, and then mechanically ground and sieved to < 2 mm. Afterward, soil EC

and pH were measured potentiometrically in a 2:1 water-volume-to-soil-mass slurry, where 40 g

(± 0.05 g) of the oven-dried, sieved soil were mixed with 40 mL of deionized water and

reciprocally shook on a mechanical shaker for 1 hr. The soil-water slurry was then filtered twice

(No.1 filter paper, Cat No 1001 125; Whatman Cytiva, Little Chalfont, Buckinghamshire, UK)

until there were 40 mL of filtrate, where the filtrate was then mixed by pouring the filtrate back-

and-forth between two plastic vails. Afterward, the volume of the filtrate was evenly split (20

mL) between the two plastic vial and the pH and EC were determined by placing a pH (Orion

9107BNMD; Thermo Scientific, Waltham, MA) and EC probe (Orion 013005MD; Thermo

Scientific, Waltham, MA) into each of the vial, which both were connected to a pH/Conductivity

Benchtop Meter (Orion Star A215; Thermo Scientific, Waltham, MA).

EMI-EC$_a$ Survey Data Processing

Prior to data analyses, survey data were cleaned, GPS coordinates adjusted, outliers

removed, and calibrated. Survey data cleaning began with the deletion of any duplicate GPS

output that were generated for a single DUALEM-1S measurement. Secondly, because the

Trimble R2 GPS unit was located 4.15 m ahead of the DUALEM-1S sensor during each scan, a

GPS adjustment between the DUALEM-1S sensor and the Trimble R2 GPS unit was needed

[41]. Because the DUALEM-1S sensor was pulled behind the side-by-side at a rate of 4.8 to 8.0

km hr^{-1} for every scan, an average of 6.4 km hr^{-1} was used to calculate the time it would take for

the center of the sensor to travel 4.15 m, which was 2.32 s. As a result, the DUALEM-1S output was adjusted to the GPS point that occurred the closest to 2.32 s earlier. Furthermore, any measurements that occurred during a stop that took place during the survey period were subsequently removed from the survey dataset. Additionally, all survey cleaning and GPS adjustments were also conducted on the calibration line data set.

The next step in the pre-analyses data cleaning was the removal of outliers. If highly conductive objects (i.e., metal) were near the DUALEM-1S when a measurement was recorded, the object can result in interference with the produced electromagnetic fields of the DUALEM-1S and cause the recording of soil EC_a values that are biologically impossible (i.e., ≤ 0.0 mS m^{-1}). Thus, the outlier removal process began with the removal of any measurement points that had an HCP or PRP EC_a conductivity measurement that were less than 0.1 mS m^{-1} for both the survey and calibration line. Additionally, similar to Rudolph et al. [42] and Martini et al. [43], any points that occurred within a 2.0-m buffer around the cables of the soil sensor network at the AF site were removed in order to remove the potential of any alteration of the EC_a data that was caused by the magnetic components of the sensors. Afterward, a Hampel filter [44] was applied to each of the survey's and calibration line's HCP and PRP EC_a data with a 10-point, half-width (i.e., 21 point moving data window) and a threshold of 3. A Hampel filter normally replaces a determined outlier with the local median; however, any measurement point that was determined to be an outlier in the HCP and/or PRP EC_a of the survey or calibration line was simply removed altogether. Similarly, Delefortrie et al. [45] applied a Hampel filter to their DUALEM collected EC_a surveys; although, they applied the Hampel filter later in the calibration procedure rather than on their original datasets and replaced the determined outliers with the local median. The

Hampel filter in this study was applied in R (version 4.05, R Core Team, Boston, MA) using the pracma package [46].

The decision to delete an entire measurement point due to either its HCP or PRP EC_a measurement being an outlier, rather than just replacing the HCP and/or PRP EC_a measurement outlier with the local median, was due to: 1) the belief that removing rather than replacing values with the local median was a better method for a more accurate dataset, 2) the attempt of being consistent with the earlier procedure of removing entire measurement points that had an HCP or PRP EC_a conductivity measurement that was < 0.1 mS m^{-1}; and 3) the belief that the removal of the relatively few measurement points with HCP or PRP EC_a outliers would only affect the overall size of the survey and calibration line datasets and the end result of kriged surveys to a small degree. Furthermore, the removal of the entire point based on whether its HCP and/or PRP EC_a was less than 0.1 mS m^{-1} or if the applied Hampel filter determined that either a point's HCP and/or PRP EC_a was an outlier was believed to be a proper method of removing outliers due to many of the removed points from all the completed survey and calibration lines occur around known locations of metal objects at the AF site. Additionally, there are groupings of removed outliers that occur in locations that do not have known metal objects. However, these isolated apparent outliers could be the result of a metal object that was placed or left in the ground prior to the establishment of the AF site.

After the survey and calibration line had been cleaned, GPS coordinates adjusted, and outliers were removed, the survey data were then ready to be calibrated. Although the DUALEM-1S sensor was turned on roughly 30 min before each survey in order to bring the sensor to a stable internal temperature, it was necessary to calibrate the collected HCP and PRP EC_a data because the internal temperature of the DUALEM-1S sensor can increase overtime

during the survey and cause EC$_a$ data to be slightly skewed. Similar calibration procedures produced by Delefortrie et al. [41], Martini et al. [43], and Simpson et al. [45] were used as references when conducting the calibration. The calibration procedure began with finding the survey points that occurred within 1.5 m of each point of the calibration line. The HCP and PRP EC$_a$ data and the measurement time of the survey points that occurred within 1.5 m of each calibration point were averaged. Similar to Martini et al. [43], a linear regression model was created based on the difference between the average HCP and PRP EC$_a$ of the survey points that occurred within 1.5 m of each calibration point and the HCP and PRP EC$_a$ of the calibration point versus the average measurement time of the survey points that occurred within 1.5 m of each calibration point. The linear regression model was applied to the cleaned, GPS-coordinate-adjusted, outlier-removed survey dataset to obtain the projected differences between the HCP and PRP EC$_a$ of the survey and calibration line throughout the survey period. The projected differences between the HCP and PRP EC$_a$ of the survey and the calibration line were subtracted from the HCP and PRP EC$_a$ of the survey points at a given time, which resulted in a drift-calibrated EC$_a$ survey dataset. The calibration procedure was performed in R Studio (version 4.05, R Core Team, Boston, MA) using the geosphere package [47].

Because the EC$_a$ surveys were conducted at relatively equal intervals throughout the year, the EC$_a$ of each survey occurred at a different soil temperature. As a result, it was necessary to standardize the EC$_a$ measurements to a reference temperature. The HCP and PRP EC$_a$ were both standardized to 25°C (EC$_{25}$) using the equation of Corwin & Lesch (2005b;1):

$$EC_{25} = EC_T \times \left(0.447 + 1.4034^{-T/26.8615}\right) \qquad (1)$$

49

In the equation, EC_T (mS m^{-1}) is the EC_a at a particular soil temperature and T (°C) is the soil

temperature [9]. The soil temperature (T) used in the EC temperature standardization equation

(1) was the average recorded soil temperature of the soil sensors at the three sentinel sites (Figure

3), at the time of a particular EC_a survey, at the 15-cm depth for the PRP EC_a standardization and

at the 50-cm depth for the HCP EC_a standardization. Additionally, any measurement point that

had an HCP and PRP EC_a value of < 0.1 mS m^{-1} after the EC temperature standardization

equation (1) was applied was removed to be consistent with earlier procedures. The HCP and

PRP EC_a of any coincidental points were then averaged. Afterward, the cleaned, GPS-

coordinate-adjusted, outlier-removed, drift-calibrated, temperature-adjusted, coincidental point-

averaged HCP and PRP EC_a survey datasets, referred to as HCP and PRP EC_a, were then ready

for interpolation procedures.

Twenty percent of the HCP and PRP EC_a survey data were selected at random and set

aside for model validation. The experimental semi-variogram was calculated with the remaining

80% and fitted with a nugget and exponential, spherical, Gaussian, Matern, circular, and linear

models. The best model minimized the sum of square of error and was selected for universal

kriging to a 5-m resolution. A 5-m resolution was chosen to be consistent with the resolution of

previous studies at the AF's site [35]. Values from the interpolated raster were then extracted to

each of the validation locations. The model residuals were calculated using Equation (2):

$$r_i = \hat{y}_i - x_i \qquad (2)$$

where r_i is the residual value in location i, $\hat{y}_i$ is the predicted value in location i, x_i is the observed value in location i, and i belongs to all locations selected at random to form the validation dataset. The model error was calculated from the model residuals using Equation (3):

$$e_i = \frac{r_i}{x_i} \qquad (3)$$

where e_i is the model error at location i. Additionally, the interpolation procedures were conducted in R Studio (version 4.05, R Core Team, Boston, MA) using the sp [48], rgdal [49], gstat [50], geodist [51], raster [52], and terra [53] packages.

Statistical Analyses

The cleaned, GPS-coordinate-adjusted, outlier-removed, drift-calibrated, temperature-adjusted, coincidental point-averaged, universally-kriged HCP and PRP EC_a survey datasets, hereafter referred to as HCP and PRP EC_a, were used to determine the mean, standard deviation (SD), and coefficient of variation (CV) among the 5-m pixels to assess the spatial variability of the AF site's HCP and PRP EC_a during the 12-month study period. Furthermore, in order to assess the AF site's temporal variability, linear regression was applied over the mean, SD, and CV across all 12 chronologically ordered survey dates for both EC_a configurations. Additionally, the mean, SD, and CV for the HCP and PRP EC_a data for each season (i.e., summer, fall, winter, and spring) determined by averaging the means, SDs, and CVs of the surveys that fell within each season. Afterward, a linear regression was also applied over the mean, SD, and CV of the HCP and PRP EC_a data for each season to assess the AF site's seasonal temporal variability across the seasons. It was decided that the order of the weather seasons would begin with summer and end with spring because the first survey took place at the end of summer.

51

Furthermore, the mean, SD, and CV of the HCP and PRP EC_a per tree growing (GS)/non-growing season (NGS) were determined by averaging the mean, SD, and CV for each survey that fell within the GS or NGS groups. The surveys that took place during the GS and NGS were determined using soil sensor and air temperature data recorded at or near the AF site along with guidelines provided by the NRCS's National Water and Climate Center [54]. Table 1 summarizes each survey's seasonal grouping (i.e., weather season and GS/NGS) and all linear regression were applied in R studio.

A one-factor analysis of variance (ANOVA) was conducted in R Studio (version 4.05, R Core Team, Boston, MA) to evaluate the effect of season and GS/NGS on HCP and PRP EC_a. When main effect differences were found, means were separated by least significant difference (LSD) at the alpha level of 0.05. Furthermore, precision soil management zones within the AF site were generated using the k-means clustering algorithm [55] by overlaying and grouping HCP and PRP EC_a surveys. The optimal number of clusters used in the k-means clustering was determined using the factoextra package [56] in R Studio.

Correlation analyses were conducted with proximally sensed and sensor-based measurements to identify potential linkages between variables. Specifically, correlations among PRP and HCP EC_a (independently and combined) and in-situ, soil-sensor-collected VWC and EC_a and benchtop-measured soil sample GWC, EC, and pH (at all depths) were analyzed using Pearson correlations at an alpha level of 0.05. Additionally, Levene's test for homogeneity of variance was conducted to assess if fewer, strategically selected EC_a surveys could have been conducted to capture the same amount of overall EC_a variance at the AF site as the 12 monthly EC_a surveys for both the HCP and PRP EC_a. The non-universally-kriged HCP and PRP EC_a

survey data sets were used in the Levene's test. Table 1 also summarizes the survey groupings used in the Levene's test.

Results and Discussion

Weather, Soil Sensor, and Soil Sample Data

Air temperature and precipitation measured at the AF site throughout the measurement period were below historical climate means. Between 1 August 2020 and 31 July 2021, the overall average daily air temperature at the AF site was 14.0°C, which was slightly numerically lower to the 30-yr mean (i.e., 1981 to 2010) of 14.6°C [25]. Conversely, the range in the recorded air temperature at the AF site differed greatly from the annual average (Figure 4) [25]. The recorded minimum and maximum daily mean air temperatures at the AF site were -18.7 (15 February 2021) and 28.3°C (28 June 2021), respectively, which were 27.4°C lower and 7.7°C greater, respectively, than the 30-yr mean annual minimum and maximum air temperatures (Figure 4) [25]. Furthermore, the AF site received a total of 818 mm of precipitation during the sampling period of the study, where the largest precipitation event occurred over a course of four days at the end of September 2020, totaling 141 mm (Figure 4). Similar to the range in recorded air temperatures, the total precipitation at the AF site differed from the mean annual precipitation of 1156 mm [25].

The daily mean soil temperatures generally followed the overall trend of the recorded daily mean air temperature. The daily mean soil temperature at the AF site averaged 15.5 and 14.9°C for the 15- and 75-cm depths and ranged between 1.6 (Logger 6b, 15-cm depth, 15 February 2021) and 26.5°C (Logger 2, 15-cm depth, 16 August 2020; Figures 1 and 5), respectively. The plunge in daily mean soil and air temperatures, which occurred in the middle of

February 2021, was due to a winter storm that occurred between 13 and 17 February 2021 (Figure 5). Furthermore, the daily mean soil VWC averaged 31.1 and 31.3 % (v v^{-1}) for the 15- and 75-cm depths and ranged between 9.9 (Logger 2, 75-cm depth, 11 September 2021) and 57.7 % (v v^{-1}) (Logger 6b, 15-cm depth, 14 July 2021; Figures 1 and 5), respectively. Fluctuations in the recorded soil VWC following precipitation events were observed, where the area with the greatest response, and generally greatest overall soil moisture, was at Logger 6b at the 15-cm depth (Figures 1 and 5). Logger 6b is positioned in the depressional area within the local drainage way, where water pools not only during precipitation events, but throughout the year (Figure 1) [24,30,36]. After the precipitation event at the end of September 2020, soils remained consistently wetter throughout the end of fall, winter, and spring compared to the summer months, especially at Logger 6b (Figures 1 and 5). The daily mean soil EC$_a$ averaged 18.0 and 18.5 mS m^{-1} for the 15- and 50-cm depths and ranged between 5.7 (Logger 2, 50-cm depth, 12-14 September 2021) and 43.7 mS m^{-1} (Logger 6b, 15-cm depth, 27 May 2021; Figures 1 and 5), respectively.

Unlike the soil sensors at the AF site, soil samples were only collected for each survey conducted. Soil GWC averaged of 26.9 and 21.8 % (m m^{-1}) for the 0-15- and 45-55-cm depth intervals and ranged between 7.9 (Logger 2, 45-55 cm depth, 18 September 2020) and 38.4 % (m m^{-1}) (Logger 6b, 0-15 cm depth, 11 June 2021; Figures 1 and 6), respectively. The measured EC of the soil samples averaged 17.8 and 8.8 mS m^{-1} for the 0-15- and 45-55-cm depth intervals and ranged between 6.3 (Logger 9, 45-55 cm depth, 18 September 2020) and 27.9 mS m^{-1} (Logger 6b, 0-15 cm depth, 14 July 2021; Figures 1 and 6), respectively. The pH of the soil samples averaged of 6.2 and 5.8 for the 0-15- and 45-55-cm depth intervals and ranged between 4.6

(Logger 2, 45-55 cm depth, 19 August 2020) and 6.7 (Logger 6b, 0-15 cm depth, 13 May 2021; Figures 1 and 6), respectively.

EMI-EC$_a$ Survey Data

Semi-variogram Information

After data processing, the EC$_a$ surveys ranged between 5,271 and 6,854 and averaged 6,108 measurement points (Table 2 and 3). The number of points used in the universal kriging and model validation averaged 4,887 and 1,222, respectively (Table 2 and 3). Additionally, the universally-kriged PRP and HCP EC$_a$ data sets totaled 1836, 5-m pixel measurements across the AF site. The experimental semi-variograms for the PRP EC$_a$ surveys primarily consisted of exponential models, but two surveys had Matern as the best-fit model (Table 2). Alternatively, the experimental semi-variograms for the HCP EC$_a$ surveys primarily consisted of Matern models, but also had spherical, circular, and exponential as best-fit models (Table 3).

For the PRP EC$_a$, the nugget ranged between 0.00 (February, May, and June 2021 surveys) and 0.61 (August 2020 survey), the sill ranged between the 3.5 (September 2020 survey) and 13.1 (June 2021 survey), and the range ranged between 24.0 (March and May 2021 surveys) and 41.4 m (November 2021 survey; Table 2). For the HCP EC$_a$, the nugget ranged between 0.00 (December 2020 and January, February, March, April, and May 2021 surveys) and 0.32 (October 2020 survey), the sill ranged between 11.8 (July 2021 survey) and 19.1 (June 2021 survey), and the range ranged between 42.1 (March 2021 survey) and 97.9 m (August 2020 survey; Table 3).

Each parameter of the experimental semi-variogram provides different information. The sill represents the value where the semi-variance of the modeled variable plateaus, and the

55

range corresponds to the distance where the sill first occurs and the distance where measurements are no longer spatially correlated [57–59]. The nugget represents small-scale, uncorrelated spatial variations within the 5-m pixels at the AF site, including measurement error [57,59]. Practically, the range indicates how within-site differences are spatially dependent, where a larger range represents greater spatial correlation, and a small range represents smaller spatial correlation [57–59]. Additionally, when data sets are kriged, the range of the semi-variogram model governs the average radius/correlation length of the nodes created and the sill governs the magnitude of the nodes [58].

The sill, range, and nugget can also be used as an indicator of the spatial structure and variability of the modeled variable [59,60]. The strength of the spatial structure (i.e., spatial pattern) can be described by the nugget to sill ratio (nugget/sill), which is the ratio of unexplained variability to the total variability [59,60]. Specifically, the nugget/sill ratio relates to the proportion of small-scale variability that cannot be characterized by the geostatistical model within the measured field [59,60]. If no small-scale variability/measurement error is present, then the nugget is 0 [61]. Originally proposed by Kravchenko (2003) [60] and similarly used by Zhu et al. [59], a nugget/sill ratio of 0.6, 0.3, and 0.1 correlates to a weak, medium, and strong spatial structure, respectively. All EC_a survey data sets (i.e., HCP and PRP), excluding the PRP EC_a August 2020 (0.13), had nugget/sill ratios of < 0.1, indicating that all EC_a survey data sets in this study had strong, or just under strong, spatial structure [60].

In addition to the nugget/sill ratio, the range can also be used to help understand the modeled variable. Specifically, increased correlation lengths/ranges are indicative that the variable of interest (e.g., EC_a in this study) varies steadily over smaller spatial distances and that the parameter's variability becomes greater at larger spatial distances, while decreased

56

correlation lengths/ranges are indicative that the variable of interest varies erratically over small distances [59,61]. The ranges of the PRP EC_a surveys were 31 to 68% less than from the corresponding HCP EC_a surveys (Tables 2 and 3), which is indicative of the PRP EC_a being more spatially erratic and variable than the HCP EC_a [61]. DeCaires et al. [62] conducted repeated DUALEM-1S surveys on a 5.81-ha cacao (*Theobroma cacao* L.) plantation, classified as an alluvially formed silty-clay Inceptisol in Trinidad, and also reported that the PRP EC_a generally had a larger nugget, smaller sill, and a shorter range than the HCP EC_a. It is important to mention that no other study has conducted similar repeated, evenly spaced EMI-EC_a surveys at a site of similar size, topography, and land management (i.e., AF) within a similar environment as the Ozark Highlands. Additionally, making exact comparisons to other similarly collected and produced EMI-EC_a data was not feasible, as no other study conducted similar data processing procedures and analyses as those conducted for this study. However, several studies exist that possess similar aspects to the current study, thus these studies have been used for indirect comparisons.

The PRP EC_a being more spatially variable than the HCP EC_a is likely a result of the HCP measuring deeper into the soil profile than the PRP. Specifically, the PRP incorporates less of the soil profile into its measurement, and the part that is incorporated into the EC_a measurement (i.e., 0-0.5 m) is generally much more variable in pedogenesis factors and soil properties (i.e., SWC, OM, nutrients, structure/porosity, and coarse fragments), hence EC_a is more variable as well. The variations in pedogenesis and soil properties are the result of the upper portion of the soil being more exposed to surface factors that are also spatially and temporally variable, such as weather (i.e., precipitation, air temperature, wind, and sunlight),

environmental processes (i.e., runoff, surface erosion/accumulation, and evapotranspiration), and land management (i.e., fertilizer/manure and type and quantity of trees/grasses/animals).

Monthly Kriged EMI-EC$_a$ Survey Data

Each monthly survey had a similar spatial pattern for both PRP and HCP EC$_a$. For the PRP configuration, the September 2020 and June 2021 surveys had the lowest (0.2 mS m^{-1}) and largest (29.1 mS m^{-1}), respectively, recorded EC$_a$ values at the AF site during the sampling period (Table 2; Figure 7). The June 2021 survey had the greatest mean (8.7 mS m^{-1}), SD (3.6 mS m^{-1}), and range (26.4 mS m^{-1}) and the September 2020 survey had the largest CV (48.1 %) for the PRP EC$_a$ (Table 2; Figure 7). Furthermore, the September 2020 survey had the smallest mean (3.4 mS m^{-1}), SD (1.7 mS m^{-1}), and range (14.2 mS m^{-1}) and the November 2020 survey had the smallest CV (32.2 %) for the PRP EC$_a$ (Table 2; Figure 7).

For the HCP configuration, the September 2020 and March 2021 surveys had the numerically smallest (0.4 mS m^{-1}) and largest (34.2 mS m^{-1}), respectively, recorded EC$_a$ values at AF site during the sampling period (Table 3; Figure 8). The December 2020 survey had the greatest mean (12.3 mS m^{-1}), the June 2021 survey had the greatest SD (5.1 mS m^{-1}), the September 2020 survey had the largest CV (61.1 %), and the March and May 2021 surveys had the greatest range (29.4 mS m^{-1}) for the HCP EC$_a$ (Table 3; Figure 8). Furthermore, the September 2020 survey had the smallest mean (6.7 mS m^{-1}), the July 2021 survey had the smallest SD (3.9 mS m^{-1}), the March 2021 survey had the smallest CV (35.5 %), and the July 2021 survey had the smallest range (18.9 mS m^{-1}) for the HCP EC$_a$ (Table 3; Figure 8).

Overall, the HCP EC$_a$ was numerically greater and more numerically variable than the PRP EC$_a$ (Table 2 and 3). The mean HCP EC$_a$ was numerically greater than the mean PRP EC$_a$

for every survey date (Table 2 and 3). Additionally, besides the CV for the October 2020 and

January, March, and April 2021 surveys, the SD, CV, and range were numerically greater from

the HCP than the PRP EC_a (Table 2 and 3). Although the HCP EC_a was generally more variable

per survey than the PRP EC_a (i.e., SD and CV), the range in the SD for the PRP EC_a surveys (1.9

mS m^{-1}) was numerically greater than that from the HCP EC_a surveys (1.2 mS m^{-1}; Table 2 and

3).

Because the PRP and HCP measure the bulk EC_a of the 0-0.5- and 0-1.6-m soil

depths, respectively, the measured PRP EC_a was more likely a reflection of soil surface

management and the HCP EC_a was more likely a reflection of pedogenic factors (i.e., time,

parent material, organisms, topography/relief, and climate). Additionally, because different soils

have varying properties, it can be expected that different mapped soils would result in varying

EC_a measurements across the AF site. However, based on the generated PRP and HCP EC_a maps

(Figures 7 and 8) and soil boundary data (Figure 1), soil boundaries were not detailed enough to

show visual correlations with the measured EC_a values for either EC_a configuration. Although

the soil boundary data were not detailed enough for visual correlations with the EC_a data, the

western portion of the AF site was still generally characterized by a shallower depth to bedrock

and an increase in chert coarse fragment abundance (Figure 1). Coarse fragments have been

shown to be negatively corelated with EC_a [63]. Thus, the increased chert coarse fragments could

have resulted in the decreased PRP and HCP EC_a values in the western portion of the AF site

(Figures 7 and 8).

An additional potential residual effect is that PL was applied between 2001 to 2007

and can be observed through increased EC_a values occurring in the eastern half of the AF site in

both EC_a configurations (Figures 7 and 8). Specifically, PL and NH_4NO_3 were annually applied

based on the annual soil total-N concentrations to the eastern and western halves of the AF site

between 2001 and 2007, respectively [26]. After the PL and NH_4NO_3 applications, Sauer et al.

[26] reported numerically larger percent changes in nutrient concentrations in 9 of the 11 soil

nutrients measured [i.e., N, P, K, magnesium (Mg), sulfur (S), sodium (Na), iron (Fe), zinc (Zn),

and copper (Cu)] in the soils that received PL, than the soils that received NH_4NO_3. Thus,

increased nutrients concentrations likely remain in the soils that received PL and may be

contributing to increased PRP and HCP EC_a measurements (Figures 7 and 8).

In addition to the PRP EC_a most likely reflecting surface management actvities, the

PRP EC_a likely varied overtime more than the HCP EC_a due to variations in soil properties from

fluctuating weather (i.e., soil moisture). Specifically, the SD for the HCP EC_a was generally

more consistent than SD for the PRP EC_a (Table 2 and 3). Additionally, the SD for the PRP EC_a

was generally smaller in the summer months than in the fall, winter, and spring (Table 2 and 3),

which was most likely a reflection of increased soil moisture [59,64]. During wetter periods (i.e.,

fall, winter, and spring), the spatial distribution of soil moisture is heavily influenced by

topography, where topography strongly controls the lateral distribution of water, which increases

soil moisture variability, and thus the variability of measured EC_a [59,64].

Although no surveys for either the HCP or PRP EC_a were exactly alike, each survey

per configuration had a similar geospatial pattern to the other (Figure 7 and 8). For both the HCP

or PRP EC_a, an elevated trail in EC_a values can been seen starting in the northwest corner,

peaking in the center (Rows 5 to 7), and trailing off to bottom middle of the AF site (Figure 7

and 8). This apparent pattern can be attributed to landscape properties that affect water flow and

runoff accumulation and factors that affect measured EC_a. Specifically, the trail of elevated EC_a

values occurs in the local drainage way of the AF site, where the northwest corner has the AF

site's greatest elevation and the local landscape depression is in the center of Rows 5 to 7 (Figures 1, 7, and 8) [30,36]. Additionally, runon from the surrounding, up-slope landscapes enters through a culvert in the northwest corner of the AF site (Figure 1). Prior to the site's conversion to an AF system, this drainage way characterized by the formation of major gullies (Figure 9) [30,36,65]. However, the gullies were subsequently filled in once the site began to be converted into an AF system. Additionally, although the gullies have been filled in, this area of the site continues to be the surface drainage way of the AF site and shows evidence of water movement, water accumulation, and landscape drainage (Figure 9) [30,36,65].

As water moves across the land surface, sediment, nutrients, and OM accumulate from up-slope and are deposited in areas of flow accumulation at a lower elevation. Overtime, the overland flow accumulation results in an accumulation of water and transported nutrients, OM, and sediment in channels or low-lying areas, which also have the potential to increase plant productivity in those areas. Furthermore, some of the major influencing factors of soil EC_a are soil salinity, SWC, and OM [8]. Additionally, saturated soil or ponded water on the soil surface was visually observed at Logger 6b during most of the surveys conducted, and the upper soil-senor VWC measurements and upper and lower soil-sample GWC measurements at Logger 6b had some of the largest VWC throughout the sampling period (Figure 5). Thus, the elevated PRP and HCP EC_a values in the northwest corner of the AF site towards the center of Rows 5 to 7 were most likely the result of greater SWC and accumulated transported materials from the local landscape, but also from the up-slope runoff into the northwest corner from the surrounding landscape (Figures 7 and 8).

Although more visible in the HCP EC_a surveys, two trails of elevated EC_a values starting at the middle-eastern edge that connect to the elevated EC_a of the local depressional area

and drainage way of the AF site can be observed in both configurations (Figures 7 and 8) [24,36]. Unlike at the local depressional area (Logger 6b; Figure 9), no visual signs of soil wetness were observed in these areas during the duration of the study. However, the lower soil sensor at Logger 9, which was located at the more southern of the two trails of elevated EC_a values, recorded similar VWC measurements as the upper soil sensor measurement at Logger 6b throughout the winter during this study (Figure 5). Additionally, Smith et al. [66] conducted ground penetrating radar surveys at the AF site and produced measurements that potentially show groundwater movement in the same areas with elevated EC_a values. Thus, the trails of elevated EC_a values starting at the middle-eastern edge of the AF site are most likely due to increased SWC from a shallow groundwater table (Figure 8).

Overall Kriged EMI-EC_a Survey Data

The spatial patterns of the overall mean, SD, and CV differed greatly between PRP and HCP EC_a. Averaged across all 12 surveys, mean PRP and HCP EC_a ranged between 1.8 and 18.0 mS m^{-1} and 3.1 and 25.8 mS m^{-1}, respectively (Figure 10), and shared a similar spatial pattern as the monthly survey (Figures 7 and 8). The SD for PRP and HCP EC_a ranged between 0.6 and 4.8 mS m^{-1} and 1.3 and 4.9 mS m^{-1} within the AF site across all surveys, respectively (Figure 10). Additionally, the CV for the PRP and HCP EC_a ranged between 15.1 and 62.9 % and 7.3 and 54.6 % within the AF site across all surveys, respectively (Figure 10).

Most of the AF site is classified as a Captina silt loam (Figure 1), which is characterized by a large increase in clay content with depth [23]. Additionally, a fine-textured soil generally has a greater water-holding capacity than a coarse-textured soil and SWC

generally increases with depth. Thus, the mean HCP EC_a being numerically greater than the mean PRP EC_a was most likely due to the SWC and clay content increasing with depth [8,59]. Additionally, measured soil EC_a is influenced both by stable and dynamic soil properties. Numerous soil properties (i.e., soil texture, clay content, OM content, and depth to bedrock) are temporally stable within short time spans (i.e., within a year). Thus, within humid regions, temporal fluctuations in the measured soil EC_a are generally reflective of variations in SWC and water movement [59].

For both the PRP and HCP EC_a, the SD was generally elevated in the NW corner and across the middle-eastern edges of the AF (Figure 10), where both were most likely a result of fluctuating SWC. The NW corner is where runon from the surrounding, up-slope landscape enters into the AF site. Therefore, runoff-producing precipitation events would cause the NW corner to have varying SWC, hence varying EC_a, throughout the year. Additionally, the elevated EC_a across the middle-eastern edges of the AF site are likely where subsurface water movement occurs [66], and thus fluctuation in the SWC in these areas would cause fluctuation in the measured EC_a throughout the year (Figure 10). However, one major difference in the SD between the PRP and the HCP was PRP had elevated SD values along the drainage way at the site and the HCP did not (Figures 9 and 10) [24,30]. Elevated SD for the PRP, and not the HCP, was also likely from fluctuating SWCs throughout the year (Figure 10). Specifically, the PRP measures the upper 0.5 m of the soil, which is going to be more affected throughout the year by changes in weather and surface conditions (i.e., precipitation, air temperature, wind, sunlight, and evapotranspiration) than the 0-1.6 m of the soil profile which the HCP measures. As a result, the SD of the HCP EC_a likely did not vary to the same extent as the PRP EC_a because SWC

varied less throughout the year due to the HCP EC_a representing the portion of the soil that is less affected by surface factors (Figure 10).

The CV of the PRP and HCP EC_a generally had a similar spatial pattern, where there were increased CVs in the west/southwest portion and small CVs occurring in the eastern portion, which slightly increase moving towards the northeast of the AF site (Figure 10). However, the CV of the PRP EC_a had a less cohesive pattern and was visually more variable across the AF site than that of the HCP EC_a CV (Figure 10). The CV of the PRP EC_a was visually more variable than the CV of the HCP EC_a, which was potentially due to two reasons (Figure 10). First, the PRP EC_a is a reflection of a smaller, upper portion of the soil profile (i.e., 0-0.5 m). Secondly, the 0-0.5-m portion of soil is generally more spatially and temporally variable in soil properties (i.e., SWC, OM, nutrients, structure/porosity, and coarse fragments) than the 0-1.6-m depth from the 0-0.5-m portion of the soil being exposed to surface factors that are also spatially and temporally variable (i.e., weather, environmental processes, and land management; Figure 10). Furthermore, the smallest CVs in the HCP EC_a were generally located in wetter areas at the AF site [30] likely due to the SWC deeper in the soil profile at these locations being consistently moist to saturated throughout the year (Figure 10). Additionally, unlike the SD, there were no elevated CVs in the NW corner or along the middle-eastern edges of the AF site for both EC_a configurations (Figure 10). Thus, the EC_a variability (i.e., SD) in the NW corner and along the middle-eastern was minimal when standardized with the mean for both EC_a configurations (Figure 10).

Elevated HCP EC_a SDs and CVs occurred under the pine tree canopies (Figure 10). Authors offer several likely explanations, including a decreased water-holding capacity from a decreased effective soil depth and increased coarse fragment concentration in the Nixa cherty silt

portion of the site (Figure 1) [31]. Additionally, it is possible that the coniferous trees may be acidifying soils relative to deciduous species at the site, thus resulting in greater EC_a, as Burgess-Conforti et al. [67] reported that coniferous was more acidic than deciduous leaf litter in northwest Arkansas.

EC_a Temporal Trends

The linear relationship between the PRP and HCP EC_a survey data and chronological season sequence was assessed. Of the 12 data sets the linear regression was applied to (i.e., HCP and PRP mean EC_a, SD, and CV across time and by weather season), only two significant ($P <$ 0.05) relationships resulted (Figure 11): PRP EC_a SD increasing over time (i.e., August 2020 to July 2021) and HCP EC_a CV decreasing across weather seasons (i.e., summer to spring; Figure 11). The mean EC_a for the PRP and HCP did not differ across time (i.e., survey dates) nor across weather seasons, the HCP EC_a SD did not differ over time or across weather seasons, the PRP EC_a SD did not differ across weather seasons, and the HCP EC_a CV did not differ over time during the sampling period ($P > 0.05$; Figure 11). Thus, the hypothesis that there would be a change in the mean EC_a and EC_a variability (i.e., SD and CV) across time and across the weather seasons was supported for some, but not all EC_a summary statistics across time (i.e., survey dates and weather season) combinations.

The significant relationship for the PRP EC_a SD across time was most likely due to a combination of reasons. First, the PRP measures the bulk EC_a of the 0-0.5 m depth, which is the soil depth interval where soil priorities (i.e., soil moisture) fluctuate across time more so than in the deeper depth measured by the HCP. Secondly, after November 2020, precipitation continued to increase at the AF site until the middle of July 2021 (Figure 4) and, during wetter periods, the

spatial variability of soil moisture also increases [59,64]. Specifically, topography heavily controls the lateral distribution of water (i.e., precipitation and overland flow), and thus the spatial distribution of soil moisture, during wetter periods, resulting in increased soil moisture content (SMC) and EC_a spatial variability [59,64]. Therefore, the local topography and increased precipitation at the AF site most likely caused the spatial variability of soil moisture, and thus measured EC_a variability (i.e., SD), to increase over time within the study period [59,64].

Unlike the PRP EC_a SD over time, the HCP EC_a CV across weather seasons decreased from summer to spring (Figure 11). The explanation for why HCP EC_a CV across the weather seasons decreased is not clear, as the PRP EC_a CV across weather seasons and the PRP and HCP EC_a over time did not widely vary (Figure 11). Additionally, there could have been a different trend over time, or no trend at all, in the EC_a data across time/season if the surveys had been conducted in a different month and/or seasonal order (i.e., spring to winter). However, perhaps the increase in precipitation between February to May 2021 (Figure 4) led to an increase in SWC and salinity homogeneity in the upper 1.6 m of the soil profile, and thus reduced variability in the measured HCP EC_a, across the AF site, resulting in the HCP EC_a CV decreasing from summer to spring (Figure 11).

Seasonal Effects on EC_a

The PRP and HCP mean EC_a, SD, and CV were unaffected ($P > 0.05$) by either weather season or tree growing season. Thus, there was no difference between the mean or variation (SD and CV) among surveys that were conducted in different weather seasons or surveys that were recorded in the tree growing season versus the tree non-growing season. Furthermore, the hypothesis that there would be significant difference between the EC_a mean,

SD, and CV of surveys that were conducted in different weather seasons and in the tree

growing/non-growing season at a 20-year AF system within the Ozark Highlands was rejected.

These results highlight that the measured EC_a at the AF site was more reflective of and

influenced by temporally stable soil (i.e., soil texture, clay content, OM content, and depth to

bedrock), vegetative (i.e., coniferous versus deciduous trees), and terrain properties than

temporally variable soil properties (i.e., SWC) within short time spans (i.e., < 1 year). Similar

results have been reported by Harvey & Morgan (2009) who conducted EMI-EC_a surveys in

Spring 2005, Fall 2005, and Spring 2006 across four different fields in north-central Texas that

primarily consisted of the Miles (Typic Paleustalfs) and Abilene (Pachic Argiustolls) soil series

and had been intensively cultivated with cotton (*Gossypium hirsutum* L.) and wheat (*Triticum

aestivum* L.) [68]. Although the effect of season on the mean EC_a or SD was not formally

evaluated, Harvey & Morgan (2009) reported relatively similar mean EC_a and SD values for the

surveys conducted during different seasons within the same field [68]. Additionally, Harvey &

Morgan (2009) also reported visual similarities among the kriged maps for the three surveys

[68].

Soil Management Zones

   Three precision soil management zones (SMZ) were delineated based on k-means

clustering at the AF site using the PRP and HCP EC_a data (Figure 12). Three SMZs were

determined to be the optimal number of zones to delineate using the factoextra package in R

Studio [56]. The location and geospatial pattern of the SMZs were similar between the PRP and

HCP (Figure 12) and both were visually similar to their respective overall means map (Figure

10). Thus, the hypothesis that the monthly EMI-EC_a surveys at a 20-year-old AF system within

the Ozark Highlands could be grouped into similar functional populations and delineated into zones for precision soil management was confirmed.

For both the PRP and HCP EC_a, SMZ 1, 3, and 2 (Figure 12) occurred where the recorded EC_a was numerically smallest, in between, and the largest throughout the sampling period, respectively (Figure 10). With the exception of the CV, all summary statistics (i.e., mean, minimum, maximum, SD, and SE) for the HCP were numerically greater than for the PRP (Figure 12; Table 4). For both the PRP and HCP, SMZ 2 was more variable (i.e., greater range, SD, and SE) than the other two SMZs (Figure 12; Table 4). However, when the SMZs' variability was standardized by the mean (i.e., CV), SMZ 1 had the numerically greatest variability relative to the mean compared to the other SMZs (Figure 12; Table 4). However, SMZ 1's numerically largest variability relative to the mean was more likely a result of just the PRP and HCP mean EC_a being 42 to 60% and 46 to 66%, respectively, than the other two SMZs, rather than a soil property or terrain attribute causing variability in the measured EC_a within SMZ 1 (Figure 12; Table 4). Additionally, SMZ 3 was generally the second numerical greatest occurring and second most variable (i.e., range, SD, CV, and SE; Figure 12; Table 4) among the three SMZs.

Except for the CV, SMZ 2 had the numerically greatest mean and variability in the PRP and HCP EC_a was most likely due to SMZ 2 encompassing the local drainage way [30,36] and areas of potential subsurface water movement (Figure 12). Soil constituents, such as water, OM, nutrients/salinity, and clay particles, can increase soil EC_a [1] and may have accumulated over time in the drainage way at the AF site, likely resulting in SMZ 2 having the greatest mean EC_a among the three SMZs (Figure 12). Additionally, because SMZ 2 includes the local drainage way and zones of potential subsurface water flow, SMZ 2 experiences the greatest fluctuations in

SWC throughout the year, likely contributing to SMZ 2 having the greatest variability in measured EC_a of the three SMZs, in three out of four variability statistics (i.e., range, SD, and SE; Figure 12).

Furthermore, SMZ 1 had the numerically smallest mean and variability in three out of four variability statistics (i.e., range, SD, and SE) in the PRP and HCP EC_a and was most likely due SMZ 1 encompassing the area of shallower depth to bedrock and increased coarse fragment abundance and SMZ 1 not being a zone of accumulation (Figure 12) [30,35]. Although no soil sensor or sample data were collected from this area, SMZ 1 likely had the smallest VWC among the three SMZs for several reasons. First, SMZ 1 is not an area of water accumulation during precipitation events, thus soil constituents (i.e., sediment, OM, and nutrients) have been eroded from the area and less water is able to infiltrate into the soil, resulting in decreased SWC and SWC variability than in SMZ 2. Secondly, increased coarse fragments increases soil BD, which, in turn, decreases porosity, soil water-holding capacity, and VWC [69], and thus EC_a. Additionally, Zhu et al. [59] and Brevik et al. [70] reported larger soil EC_a responses to SWC fluctuations at wetter positions in the landscape than in drier locations, suggesting that soil EC_a is less dependent on SWC in drier locations than in wetter locations. Zhu et al. [59] also reported that at drier landscape positions or during drier time periods, the influence of water flow paths and SWC were masked by other soil and terrain attributes. Thus, the EC_a values that resulted in the delineation of SMZ 1 and 2 could have been primarily influenced by SWC in SMZ 2, primarily influenced by soil and terrain properties in SMZ 1 (Figure 12).

The EC_a-derived SMZs were produced in order to delineate soils with similar properties for precision/site-specific soil management. Adhikari et al. [30] created four topographical functional units (TFUs) at the AF site from a principal component analysis and k-

69

means clustering of 14 terrain attributes (i.e., flow accumulation, slope length factor, mid-slope position, multi-resolution ridge top flatness index, multi-resolution valley bottom flatness index, normalized height, slope percent, slope height, system for automated geoscientific analysis wetness index, valley depth, altitude above channel network). However, the four terrain attribute-derived TFUs of Adhikari et al. [30] did not show any major visual similarities with the three EC_a-derived SMZs created in this study (Figure 12). Additionally, for actual management of this 4.25-ha AF site, the grid size would likely need to be increased from the current 5-m grid to perhaps a 10-x 10-m grid in order improve manageability of the AF site and its SMZs.

Either the PRP or HCP EC_a may be more beneficial for creating SMZs depending on the land use/management system. For example, the PRP EC_a configuration would be the most beneficial to use when creating SMZs for precision soil management because topsoil is the layer that agricultural production is most concerned with. Furthermore, EC_a measurements and/or EC_a-derived SMZs can be used as a blueprint for where to collect future soil samples, referred to as EC_a-directed soil sampling [1,4,9]. Because the EC_a-derived SMZs delineate areas of potential differing soil properties, EC_a-directed soil sampling can reduce the degree of soil surface disturbance and the quantity of necessary soil samples, and thus time, energy, and cost spent on soil sampling compared to traditional grid soil sampling schemes [3–5,8]. Additionally, collecting soil samples and soil property data from each SMZ potentially allows for the characterization of the most spatially and temporally influential soil properties effecting the measured EC_a within each SMZ.

Apparent EC measurements and EC_a-derived SMZs can also be used to explain crop yield variability. Specifically, when the EC_a is correlated with crop yield, the EC_a-directed soil sampling method can be used to help characterize the soil properties that are causing crop yield

variations [3,71], and potentially variations in forage and/or tree growth. Through establishing SMZs and identifying soil properties most effecting their crop yield, producers have the potential to spatially and temporally target fertilizer, pesticide, and irrigation. As a result, SMZ-targeted resource applications have the potential to increase resource-use efficiency, yield, and profits, while reducing excess resource applications, loss of applied nutrients and pesticides, unintended environmental damage (i.e., surface and groundwater degradation), labor, and costs for the producer [72]. Additionally, establishing EC_a-derived SMZs with soil property data before the establishment of an agricultural system can allow the producer to not only decide what type of crops to use and where to plant them, but also what type of agricultural system to establish (i.e., conservation agricultural, agroforestry, or pastoral) in order to have the most productive agricultural system based on the present soil and land properties.

Correlations Among EC_a and Soil Properties

There were positive correlations between the EMI-EC_a data [i.e., PRP, HCP, and combined (PRP and HCP)] and at least two measured soil properties ($P < 0.05$; Table 5; Figure 13). The HCP EC_a and soil-sample GWC from the 45-55 cm depth interval ($r = 0.71$) and the PRP EC_a and the soil-sample GWC in the 0-15 cm depth interval ($r = 0.70$) were significantly, positively correlated (Table 5; Figure 13). The PRP EC_a and the soil-sensor-measured EC_a from the 15-cm soil depth ($r = 0.84$), the HCP EC_a and the soil-sensor-measured EC_a from the 50-cm soil depth ($r = 0.74$), and the combined EC_a and the soil-sensor-measured EC_a combined across soil depths ($r = 0.65$) were also positively correlated (Table 5; Figure 13).

The PRP EC_a and the 15-cm, soil-sensor-measurement correlation was the only comparison where the soil-sensor-measured VWC was correlated to EMI-EC_a but had a low

71

correlation coefficient ($r = 0.09$; Table 5; Figure 13). Additionally, the HCP EC_a and the 45-55 cm soil-sample-measurement correlation was the only comparison where the soil-sample-measured EC and pH were significant correlated to any EMI-EC_a measurement. Specifically, HCP EC_a and the 45-55 cm EC and pH had a positive correlation ($r = 0.37$ and $r = 0.42$, respectively; Table 5; Figure 13). As a result, the hypothesis that the monthly EMI-EC_a surveys were correlated with soil-sensor- and/or soil-sample-based soil properties at a 20-year-old AF system within the Ozark Highlands was supported for some, but not all, soil parameters.

Because the sensor-measured EC_a is a point measurement within what the PRP and HCP EC_a measure (i.e., 0-0.5- and 0-1.6-m, respectively), it was expected that sensor-measured EC_a would have positive relationships with the PRP, HCP, and combined EC_a data (Table 5; Figure 13). Furthermore, the lack of a relationship between the HCP EC_a and the lower VWC measurement was potentially due to the VWC only representing the VWC at a discrete depth (i.e., 75 cm), whereas the HCP represents the EC_a of the 0-1.6-m depth range. With the exception of the sensor-measured EC_a, GWC had the strongest correlation with EMI-EC_a in the PRP, HCP, and combined EC_a data sets (Table 5; Figure 13). Thus, of the measured soil properties, GWC most likely contributed to the greatest extent of the measured EC_a variability for both the PRP and HCP configurations (Table 5; Figure 13). Additionally, PRP and HCP EC_a correlations were likely due to different soil properties (i.e., pH and EC) contributing varying degrees to the EC_a variability for the PRP and HCP configurations (Table 5; Figure 13).

The resulting EC_a and soil property correlations in this study were similar to previous results. Abdu et al. [6], Martini et al. [43], and Zhu et al. [59] conducted repeated EC_a surveys with SMC measurements at fixed locations across each of their fields. Abdu et al. [6] conducted their study in north-central Utah over a soil of the Millville soil series (Typic Haploxerolls),

Martini et al. [43] conducted their study in central Germany over soils primarily consisting of Cambisols, Luvisols, and Gleyols [73], and Zhu et al. [59] conducted their study in central Pennsylvania over soils primarily consisting of the Hagerstown (Typic Hapludalfs), Opequon (Lithic Hapludalfs), Murrill (Typic Hapludults), Nolin (Dystric Fluventic Eutrudepts), and Melvin (Fluvaquentic Endoaquepts) series. Similar to the results of this study, Abdu et al. [6], Martini et al. [43], and Zhu et al. [59] reported positive relationships between the EC_a and SMC. Using a Spearman rank correlation, DeCaires et al. [62] also conducted repeated EC_a surveys and random soil sample measurements on a 5.81-ha cacao plantation with a silty-clay Inceptisol soil in Trinidad and reported a strong positive relationship between both the PRP and HCP EC_a and soil EC. Additionally, DeCaires et al. [62] reported significant relationships between both the PRP and HCP EC_a and soil pH and a weak, but significant, positive correlation between the PRP and HCP EC_a and GWC. Furthermore, Corwin et al. [71] conducted one EC_a survey and collected multi-depth soil sample measurements at a site classified as Panoche silty clay (Thermic Xerorthents) and located within the San Joaquin Valley in central California. Corwin et al. [71] collected EC_a and soil sample measurements for mapping and correlating EC_a and soil properties to cotton yield variations and reported significant positive relationships between the 0-1.5-m EC_a and the 0-1.5-m GWC, EC, and pH.

Homogeneity of Variance Assessment

Homogeneity of variance was used to assess whether fewer, strategically selected EC_a surveys could be conducted to capture the same amount of overall EC_a variance at the AF site as the 12 monthly EC_a surveys captured. The five reduced survey groupings that were used for the homogeneity of variance assessment are summarized in Table 1. For the PRP EC_a, there were

differences between the variance of all 12 surveys and the variance of all five of the reduced number of survey groupings [i.e., odd half of surveys in sequential order of conduction (H1), even half of surveys in sequential order of conduction (H2), middle of the season (MS), middle of Fall and Spring (MFS), middle of Winter and Summer (MWS); $P < 0.05$; Table 1 and 6]. Except for when compared to the H1 survey group, the variance of all 12 PRP EC_a surveys was greater than the variance of the other four reduced number of survey groupings for the PRP EC_a (i.e., H2, MS, MFS, and MWS; Table 6). Consequently, for the PRP configuration, with the exception of the H1 survey grouping, conducting an EC_a survey every month for one year captured more numerical EC_a variability than conducting six, four, or two evenly temporally spaced EC_a surveys within a year (Table 6). It is not clear why the H1 grouping for the PRP EC_a had greater EC_a variance than all 12 surveys combined; however, perhaps the greater EC_a variance in the H1 grouping was potentially due the H1 grouping dataset having fewer observations than the 12-survey dataset (Table 6).

In contrast to the PRP, for the HCP configuration, there were differences between the variance of all 12 monthly surveys and the variance of MS and MFS reduced groupings (Table 6). Specifically, the variance of all 12 monthly HCP EC_a surveys was greater than the variance of both the MS and MFS groupings (Table 6). Consequently, only conducting four HCP EC_a surveys in the middle of the weather seasons (i.e., summer, fall, winter, and spring) or two HCP EC_a surveys in the middle of fall and spring at this AF site would potentially result in not capturing all of the EC_a variability within one year. Conversely, there was no difference between the variance of all 12 monthly HCP EC_a surveys and the reduced H1, H2, and MWS survey groupings (Table 6). Therefore, one could potentially conduct only six evenly temporally spaced HCP EC_a surveys within a one-year period and/or one HCP EC_a survey in the middle of winter

and summer and obtain the same numerical EC_a variability as 12 monthly EC_a surveys across

one year (Table 6). As a result, the hypothesis that fewer EC_a surveys could have been conducted

in one year to capture the same amount of overall EC_a variance as the 12, mid-monthly EMI-EC_a

surveys was supported for the HCP EC_a, but not for the PRP EC_a. Being able to capture the same

amount of EC_a variability with fewer surveys would be greatly beneficial for researchers,

agricultural consultants, and producers due to reduced time and energy spent collecting and

processing the data and would reduce surface traffic within the AF site, which could positively

contribute to maintaining good soil surface health.

Summary and Conclusions

Repeated EMI-based EC_a surveys have been widely used to assess the spatial and

temporal variability of a multitude of soil properties within different ecosystems and land

management systems. However, little work has been conducted on the spatiotemporal

relationship among repeated EMI-EC_a surveys and soil property variations in AF systems within

regions that have similar features to the Ozark Highlands. As a consequence, the objectives of

this study were to i) use 12 mid-monthly EMI-EC_a surveys to assess the spatiotemporal pixel

variation of the measured EC_a; ii) use k-means to identify clusters of similarly behaving

populations for precision soil management; iii) identify correlations among EMI-EC_a data and

in-situ VWC and EC_a measurements at two depths and soil-sample EC, GWC, and pH in two

depth intervals; and iv) determine whether fewer, evenly spaced, strategically selected EMI-EC_a

surveys could have been conducted in one year to capture the same amount of overall EC_a

variance as the 12 mid-monthly EMI-EC_a surveys conducted.

Results of this study demonstrated measured EC_a at the AF site was spatially variable. The experimental semi-variogram models of all mid-monthly PRP and HCP EC_a data sets had a strong, or nearly strong, spatial structure. Additionally, the experimental semi-variogram model ranges of the PRP EC_a surveys indicated that the PRP EC_a was more spatially erratic and variable than the HCP EC_a. Although no surveys for either the HCP or PRP EC_a were exactly alike, each survey per configuration had a similar geospatial pattern to the other. Additionally, potential effects of pedogenic (i.e., topography, depth to bedrock, and coarse fragments), biologic (i.e., pine trees) and surface management factors (i.e., PL applications) were observed on the measured EC_a. The overall mean HCP EC_a was numerically greater than that of the PRP EC_a and was likely due to increases in SWC and clay content with depth. The greatest measured EC_a values in both the PRP and HCP were recorded in the local drainage way or areas of potential groundwater movement at the AF site. Additionally, the temporal variability of SWC and water movement were likely the primary cause of the temporal fluctuations in the measured PRP and HCP EC_a at the AF site. The overall PRP EC_a SD and CV were more visually variable than the HCP EC_a SD and CV, likely as a result of the 0-0.5-m portion of soil generally being more spatially and temporally variable in soil properties (i.e., SWC, OM, nutrients, structure/porosity, and coarse fragments) than the 0-1.6-m depth, as the 0-0.5-m portion of the soil was more exposed to surface factors that are also spatially and temporally variable (i.e., weather, environmental processes, and land management).

Results of this study partially supported the hypothesis that there would be a significant change in the mean EC_a and EC_a variability (i.e., SD and CV) across time and the weather seasons. Through the linear regression analyses, only a positive relationship between PRP EC_a SD over time (i.e., August 2020 to July 2021) and a negative relationship between HCP EC_a CV

76

across weather seasons (i.e., summer to spring) was observed. Furthermore, results of this study did not support the hypothesis that there would be differences between the EC_a mean, SD, and CV of surveys that were conducted in different weather seasons and in the tree growing/non-growing season at a 20-year AF system within the Ozark Highlands. Through the ANOVA, there was no difference between the PRP and HCP EC_a mean or variation (i.e., SD and CV) among surveys that were conducted in different weather seasons or surveys that were recorded in the tree growing season versus the non-growing season. Thus, the measured EC_a at the AF site was more reflective of and influenced by temporally stable soil (i.e., soil texture, clay content, OM content, and depth to bedrock), vegetative, and terrain properties than temporally variable soil properties (i.e., SWC) within short time spans (i.e., < 1 year). The results of this study demonstrated that the repeated EMI-EC_a surveys can be used to assess the spatiotemporal pixel variation of the measured EC_a of a 20-year-old AF system within the Ozark Highlands. However, further research needs to be conducted to better understand and provide more information on the spatiotemporally variability of measured EC_a, not just within AF systems, but AF systems within similar environments as the Ozark Highlands.

Results of this study supported the hypothesis that monthly EMI-EC_a surveys at a 20-year-old AF system within the Ozark Highlands can be grouped into similar functional populations and be made into zones for precision soil management. The k-means clustering method delineated three SMZs that were reflective of areas of similar EC_a and EC_a variability, and thus areas of similar soil properties (i.e., increased SWC and coarse fragment and decreased depth to bedrock areas). However, future EC_a-directed soil sampling and further *in-situ* terrain and soil property investigations are required to fully understand the causes of the measured EC_a variations that defined the SMZs and to know how to properly manage each of the SMZs.

Results of this study partially supported the hypothesis that monthly EMI-EC$_a$ survey data are correlated with soil-sensor-based VWC and EC$_a$ and soil-sample-based EC, GWC, and pH. Within each of the correlation pairs assessed (i.e., PRP EC$_a$ and upper, HCP EC$_a$ and lower, and combined EC$_a$ and combined soil property measurement), the EMI-collected EC$_a$ was only correlated with two to four of the five measured soil properties (i.e., soil-sensor-measured VWC and EC$_a$ and soil-sample-derived GWC, EC, and pH). However, the EMI-collected EC$_a$ was correlated to the soil-sensor-measured EC$_a$ and soil-sample-derived GWC in all three correlation pairs assessed, where GWC likely contributed to the greatest extent of the measured EC$_a$ variability for both the PRP and HCP configurations. Furthermore, not only would further EC$_a$ surveys with increased in-field soil property measurement locations and additional soil properties measured help better understand the causes of the measured EC$_a$ variation at the AF site, but also EC$_a$-directed soil property investigations in each SMZs have the potential to identify the most influential soil property related to the measured EC$_a$, thus plant response, in each SMZ.

Results of this study also partially supported the hypothesis that fewer, strategically timed, and evenly spaced EC$_a$ surveys could be conducted to capture the same amount of overall EC$_a$ variance at the AF site as the 12 monthly EC$_a$ surveys conducted. With the exception of the H1 survey group, the variance of the 12 monthly EC$_a$ surveys conducted was greater than the variance of the other reduced number of survey groupings for the PRP EC$_a$ (i.e., H2, MS, MFS, and MWS). Although, there was no difference between the variance of all 12 monthly EC$_a$ surveys conducted and the reduced H1, H2, and MWS survey groupings for the HCP EC$_a$. Thus, it is recommended that at least 12 monthly EC$_a$ surveys are necessary to be conducted to capture the full EC$_a$ variance in the 0-0.5-m soil depth of AF site within a 1-year period. However, to capture the full EC$_a$ variance in the 0-1.6-m soil depth of AF site within a 1-year period, it is

recommended to conduct either six EC_a surveys every other month or one EC_a survey in the middle of Winter and Summer to limit soil surface disturbance and to save time resources.

Results of this study provided beneficial and valuable insight on the spatial and temporal variability of measured EMI-EC_a over time, not only in an AF system, but also an AF system that is located within a unique environment like the Ozark Highlands. Results of this study demonstrated that a variety of different methods can be used to assess spatial and temporal changes in measured EMI-EC_a, and that the effects of pedogenic and anthropogenic factors on measured EMI-EC_a can be observed in an AF system within the Ozark Highlands. Results of this study also demonstrated that measured EMI-EC_a can be correlated to multiple soil properties and used to create precision SMZs in an AF system within the Ozark Highlands. Thus, results of this study provide further evidence of the potential versatility, applicability, and ability of an EMI-EC_a survey device to quickly and accurately delineate in-field variability in a multitude of landscapes with different land uses and management systems.

References

1. Corwin, D. L.; Scudiero, E. Mapping Soil Spatial Variability with Apparent Soil Electrical Conductivity (ECa) Directed Soil Sampling. *Soil Sci. Soc. Am. J.* **2019**, *83*, 3–4.

2. Garcia-Tomillo, A.; Miras-Avalos, J.; Dafonte-Dafonte, J.; Paz-Gonzalez, A. Mapping Soil Texture Using Geostatistical Interpolation Combined with Electromagnetic Induction Measurements. *Soil Sci.* **2017**, *182*, 278–284.

3. Corwin, D. L.; Lesch, S. M. Characterizing Soil Spatial Variability with Apparent Soil Electrical Conductivity – Survey Protocols. *Comput. Electron. Agric.* **2005**, *46*, 103–133.

4. Johnson, C. K.; Doran, J. W.; Duke, H. R.; Wienhold, B. J.; Eskridge, K. M.; Shanahan, J. F. Field scale Electrical Conductivity Mapping for Delineating Soil Condition. *Soil Sci. Soc. Am. J.* **2001**, *65*, 1829–1837.

5. Johnson, C. K.; Mortensen, D. A.; Wienhold, B. J.; Shanahan, J. F.; Doran, J. W. Site-Specific Management Zones Based on Soil Electrical Conductivity in a Semiarid Cropping System. *Agron. J.* **2003**, *95*, 303–315.

6. Abdu, H.; Robinson, D. A.; Boettinger, J.; Jones, S. B. Electromagnetic Induction Mapping at Varied Soil Moisture Reveals Field-Scale Soil Textural Patterns and Gravel Lenses. *Front. Agric. Sci. Eng.* **2017**, *4*, 135–145.

7. Serrano, J.; Shahidian, S.; Silva, J. Spatial and Temporal Patterns of Apparent Electrical Conductivity: DUALEM vs. Veris Sensors for Monitoring Soil Properties. *Sensors* **2014**, *14*, 1–19.

8. Corwin, D. L.; Scudiero, E. Field-Scale Apparent Soil Electrical Conductivity. In *Methods of soil analysis*; Logsdon, S., Ed.; Soil Science Society of America: Madison, WI, US, 2017; Volume 1, pp 1–29.

9. Corwin, D. L.; Lesch, S. M. Apparent soil electrical conductivity measurements in agriculture. *Comput. Electron. Agric.* **2005**, *46*, 11–43.

10. Heil, K.; Schmidhalter, U. The Application of EM38: Determination of Soil Parameters, Selection of Soil Sampling Points and Use in Agriculture and Archaeology. *Sensors* **2017**, *17*, 1–44.

11. Agroforestry. Available online: https://www.usda.gov/topics/forestry/agroforestry (accessed 23 April 2022).

12. Dollinger, J.; Jose, S. Agroforestry for Soil Health. *Agrofor. Syst.* **2018**, *92*, 213–219.

13. Jose, S. Agroforestry for Ecosystem Services and Environmental Benefits: An Overview. *Agrofor. Syst.* **2009**, *76*, 1–10.

14. Schoeneberger, M.; Bentrup, G.; Gooijer, H.; Soolanayakanahally, R.; Sauer, T.; Brandle, J.; Zhou, X.; Current, D. Branching out: Agroforestry as a Climate Change Mitigation and Adaptation Tool for Agriculture. *J. Soil Water Conserv.* **2012**, *67*, 128–136.

15. Udawatta, R. P.; Jose, S. Agroforestry Strategies to Sequester Carbon in Temperate North America. *Agrofor. Syst.* **2012**, *86*, 225–242.

16. Lorenz, K.; Lal., R. Soil Organic Carbon Sequestration in Agroforestry Systems. A Review. *Agron. Sustain. Dev.* **2014**, *34*, 443–454.

17. Gelaw, A. M.; Singh, B. R.; Lal, R. Soil Quality Indices for Evaluating Smallholder Agricultural Land Uses in Northern Ethiopia. *Sustainability* **2015**, *7*, 2322–2337.

18. Nair, P. K. R. Agroforestry Systems and Environmental Quality: Introduction. *J. Environ. Qual.* **2011**, *40*, 784–790.

19. Brye, K. R.; West, C. P. Grassland Management Effects on Soil Surface Properties in the Ozark Highlands. *Soil Sci.* **2005**, *170*, 63–73.

20. Natural Resources Conservation Service. Land Resource Regions and Major Land Resource Areas of the United States, the Caribbean, and the Pacific Basin. In *USDA Handbook 296*; Government Printing Office: Washington, DC, US, 2006; pp 373–375.

21. Brion, G.; Brye, K. R.; Haggard, B.; West, C. P.; Brahana, J. Land☐use Effects on Water Quality of a First☐order Stream in the Ozark Highlands, Mid☐southern United States. *River Res. Appl.* **2011**, *27*, 772–790.

22. Major Land Resource Areas. Available online: https://data.nal.usda.gov/dataset/major-land-resource-areas-mlra (accessed 23 June 2022).

23. Web Soil Survey. Available online: https://websoilsurvey.sc.egov.usda.gov/App/WebSoilSurvey.aspx (accessed 23 June 2022).

24. Ashworth, A. J.; Adams, T. C.; Kharel, T.; Philip, D.; Owens, P. R.; Sauer, T. Root Decomposition in Silvopastures Is Influenced by Grazing, Fertility, and Grass Species. *Agrosystems Geosci. Environ.* **2021**, *4*, 1–15.

25. Data tools: 1981-2010 Normals. Fayetteville experimental station, AR US. Available online: https://www.ncei.noaa.gov/access/us-climate-normals/#dataset=normals-monthly&timeframe=81 (accessed 23 June 2022).

26. Sauer, T. J.; Coblentz, W. K.; Thomas, A. L.; Brye, K. R.; Brauer, D. K.; Skinner, B.; J.V., D.; S.L., H.; P.D., M.; D.C., R.; J.L., J.; T.A.; Hickie, K. A. Nutrient Cycling in an Agroforestry Alley Cropping System Receiving Poultry Litter or Nitrogen Fertilizer. *Nutr. Cycl. Agroecosystems* **2014**, *101*, 167–179.

27. Niyigena, V.; Ashworth, A. J.; Nieman, C.; Acharya, M.; Coffey, K. P.; Philipp, D.; Meadors, L.; Sauer, T. J. Factors Affecting Sugar Accumulation and Fluxes in Warm- and Cool-Season Forages Grown in a Silvopastoral System. *Agronomy* **2021**, *11*, 1–14.

28. Gurmessa, B.; Ashworth, A. J.; Yang, Y.; Adhikari, K.; Savin, M.; Owens, P. R.; Sauer, T. J.; Pedretti, E. F.; S., C.; Corti, G. Soil Bacterial Diversity Based on Management and Topography in a Silvopastoral System. *Appl. Soil Ecol.* **2021**, *163*, 1–10.

29. Adams, T.; Ashworth, A. J.; Sauer, T. Soil CO2 Evolution Is Driven by Forage Species, Soil Moisture, Grazing Pressure, Poultry Litter Fertilization, and Seasonality in Silvopastures. *Agrosystems Geosci. Environ.* **2021**, *4*, 1–10.

30. Adhikari, K.; Owens, P. R.; Ashworth, A. J.; Sauer, T. J.; Libohova, Z.; Miller, D. M. Topographic controls on soil nutrient variations in a silvopasture system. *Agrosystems Geosci. Environ.* **2018**, *1*, 1–15.

31. Amorim, H. C. S.; Ashworth, A. J.; Sauer, T. J.; Zinn, Y. L. Soil Organic Carbon and Fertility Based on Tree Species and Management in a 17-Year Agroforestry Site. *Agronomy* **2022**, *12*, 1–13.

32. Ashworth, A. J.; Kharel, T.; Sauer, T.; Adams, T. C.; Philip, D.; Thomas, A. L.; Owens, P. R. Spatial Monitoring Technologies for Coupling the Soil Plant Water Animal Nexus. *Sci. Rep.* **2022**, *12*, 1–14.

33. DeFauw, S. L.; Brye, K. R.; Sauer, T. J.; Hays, P. Hydraulic and Physiochemical Properties of a Hillslope Soil Assemblage in the Ozark Highlands. *Soil Sci.* **2014**, *179*, 107–117.

34. Dold, C.; Thomas, A. L.; Ashworth, A. J.; Philipp, D.; Brauer, D. K.; Sauer, T. J. Carbon Sequestration and Nitrogen Uptake in a Temperate Silvopasture System. *Nutr. Cycl. Agroecosystems* **2019**, *114*, 85–98.

35. Jiang, Z.-D.; Owens, P. R.; Ashworth, A. J.; Ponce, B. F.; Thomas, A. L.; Sauer, T. Evaluating Tree Growth Factors into Species-Specific Functional Soil Maps for Improved Agroforestry System Efficiency. *Agrofor. Syst.* **2021**, *96*, 479–490.

36. Kharel, T. P.; Ashworth, A. J.; Owens, P. R.; Philipp, D.; Thomas, A. L.; Sauer, T. Teasing Apart Silvopasture System Components Using Machine Learning for Optimization. *Soil Syst.* **2021**, *5*, 1–16.

37. O'Brien, P. L.; Thomas, A. L.; Sauer, T. J.; Brauer, D. K. Foliar nutrient concentrations of three economically important tree species in an alley-cropping system. *J. Plant Nutr.* **2020**, *43*, 1–12.

38. Thomas, A. L.; Brauer, D. K.; Sauer, T. J.; Coggeshall, M. V.; Ellersieck, M. R. Cultivar Influences Early Rootstock and Scion Survival of Grafted Black Walnut. *J. Am. Pomol. Soc.* **2008**, *62*, 3–12.

39. Ylagan, S.; Amorim, H. C. S.; Ashworth, A. J.; Sauer, T.; Wienhold, B. J.; Owens, P. R.; Zinn, Y. L.; Brye, K. R. Soil Quality Assessment of an Agroforestry System Following Long-Term Management in the Ozark Highlands. *Agrosystems Geosci. Environ.* **2021**, *4*, 1–15.

40. Abdu, H.; Robinson, D.; Jones, S. Comparing Bulk Soil Electrical Conductivity Determination Using the DUALEM□1S and EM38□DD Electromagnetic Induction Instruments. *Soil Sci. Soc. Am. J.* **2007**, *71*, 189–196.

41. Simpson, D.; Lehouck, A.; Verdonck, L.; Vermeersch, H.; Meirvenne, M.; Bourgeois, J.; Thoen, E.; Docter, R. Comparison between Electromagnetic Induction and Fluxgate Gradiometer Measurements on the Buried Remains of a 17th Century Castle. *J. Appl. Geophys.* **2009**, *68*, 294–300.

42. Rudolph, S.; Wongleecharoen, C.; Lark, R. M.; Marchant, B. P.; Garré, S.; Herbst, M.; Vereecken, H.; Weihermüller, L. Soil Apparent Conductivity Measurements for Planning and Analysis of Agricultural Experiments: A Case Study from Western-Thailand. *Geoderma* **2016**, *267*, 220–229.

43. Martini, E.; Werban, U.; Zacharias, S.; Pohle, M.; Dietrich, P.; Wollschläger, U. Repeated Electromagnetic Induction Measurements for Mapping Soil Moisture at the Field Scale: Validation with Data from a Wireless Soil Moisture Monitoring Network. *Hydrol. Earth Syst. Sci.* **2017**, *21*, 495–513.

44. Pearson, R. K.; Neuvo, Y.; Astola, J.; Gabbouj, M. Generalized Hampel Filters. *EURASIP J. Adv. Signal Process.* **2016**, 1–18.

45. Delefortrie, S.; Smedt, P.; Saey, T.; Vijver, E.; Meirvenne, M. An efficient calibration procedure for correction of drift in EMI survey data. *J. Appl. Geophys.* **2014**, *110*, 115–125.

46. Borchers, H. W. Pracma: Practical Numerical Math Functions. R package version 2.3.3., 2021.

47. Hijmans, R. J. Geosphere: Spherical Trigonometry. R package version 1.5.10., 2019.

48. Pebesma, E.; Bivand, R.; Rowlingson, B.; Gomez-Rubio, V. Sp: Package Providing Classes and Methods for Spatial Data: Points, Lines, Polygons and Grids. R package version 2.0.7., 2005.

49. Bivand, R.; Keitt, T.; Rowlingson, B. Rgdal: Bindings for the "geospatial" Data Abstraction Library. R package version 1.5.23., 2021.

50. Pebesma, E. J. gstat: Multivariable geostatisitcs in S. R package version 2.0.8., 2004.

51. Padgham, M.; Sumner, M. D. geodist: Fast, dependency-free geodesic distance calculations. R package version 0.0.7., 2021.

52. Hijmans, R. J. Raster: Geographic Data Analysis and Modeling. R package version 3.4.10., 2021.

53. Hijmans, R. J. terra: Spatial data analysis. R package version 1.2.10., 2021.

54. Growing Season Dates and Length. Available online: https://www.nrcs.usda.gov/wps/portal/wcc/home/climateSupport/wetlandsClimateTables/growingSeasonDatesLength/ (accessed 23 June 2022).

55. Hartigan, J. A. *Clustering Algorithms*; John Wiley & Sons: Hoboken, NJ, US, 1975; pp 1–351.

56. Kassambara, A.; Mundt, F. factoextra: Extract and visualize the results of multivariate data analyses. R package version 1.0.7., 2020.

57. Chilés, J.-C.; Delfiner, P. Structural Analysis. In *Geostatisitcs: Modeling spatial uncertainty*; Balding, D. J., Cressie, N. A. C., Fitzmaurice, G. M., Goldstein, H., Johnstone, I. M., Molenberghs, G., Scott, D. W., Smith, A. F. M., Tsay, R. S., Weisberg, S., Eds.; John Wiley & Sons: Hoboken, NJ, US, 2012; pp 28–146.

58. Fortin, M.-J.; Dale, M. R. T.; Ver Hoef, J. Spatial Analysis in Ecology. In *Encyclopedia of environmetrics*; El-Shaarawi, A. H., Pieforsch, W. W., Eds.; John Wiley & Sons: Chichester, England, UK, 2002; Volume 4, pp 2051–2058.

59. Zhu, Q.; Lin, H.; Doolittle, J. Repeated Electromagnetic Induction Surveys for Determining Subsurface Hydrologic Dynamics in an Agricultural Landscape. *Soil Sci. Soc. Am. J.* **2010**, *74*, 1750–1762.

60. Kravchenko, A. N. Influence of Spatial Structure on Accuracy of Interpolation Methods. *Soil Sci. Soc. Am. J.* **2003**, *67*, 1564–1571.

61. Skøien, J. O.; Blöschl, G. Scale Effects in Estimating the Variogram and Implications for Soil Hydrology. *Vadose Zone J.* **2006**, *5*, 153–167.

62. DeCaires, S. A.; Wuddivira, M. N.; Bekele, I. Assessing the Temporal Stability of Spatial Patterns of Soil Apparent Electrical Conductivity Using Geophysical Methods. *Int. Agrophysics* **2014**, *28*, 423–433.

63. Khakural, B. R.; Robert, P. C.; Hugins, D. R. Use of non□contacting electromagnetic inductive method for estimating soil moisture across a landscape. *Commun. Soil Sci. Plant Anal.* **1998**, *29*, 2055–2065.

64. Western, A. W.; Blöschl, G.; Grayson, R. B. Geostatistical Characterization of Soil Moisture Patterns in the Tarrawarra Catchment. *J. Hydrol.* **1998**, *205*, 20–37.

65. General Reference and Data Downloads. Available online: https://maps.fayetteville-ar.gov/viewer/index.html?webmap=46ac3a6201624738a961f1f3123d7d5b (accessed 23 June 2022).

66. Smith, H.; Ashworth, A.J.; Owens, P. R. Applications and Analytical Methods of Ground Penetrating Radar for Soil Characterization in a Silvopastoral System. *J. Environ. Eng. Geophys.* **2022**, accepted.

67. Burgess-Conforti, J. R.; Moore, P. A.; Owens, P. R.; Miller, D. M.; Ashworth, A. J.; Hays, P. D.; Evans-White, M. A.; Anderson, K. R. Are Soils beneath Coniferous Tree Stands More Acidic than Soils beneath Deciduous Tree Stands? *Environ. Sci. Pollut. Res.* **2019**, *26*, 14920–14929.

68. Harvey, O. R.; Morgan, C. L. S. Predicting Regional-Scale Soil Variability Using a Single Calibrated Apparent Soil Electrical Conductivity Model. *Soil Sci. Soc. Am. J.* **2009**, *73*, 164–169.

69. Chow, T. L.; Rees, H. W.; Monteith, J. O.; Toner, P.; Lavoie, J. Effects of Coarse Fragment Content on Soil Physical Properties, Soil Erosion and Potato Production. *Can. J. Soil Sci.* **2007**, *87*, 565–577.

70. Brevik, E. C.; Fenton, T. E.; Lazari, A. Soil Electrical Conductivity as a Function of Soil Water Content and Implications for Soil Mapping. *Precis. Agric.* **2006**, *7*, 393–404.

71. Corwin, D. L.; Lesch, S. M.; Shouse, P. J.; Soppe, R.; Ayars, J. E. Identifying Soil Properties That Influence Cotton Yield Using Soil Sampling Directed by Apparent Soil Electrical Conductivity. *Agron. J.* **2003**, *95*, 352–364.

72. Bongiovanni, R.; Lowenberg-Deboer, J. Precision Agriculture and Sustainability. *Precis. Agric.* **2004**, *5*, 359–387.

73. Food Agriculture Organization. FAO/Unesco Soil Map of the World, Revised Legend, with Corrections and Updates (Technical paper 20); FAO: Rome, Italy, 1988; pp. 1–146.

Tables and Figures

Table 1. Summary of the seasonal [i.e., weather season (summer, fall, winter, and spring) and tree growing season (growing season and non-growing season)] groupings and the survey groupings compared against all 12 monthly conducted electromagnetic-induction (EMI) apparent electrical conductivity (EC_a) surveys for the homogeneity of variance assessment. The EMI EC_a surveys were conducted at an agroforestry site in Fayetteville, AR between August 2020 and July 2021.

Survey	Survey (Month-Year)	Seasonal Groupings		Test Groupings[††]				
		Weather Season	Growing[†] Season	H1	H2	MS	MFS	MWS
1	Aug-2020	Summer	GS	X				
2	Sep-2020	Fall	GS		X			
3	Oct-2020	Fall	GS	X		X	X	
4	Nov-2020	Fall	NGS		X			
5	Dec-2020	Winter	NGS	X				
6	Jan-2021	Winter	NGS		X	X		X
7	Feb-2021	Winter	GS	X				
8	Mar-2021	Spring	GS		X			
9	Apr-2021	Spring	GS	X		X	X	
10	May-2021	Spring	GS		X			
11	Jun-2021	Summer	GS	X				
12	Jul-2021	Summer	GS		X	X		X

[†] Growing season (GS), non-rowing season (NGS)

[††] Odd half of surveys in sequential order of conduction (H1), even half of surveys in sequential order of conduction (H2), middle of climate season (MS), middle of Fall and Spring (MFS), middle of Winter and Summer (MWS)

Table 2. Summary of the perpendicular geometry (PRP) apparent electrical conductivity (EC_a) survey dates, number of measurements per survey, semi-variogram information (i.e., experimental model, nugget, sill, and range), and resulting summary statistics [i.e., mean, minimum (min), maximum (max), standard deviation (SD), and coefficient of variation (CV)] of each PRP EC_a survey after universal kriging at an agroforestry site in Fayetteville, AR between August 2020 and July 2021.

Survey	Date (Month-Year)	Survey Points	PRP EC_a								
			Semi-variogram Information				Kriged Survey Summary Statistics				
			Model	Nugget	Sill	Range	Mean	Min	Max	SD	CV
						m	——— mS m^{-1} ———				%
1	Aug-2020	5271	Exponential	0.61	4.8	39.4	4.2	1.0	17.0	1.9	44.1
2	Sep-2020	5422	Matern	0.18	3.5	34.4	3.4	0.4	14.6	1.7	48.1
3	Oct-2020	5769	Exponential	0.17	3.7	28.9	4.6	0.9	16.6	1.9	42.1
4	Nov-2020	6083	Exponential	0.38	5.0	41.4	7.4	2.3	18.2	2.4	32.2
5	Dec-2020	6085	Exponential	0.30	4.8	29.3	6.7	2.6	21.0	2.3	34.1
6	Jan-2021	6340	Exponential	0.10	3.6	27.8	5.5	1.4	17.2	2.1	38.0
7	Feb-2021	5777	Exponential	0.00	3.7	26.8	6.2	1.7	20.5	2.3	36.3
8	Mar-2021	6173	Exponential	0.10	5.6	24.0	5.9	1.3	21.9	2.5	41.8
9	Apr-2021	6329	Exponential	0.03	6.0	25.3	5.5	0.6	17.6	2.6	46.8
10	May-2021	6854	Exponential	0.00	8.4	24.0	7.5	2.2	21.4	2.9	38.6
11	Jun-2021	6671	Matern	0.00	13.1	27.6	8.7	2.7	29.1	3.6	41.2
12	Jul-2021	6527	Exponential	0.18	4.2	27.7	5.1	0.2	15.9	2.1	40.3

Table 3. Summary of the horizontal coplanar geometry (HCP) apparent electrical conductivity (EC_a) survey dates, number of measurements per survey, semi-variogram information (i.e., experimental model, nugget, sill, and range), and resulting summary statistics [i.e., mean, minimum (min), maximum (max), standard deviation (SD), and coefficient of variation (CV)] for each HCP EC_a survey after universal kriging at an agroforestry site in Fayetteville, AR between August 2020 and July 2021.

Survey	Date (Month-Year)	Survey Points	HCP EC_a								
			Semi-variogram Information				Kriged Survey Summary Statistics				
			Model	Nugget	Sill	Range	Mean	Min	Max	SD	CV
						m	——————— mS m^{-1} ———————				%
1	Aug-2020	5271	Spherical	0.25	16.5	97.9	8.6	1.6	25.5	4.4	51.2
2	Sep-2020	5422	Circular	0.14	13.8	84.0	6.7	0.4	19.7	4.1	61.1
3	Oct-2020	5769	Spherical	0.32	14.3	91.6	9.9	3.6	25.6	4.1	41.2
4	Nov-2020	6083	Matern	0.08	15.9	60.0	9.8	2.9	26.2	4.2	42.1
5	Dec-2020	6085	Matern	0.00	15.7	50.0	12.3	3.6	28.4	4.4	35.9
6	Jan-2021	6340	Matern	0.00	14.6	48.9	11.7	4.4	29.2	4.2	36.4
7	Feb-2021	5777	Matern	0.00	15.2	58.9	8.8	2.2	23.6	4.2	47.5
8	Mar-2021	6173	Matern	0.00	16.0	42.1	11.9	4.8	34.2	4.2	35.5
9	Apr-2021	6329	Exponential	0.00	16.5	43.2	11.6	4.1	27.2	4.2	36.3
10	May-2021	6854	Matern	0.00	18.9	46.1	9.7	2.0	31.4	4.4	45.6
11	Jun-2021	6671	Spherical	0.13	19.1	69.3	10.1	1.7	28.6	5.1	50.1
12	Jul-2021	6527	Spherical	0.18	11.8	77.7	7.2	1.0	19.9	3.9	53.2

Table 4. Summary of the perpendicular (PRP) and horizontal coplanar geometry (HCP) apparent electrical conductivity (EC$_a$) for each cluster generated by the k-means clustering algorithm (Hartigan, 1975) using 12 electromagnetic-induction EC$_a$ surveys conducted at an agroforestry site in Fayetteville AR between August 2020 and July 2021.

		Summary Statistics[†]					
EC$_a$	Cluster	Mean	Min	Max	SD	CV	SE
		——————— mS m^{-1} ———————				%	
HCP	1	5.7	0.4	15.0	2.2	38.8	0.024
	2	16.6	7.5	34.2	3.2	19.3	0.050
	3	10.5	2.4	19.2	2.4	22.6	0.024
PRP	1	3.6	0.2	9.0	1.4	38.3	0.016
	2	9.0	3.1	29.1	2.8	31.3	0.042
	3	6.2	1.3	13.4	1.9	29.9	0.019

[†] Minimum (Min), maximum (Max), standard deviation (SD), coefficient of variation (CV), standard error (SE)

Table 5. Summary of the resulting correlation coefficients (r) and *P*-values from Pearson linear correlations evaluating the relationship between the perpendicular (PRP), horizontal coplanar geometry (HCP), and combined (PRP and HCP) apparent electrical conductivity (EC_a) and the upper, lower, and combined (upper and lower) soil-sensor-measured volumetric water content (VWC) and EC_a measurements and the upper, lower, and combined soil-sample-derived gravimetric water content (GWC), electrical conductivity (EC), and pH, respectively. Figures for each correlation are presented on Figure 12. Electromagnetic-induction EC_a survey, soil sensor, and soil sample data were collected from an agroforestry site in Fayetteville AR between August 2020 and July 2021.

Correlation Data Set		*r*	*P*
PRP EC_a & Upper			
	VWC	0.09	**< 0.01[†]**
	EC_a	0.84	**0.01**
	GWC	0.70	**< 0.01**
	EC	0.57	0.17
	pH	0.61	0.13
HCP EC_a & Lower			
	VWC	0.62	0.79
	EC_a	0.74	**< 0.01**
	GWC	0.71	**< 0.01**
	EC	0.37	**< 0.01**
	pH	0.42	**< 0.01**
Combined EC_a & Combined			
	VWC	0.25	0.24
	EC_a	0.65	**< 0.01**
	GWC	0.36	**0.03**
	EC	-0.22	0.28
	pH	0.15	0.49

[†] Bolded values are significant at $P < 0.05$

Table 6. Summary of the homogeneity of variance between all 12 monthly perpendicular (PRP) and horizontal coplanar geometry (HCP) apparent electrical conductivity (EC_a) surveys and five reduced survey groupings (i.e., H1, H2, MS, MFS, and MWS). Additional details of the survey groupings are presented on Table 1. Homogeneity of variance was evaluated using the Levene's test.

EC_a	Survey grouping comparison	P	Survey grouping with greater variance
PRP	H1[†]	**< 0.01**[††]	H1
	H2	**< 0.01**	All
	MS	**< 0.01**	All
	MFS	**< 0.01**	All
	MWS	**< 0.01**	All
HCP	H1[†]	0.60	-
	H2	0.93	-
	MS	**< 0.01**	All
	MFS	**< 0.01**	All
	MWS	0.87	-

[†] Odd half of surveys in sequential order of conduction (H1), even half of surveys in sequential order of conduction (H2), middle of season (MS), middle of Fall and Spring (MFS), middle of Winter and Summer (MWS)

[††] Bolded values are significant at $P < 0.05$

Figure 1. The agroforestry site in Fayetteville, AR is organized into 16 rows, where Row 1 starts at the northern most row. Rows 1-5 consists of the northern red oak; the western, central, and eastern portion of Rows 6-10 consists of the pitch/loblolly pine, cottonwood, and American Sycamore; and Rows 11-16 consist of pecan. The three sampling/logger locations are located at a local summit (Logger 2), depression area (Logger 6b), and mid-slope area between the summit and depression (Logger 9). The soils at the site include Captina silt loam (CaB), Pickwick silt loam (PsC2), Nixa cherty silt loam (NaC), Johnsburg silt loam (Js), and Cleora fine sandy loam (Cr; Soil Survey Staff, 2019b). The alleys between the tree rows consist of either orchardgrass or a native grass mix (big bluestem, little bluestem, and Indiangrass), where fertility treatments were fertilized with poultry litter in 2017, 2018, and 2019. Maps were created in ArcGIS (ArcGISmap version 10.6.1, Esri, Redlands, CA).

Figure 2. The survey setup included a DUALEM-1S sensor that was suspended on a sled that was tied to a Side-by-Side vehicle, a Trimble R2 global positioning system unit mounted inside of the Side-by-Side, and both the DUALEM-1S and Trimble R2 were connected to a Trimble Yuma 2 field computer inside the Side-by-Side that interpolated the data in a hand-held geoinformation system.
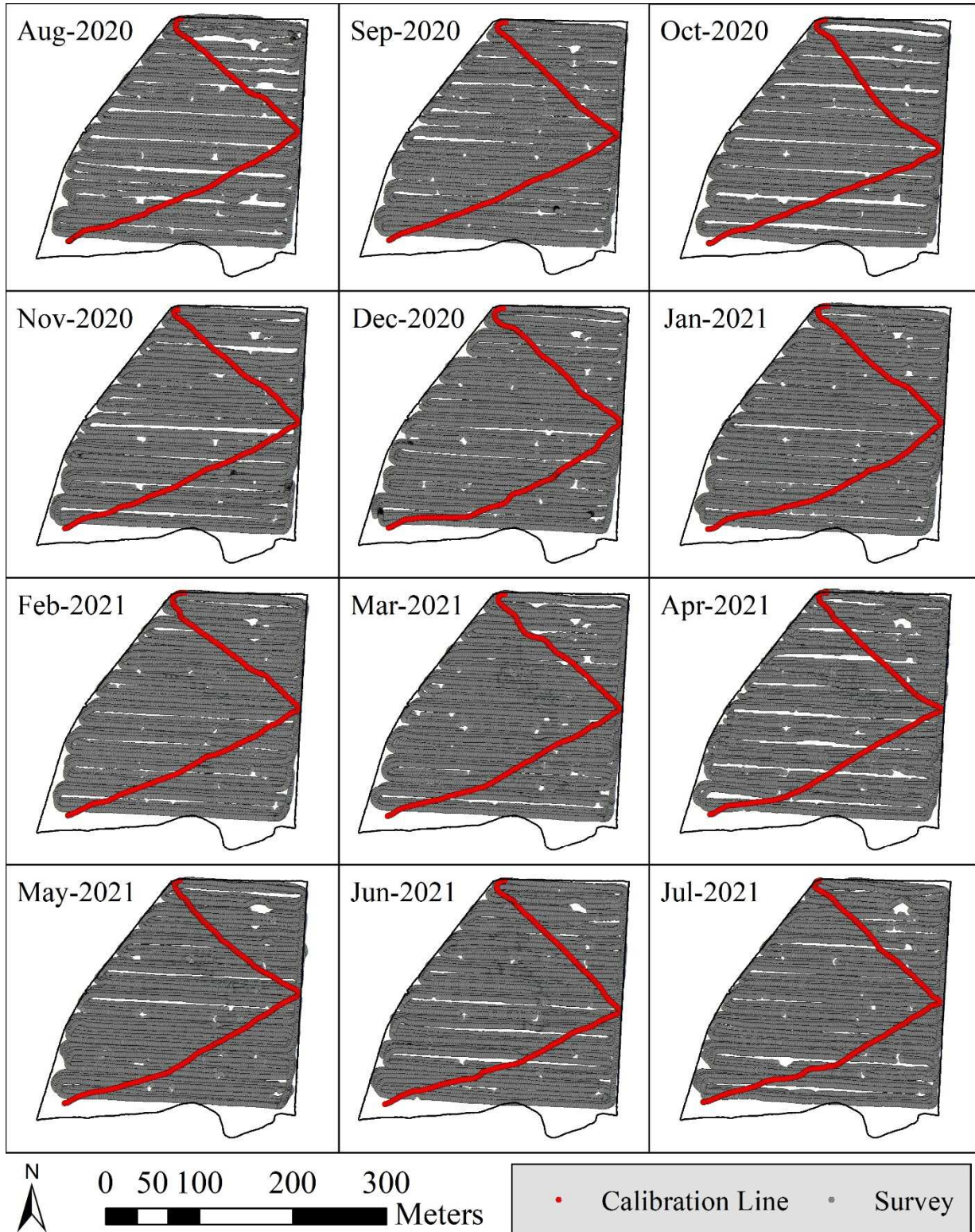
Figure 3. The measurement locations of the EMI-EC$_a$ survey (grey dots) and calibration line (red dots) for all 12, mid-monthly scans conducted at the agroforestry site in Fayetteville, AR. Maps were created in ArcGIS (ArcGISmap version 10.6.1, Esri, Redlands, CA).
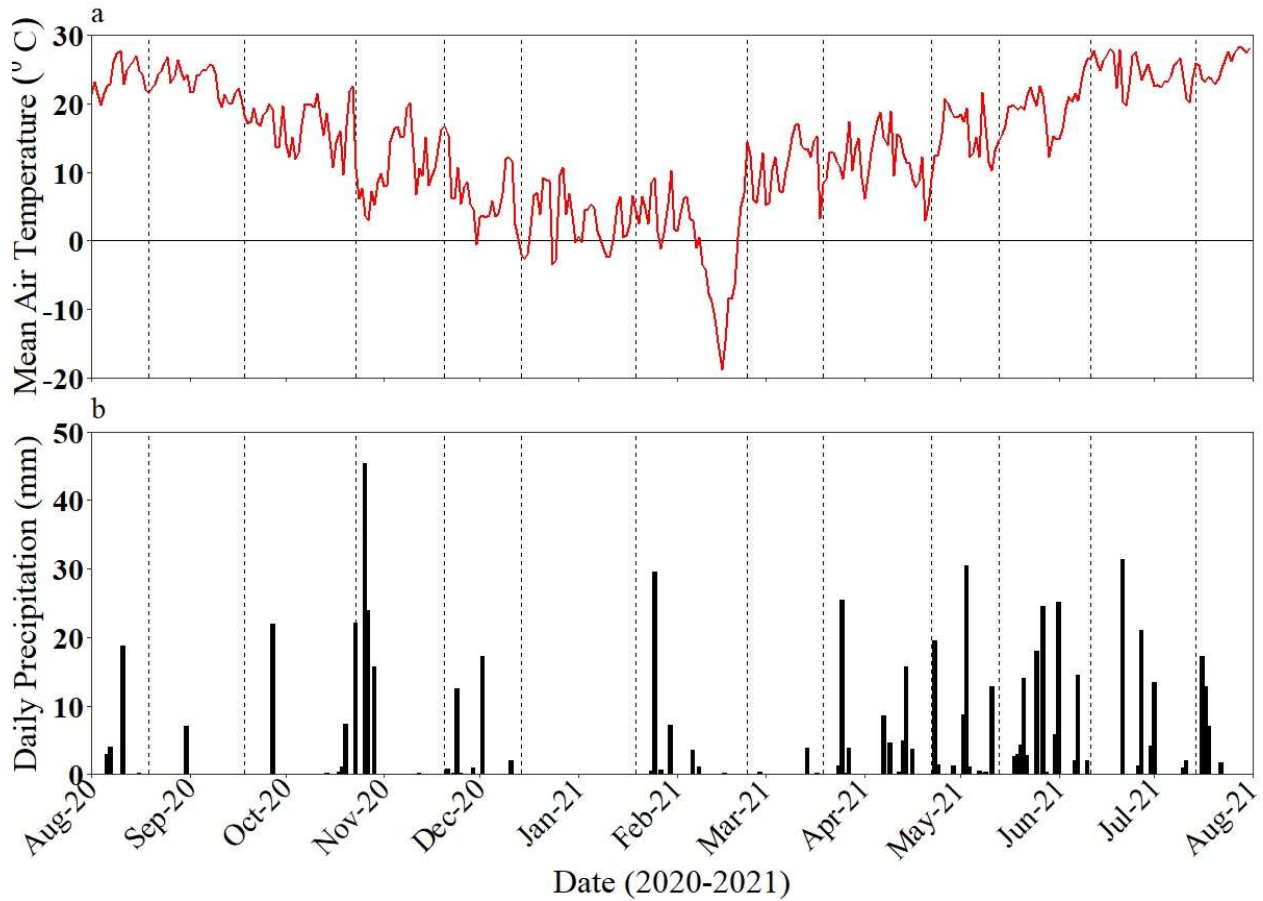
Figure 4. The local, daily average air temperature and total daily precipitation at the University of Arkansas' Milo J. Shult Agricultural Research and Extension Center, recorded on a micrometeorological weather station (36.101002°N, 94.173728°W) from 1 August 2020 to 31 July 2021. Electromagnetic-induction apparent electrical conductivity surveys dates are represented by the vertical dashed lines.
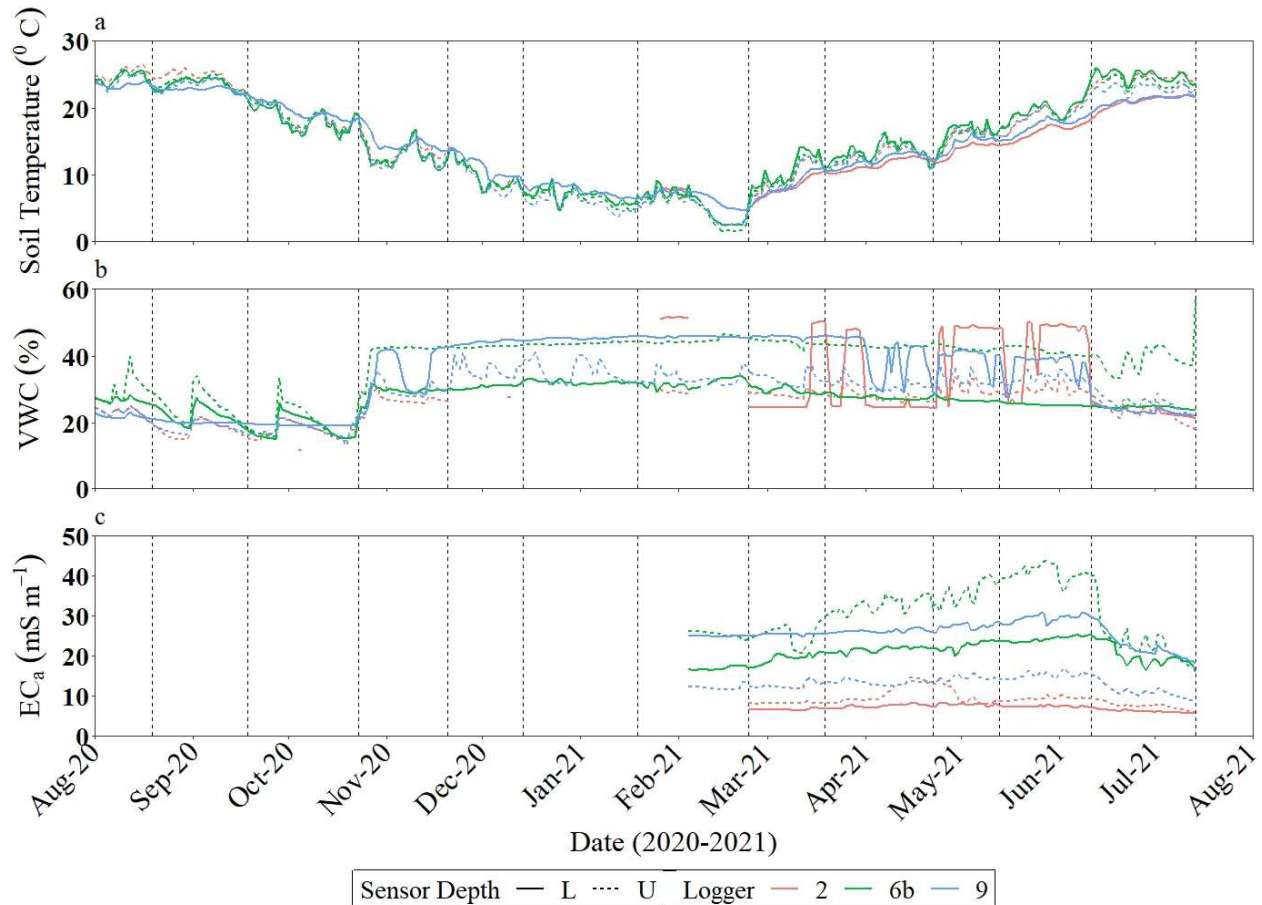
Figure 5. The recorded daily mean soil temperature (temp; a), volumetric water content (VWC; b), and apparent electrical conductivity (EC$_a$; c) for the upper (U; 15, 15, 15 cm, respectively) and lower (L; 75, 75, and 50 cm, respectively) soil sensor depths at logger 2, 6b, and 9, at the agroforestry site in Fayetteville, AR. Electromagnetic-induction EC$_a$ surveys dates are represented by the vertical dashed lines. Figures were created in R Studio (version 4.05, R Core Team, Boston, MA).
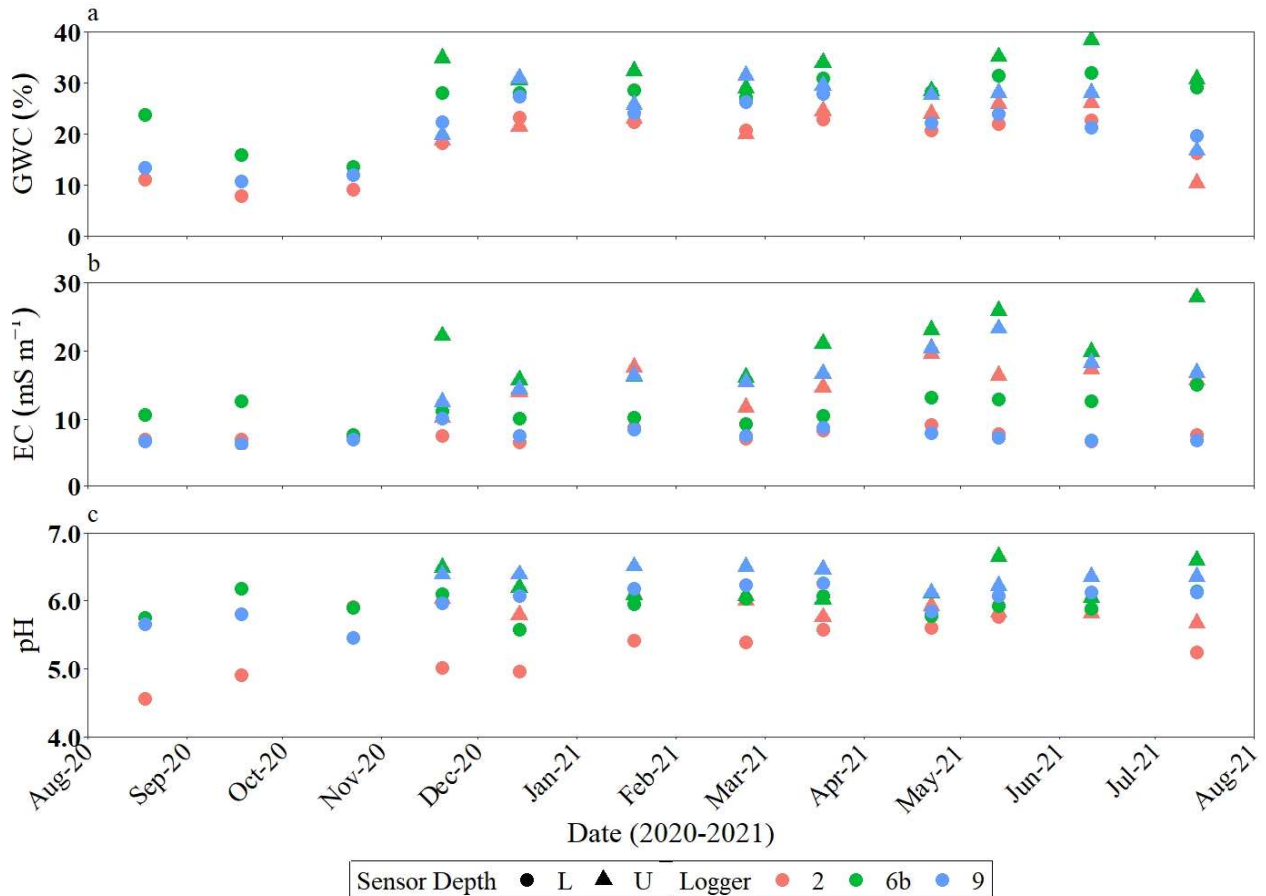
Figure 6. The lab measured gravimetric water content (GWC; a), electrical conductivity (EC; b), and pH for the upper (U; 0-15 cm) and lower (L; 45-55 cm) soil sample depth intervals at logger 2, 6b, and 9 for each electromagnetic-induction apparent electrical conductivity survey, at the agroforestry site in Fayetteville, AR. Figures were created in R Studio (version 4.05, R Core Team, Boston, MA).
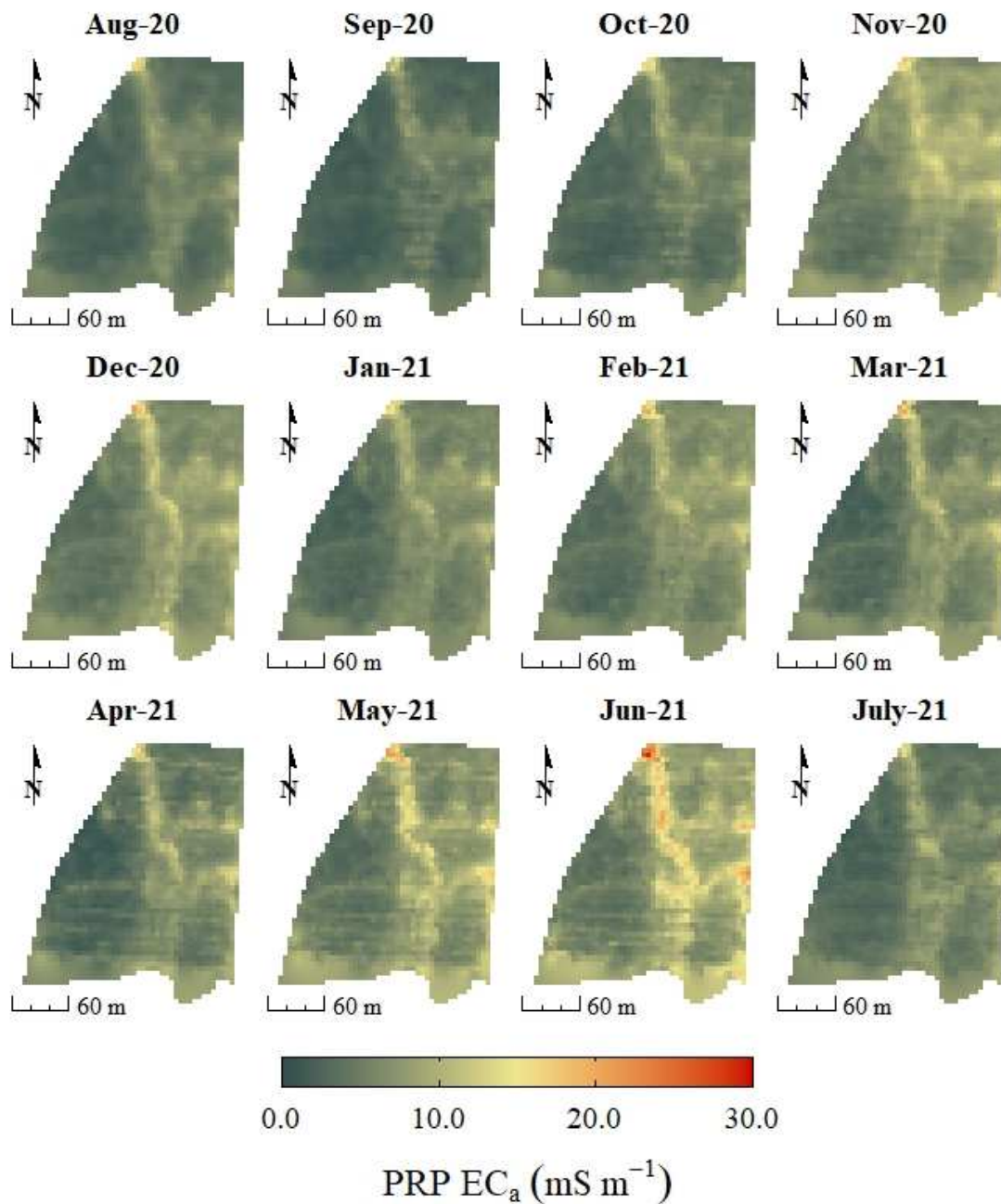
Figure 7. The perpendicular geometry (PRP) apparent electrical conductivity (EC$_a$) after universal kriging for all 12 survey months (2020-2021) at the agroforestry site in Fayetteville, AR. Maps were created in R Studio (version 4.05, R Core Team, Boston, MA).
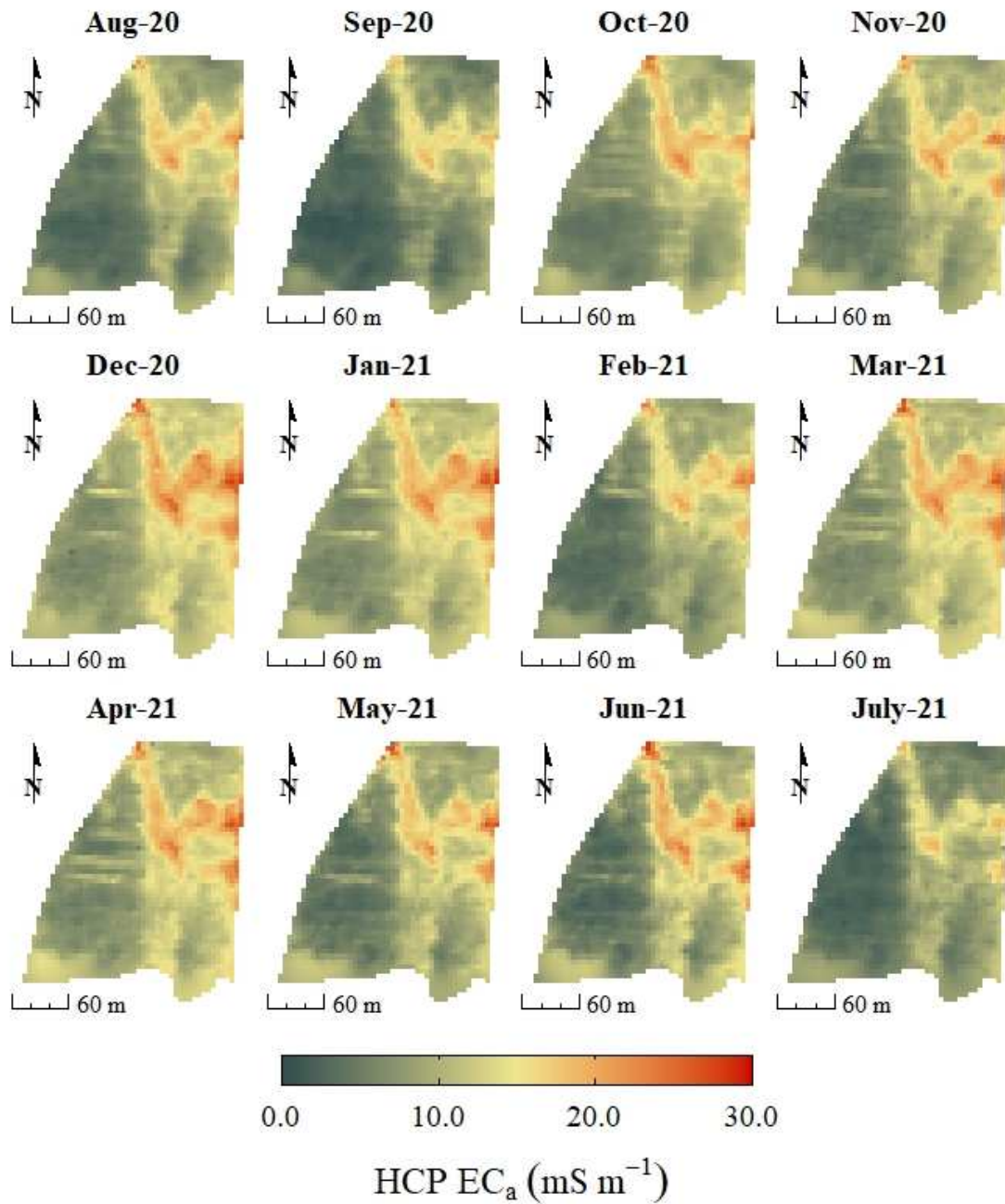
Figure 8. The horizontal coplanar geometry (HCP) apparent electrical conductivity (EC$_a$) after universal kriging for all 12 survey months (2020-2021) at the agroforestry site in Fayetteville, AR. Maps were created in R Studio (version 4.05, R Core Team, Boston, MA).
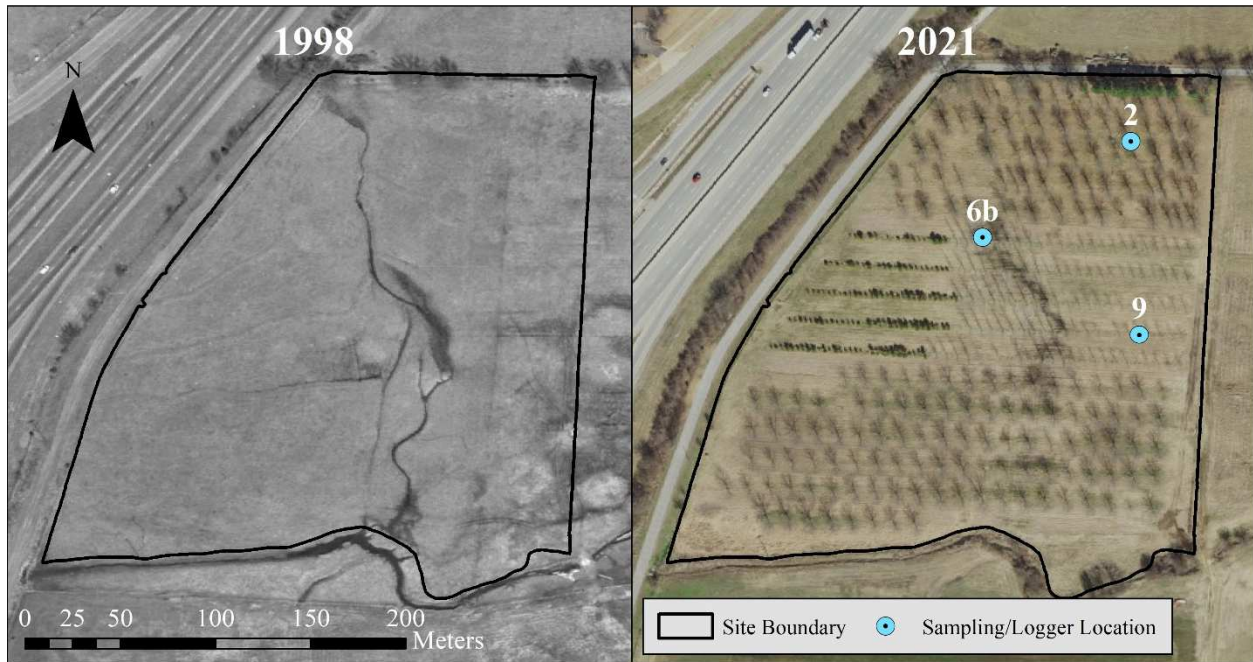
Figure 9. A satellite image of the agroforestry site in Fayetteville, AR prior to being converted into an agroforestry system in 1998 (left image) and the agroforestry site in 2021 (right image) with the three sampling/logger locations. The three sampling/logger locations are located at a local summit (Logger 2), depression area (Logger 6b), and mid-slope area between the summit and depression (Logger 9). Imagery was obtained from City of Fayetteville, AR (2022) and the maps were created in ArcGIS (ArcGISmap version 10.6.1, Esri, Redlands, CA).
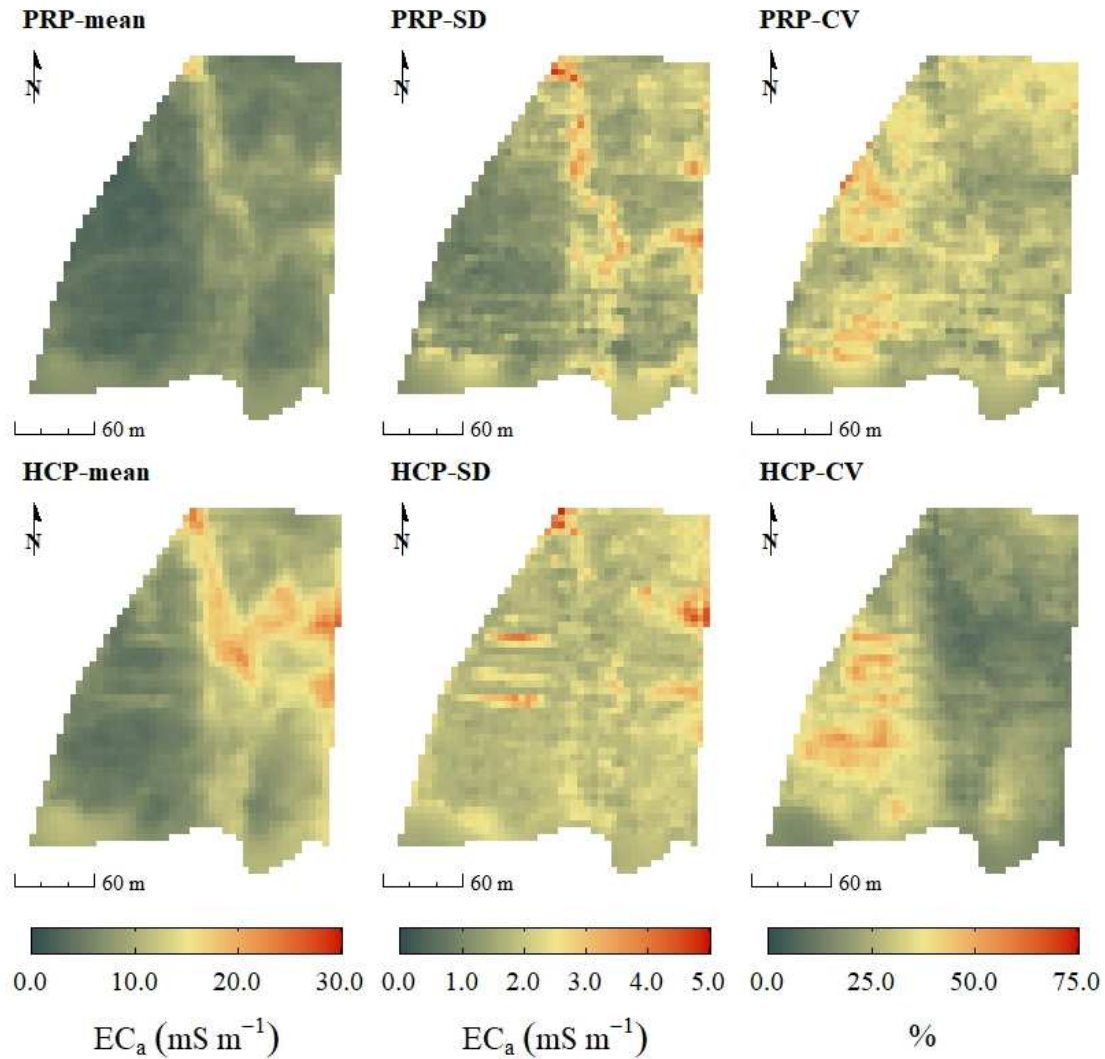
Figure 10. The overall mean, standard deviation (SD), and coefficient of variation (CV) for all 12 perpendicular (PRP) and horizontal coplanar geometry (HCP) apparent electrical conductivity (EC$_a$) surveys after universal kriging at the agroforestry site in Fayetteville, AR. Maps were created in R Studio (version 4.05, R Core Team, Boston, MA).
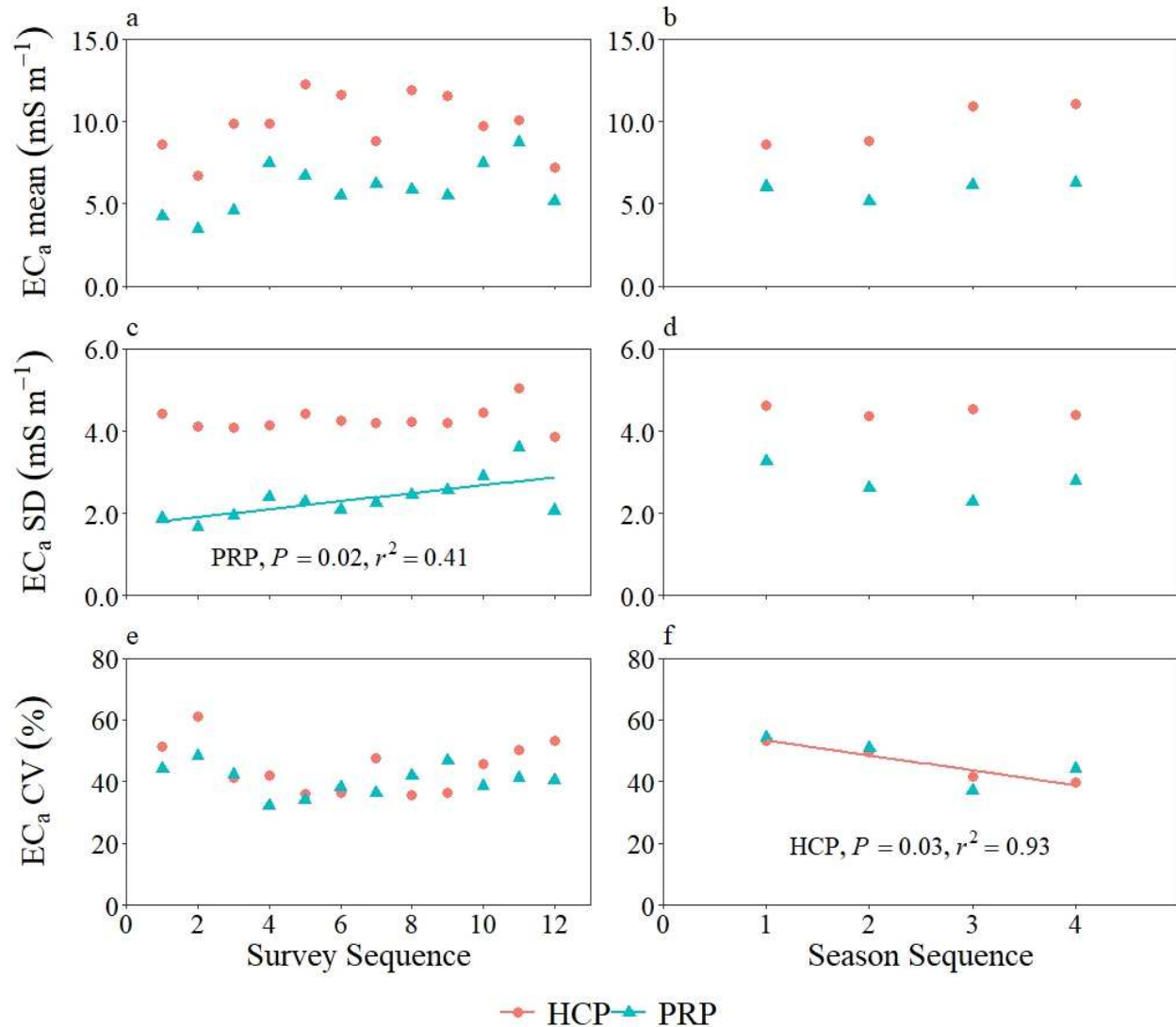
Figure 11. Relationship between mean apparent electrical conductivity (EC_a; a), standard deviation (SD; c), and coefficient of variation (CV; e) and survey sequence (i.e., time; 1, August 2020; 2, September 2020; 3, October 2020; 4, November 2020; 5, December 2020; 6, January 2021; 7, February 2021; 8, March 2021; 9, April 2021; 10, May 2021; 11, June 2021; 12, July 2021), and the relationship between mean EC_a (b), SD (d), and CV (f) and season sequence (i.e., time; 1, summer; 2, fall; 3, winter; 4, spring) for both the perpendicular (PRP) and horizontal coplanar geometry (HCP) configurations. Linear regression fit to the data are also plotted when the regression slope was significant ($P < 0.05$).
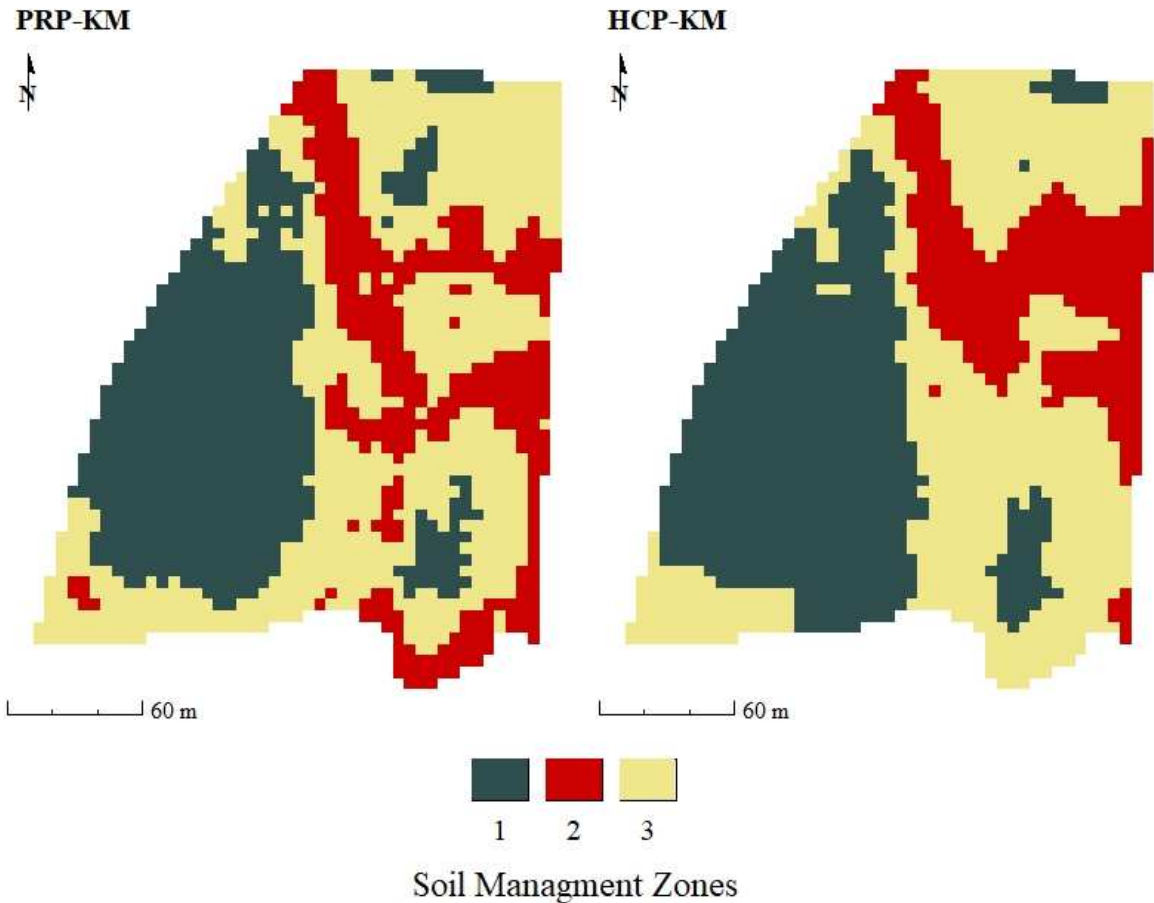
Figure 12. Precision soil management zones within the agroforestry site in Fayetteville, AR that were generated by the k-means (KM) clustering algorithm using all 12, perpendicular (PRP) and horizontal coplanar geometry (HCP) apparent electrical conductivity surveys.
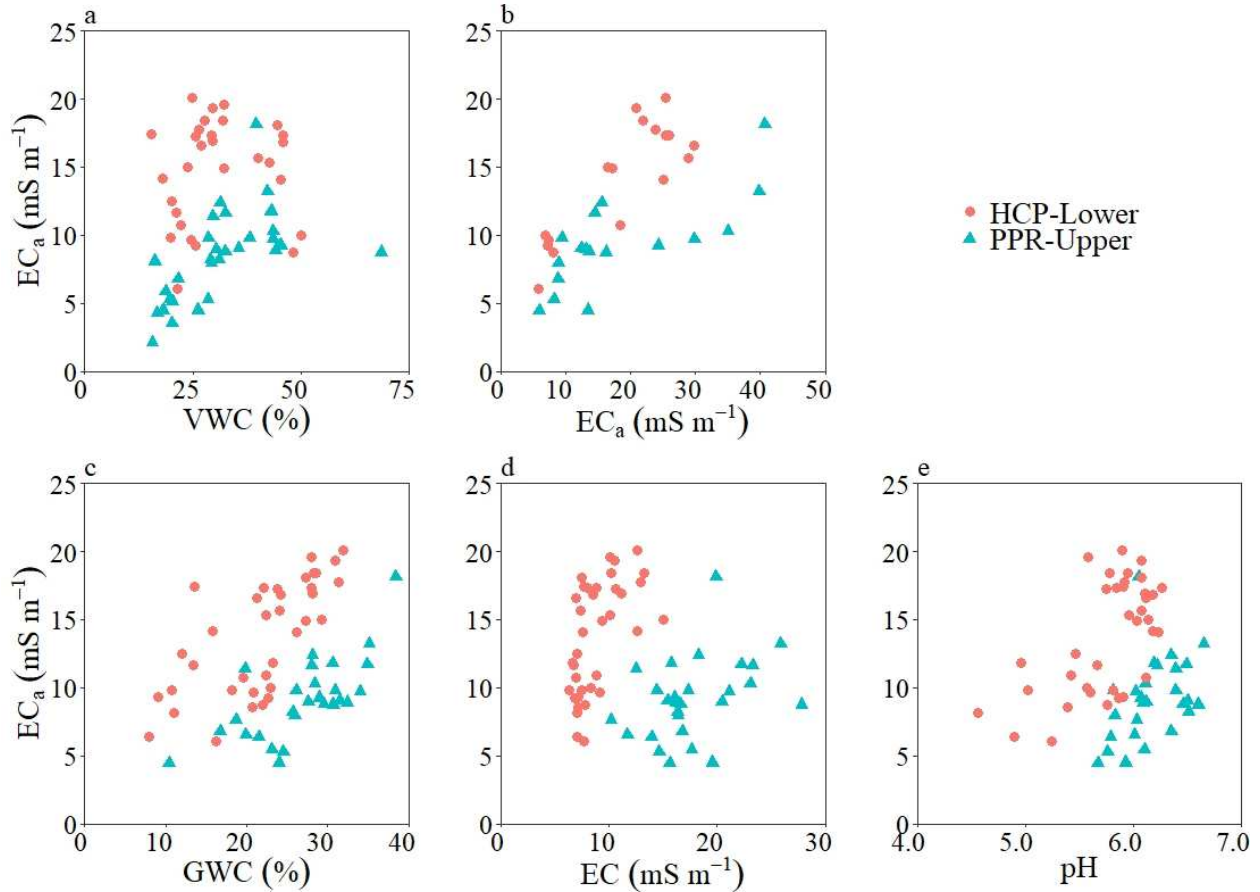
Figure 13. Relationship between the perpendicular (PRP) and horizontal coplanar geometry (HCP) apparent electrical conductivity (EC_a) and the a) upper (15 cm) and lower (75 cm) *in situ* soil sensor based volumetric water content (VWC), respectively; b) upper (15 cm) and lower (50 cm) *in situ* soil sensor based EC_a, respectively; c) upper (0-15 cm) and lower (45-55 cm) field collected gravimetric water content (GWC), respectively; d) upper (0-15 cm) and lower (45-55 cm) field collected EC, respectively; and e) upper (0-15 cm) and lower (45-55 cm) soil sample collected pH, respectively. Measurements were made at three sentinel sampling/logger locations at an agroforestry site in Fayetteville, AR from 2020 to 2021. Each figure's resulting r- and p-value from the Pearson correlation are reported on Table 6.

Chapter 3

Relationships Among Apparent Electrical Conductivity and Plant and Terrain Data in an Agroforestry System in the Ozark Highlands

Abstract

　　Minimal research has been conducted relating electromagnetic induction (EMI) apparent electrical conductivity (EC$_a$) surveys to plant and terrain properties in agroforestry (AF) systems. Objectives of this study were to i) evaluate correlations between EC$_a$ and forage yield, tree growth, and terrain attributes based on plant (forage and tree) species, and fertility treatments, and EC$_a$-derived soil management zones (SMZs), and ii) identify terrain attributes that have the largest contribution to EC$_a$ variability at a 20-year-old, 4.25-ha, AF system in the Ozark Highlands of northwest Arkansas. Fourteen terrain attributes and average of 12 mid-monthly EC$_a$ surveys (August 2020 to July 2021) were obtained. Tree diameter at breast height (DBH) and tree height (TH) measurements were made in December 2020 and March 2021, respectively, and forage yield samples were collected seven times during Summer 2018 and 2019. Perpendicular geometry (PRP) and horizontal coplanar geometry (HCP) EC$_a$ ranged between 1.8 and 18.0 and 3.1 and 25.8 mS m^{-1}, respectively. Relationships between EC$_a$ and tree properties were generally stronger within the whole-site (averaged across tree property and EC$_a$ configuration, $|r| = 0.38$) than the SMZs (averaged across tree property, EC$_a$ configuration, and SMZ, $|r| = 0.27$). The strength of the SMZs' terrain-attribute-PRP-EC$_a$ relationships were 9 to 205% greater than that for the whole-site. Whole-site, multi-linear regressions, Slope Length and Steepness (LS)-Factor (10.5%), Mid-slope (9.4%), and Valley Depth (7.2%) had the greatest influence (i.e., largest percent of total sum of squares) on PRP EC$_a$ variability, whereas Valley Depth (15.3%), Wetness Index (11.9%), and Mid-slope (11.2%) had the greatest influence on HCP EC$_a$ variability. Results of this study show how EC$_a$ relates to plant properties (i.e., tree DBH and TH and forage yield) and terrain attributes within SMZs in AF systems with varying topography that could be used to influence AF management.

Introduction

Crop yield variability due to spatially heterogeneous soil properties has been well recognized. As a result, whole-field land management has increasingly been identified as inefficient, as whole-field land management causes the under- and over-application of resources in regions of high- and low-yield potential, respectively [1]. Intra-field management, the spatially directed management of pests, crops, and soils based on differing characteristics within a field, is a precision agriculture management approach that produces smaller management units and optimizes field production and sustainability [1,2]. However, site-specific management requires the characterization of within-field variability and the identification of areas of homogeneous characteristics, or soil management zones (SMZs) [2].

Several methods have been used to map spatial variability and delineate management zones within a field. These methods include soil sampling for digital soil mapping yield monitoring and geophysical methods for proximal soil sensing [i.e., ground-penetrating radar (GPR), electrical resistivity (ER), electromagnetic induction (EMI), optical reflectance, gamma-ray spectrometry, time domain reflectometry (TDR)] [3,4], with EMI-based methods being the most frequently used for proximal soil sensing [5]. Electromagnetic induction-based methods use ground conductivity meters, which are non-invasive, simple to implement, and are capable of measuring large areas relatively quickly [6,7]. Electromagnetic-induction sensors are able to help delineate soil property variability through proximally sensing the soil's apparent electrical conductivity (EC_a), which is the ability of a soil to conduct an electrical current. Lab-measured EC has commonly been used has a measurement of soil salinity [8,9]; however, in-field EMI-EC_a is the result of complex interactions of many soil properties [i.e., base saturation (BS), bulk density (BD), cation exchange capacity (CEC), clay content and mineralogy, soil organic matter

(SOM), soil salinity, soil temperature, and soil water content (SWC)] and, in turn, can be used to help identify within-field soil property variability through correlations [10]. In addition to establishing relationships between measured EMI-EC$_a$ and soil properties, EMI-EC$_a$ surveys have been used in digital soil mapping, optimizing soil sampling strategies, and delineating crop/soil management zones [11,12].

Electromagnetic induction-EC$_a$ surveys have been used to evaluate variations in a multitude of soil and crop responses within a variety of different land management systems and ecosystems across the world. In addition to soil properties, relationships between EMI-EC$_a$ and crop yield have been assessed [1,13,14]. However, minimal work has been conducted exploring the relationships between EMI-EC$_a$ and pasture forage yield and tree growth in agroforestry (AF) systems, or whether the relationships could be improved with EC$_a$-derived SMZs within an AF system in an environment similar to the Ozark Highlands. Similarly, relationships between terrain attributes and EMI-EC$_a$ have been evaluated and both have been used to create management zones or functional units and for predictive mapping, individually or in combination [13,15–22]. However, no work has been conducted evaluating relationships between terrain attributes and EMI-EC$_a$ within an AF system in an environment like the Ozark Highlands.

The Ozark Highlands is a region with unique characteristics that result in the area having increased potential for conservation issues. Specifically, the Ozark Highlands is characterized by a relatively warm and wet climate, rolling topography, inclusions of shallow, cherty soils overlying karst limestone geology, rapid urbanization, and pastoral systems with repeated, excess applications of poultry litter (PL). The characteristics of the Ozark Highlands, in turn, cause the region to have an elevated potential for surface and sub-surface water quality degradation via

nutrient-rich runoff to surface waters and leaching to shallow and/or easily accessed groundwater sources. Considering the conservation issues in the Ozark Highlands, AF systems may be beneficial due to the many potential ecosystem services that AF systems offer (i.e., reduced soil erosion and runoff and water and soil quality enhancement).

Considering the lack of information relating EMI-EC$_a$ surveys to plant characteristics and terrain attributes in a sloped, topographically variable AF system in the Ozark Highlands, the objectives of this study were to identify: i) correlations between EMI-EC$_a$ and forage yield, tree growth, and terrain attribute data at the whole-site and EC$_a$-derived SMZs level, ii) correlations between EC$_a$ and forage yield and tree growth data per species and fertility treatments within the whole site and three EC$_a$-derived SMZs, and iii) terrain attributes that drive EMI-EC$_a$ variations at a 20-year AF system in the Ozark Highlands of northwest Arkansas. It was hypothesized that EMI-EC$_a$ data will be correlated with forage yield, tree growth characteristics, and terrain attributes and that correlations among EMI-EC$_a$ and forage yield, tree growth data, and terrain attributes can be improved with EC$_a$-derived SMZs. It was also hypothesized that terrain attributes would contribute to the EC$_a$ variability to varying degrees within the AF site and across the SMZs.

Materials and Methods

Site Description

Mapped Soils and Tree and Forage Establishment

The study site was located in the Ozark Highlands, Major Land Resource Area (MLRA) 116A [23], at the University of Arkansas Milo J. Shult Agricultural Research and Extension Center (SAREC) in Fayetteville, AR (36.09°N, 94.19°W). The study site was a 4.25-ha paddock

primarily mapped as Captina silt loam (fine-silty, siliceous, active, mesic Typic Fragiudults), but contains some Pickwick silt loam (fine-silty, mixed, semiactive, thermic Typic Paleudults), Nixa cherty silt loam (loamy-skeletal, siliceous, active, mesic Glossic Fragiudults), Johnsburg silt loam (fine-silty, mixed, active, mesic Aquic Fragiudults), and Cleora fine sandy loam (Coarse-loamy, mixed, active, thermic Fluventic Hapludolls; Figure 1) [24]. The research area also contained a dissimilar soil inclusion that is consistently wetter and lower in elevation than the immediate surrounding areas at the AF site. The dissimilar inclusion within the study site is not captured in the formal soil mapping units across the site, but is classified as fine, mixed, active, thermic Typic Endoaqualfs [25]. The AF site receives an average of 1156 mm of precipitation annually and has annual minimum, maximum, and average air temperature of 8.7, 20.3, and 14.6°C, respectively, based on 30-yr means (1981 to 2010) [26].

Before the AF site was established, the paddock was split into two paddocks by a north-south fence, which were poorly managed, covered in weeds, and only used for equipment storage. Additionally, the paddocks had small terraces from previous management and had a gully forming. Prior to the site's conversion to an AF system, the fences were removed, the gully was filled in, the soil was leveled, and the vegetation was killed. Sixteen rows of northern red oak (*Quercus rubra* L.), pecan (*Carya illinoinensis* Wangenh. K. Koch), and eastern black walnut (*Juglans nigra* L.) were established at the study site in 2000 in an east-west orientation with 15-m spacing between tree rows (Figure 1). The eastern black walnut trees grew adequately on the east side, but struggled to grow in the central, wetter area and in the dry Nixa soil on the west side of the tree rows. Consequently, in 2014, the eastern black walnut trees were removed and replaced with three fast-growing tree species: pitch/loblolly pine (*Pinus rigida x Pinus taeda*) in the drought-prone portion, American sycamore (*Plantanus occidentalis* L.) in the well-

drained portion, and cottonwood (*Populus deltoides* W. Bartram ex Marshall) in the poorly

drained portion of the study site (Figure 1). Furthermore, two forage-species treatments were

established in the tree-row alleys, which included a cool-season species [orchardgrass (*Dactylis*

glomerata L., var. Tekapo)] that was seeded in Fall 2015 at 17 kg pure live seed (PLS) ha^{-1} and a

native warm-season mix [8:1:1 big bluestem (*Andropogon gerardii* Vitman), little bluestem

(*Schizachyrium scoparium* {Michx. Nash}, indiangrass (*Sorghastrum nutans* L.)] seeded in

spring 2016 at 10 kg PLS ha^{-1} (Figure 1). To remove any existing vegetation from the alleys

before forage establishment, Cornerstone$^®$ Plus (N-[phosphonomethyl] glycine, Winfield

Solutions, St. Paul, MN) was applied at a 2.2 kg ha^{-1} rate [41% active ingredient (ai)].

Additionally, a Haybuster 107C no-tillage drill (DuraTech, Jamestown, ND) was used to plant

the alleys and Plateau^{TM} (ammonium salt of imazapic) was applied after establishment at a rate

of 0.28 kg ha^{-1} (23.6% ai) to remove any remaining non-forage vegetation.

Fertilizer Applications

Between 2001 and 2007, except for 2005, 50 to 76 kg nitrogen (N) ha^{-1}, as ammonium

nitrate (NH_4NO_3), and 3.9 to 6.7 Mg PL ha^{-1} were broadcast applied over the western and eastern

halves, respectively, of the AF site each spring (Figure 2) [27]. In 2005, NH_4NO_3 and PL were

applied in the spring and fall at rates of 123 kg N ha^{-1} and 8.9 Mg PL ha^{-1} to evaluate the impacts

of nutrient source on soil physiochemical properties [27]. Additionally, annual applications of

Osmocote (The Scotts Miracle-Grow Co., Marysville, OH), a slow-release fertilizer that

contained 5.6, 2.4, and 4.6 g of N, phosphorus (P), and potassium (K), respectively, began in

June 2004 and were surface-applied to the surrounding ground near each tree [27]. Between

2016 and 2021, trees were annually fertilized in the spring/summer with variable rates and

combinations of NH_4NO_3 or a 32-0-0 fertilizer blend, a 13-13-13 fertilizer (Greenkeeper's Secret 13-13-13 Premium Fertilizer, T&M, Inc., Foristell, MO), and gypsum ($CaSO_4$). The 2016 to 2021 tree fertilizer application rates were based on the nutrient concentrations of 2016 soil samples and the fertilizer combinations applied to the trees were based on fertility treatment. Further information regarding the 2016 to 2021 tree fertilization scheme was previously summarized [28].

Native grass (NG) and orchardgrass (OG) forage treatments in the alleys between tree rows (15 m wide) received 84 kg N ha^{-1} (4.94 Mg ha^{-1}, fresh weight basis) of locally sourced PL in March 2017 and 2018 and April 2019 (Figure 2). The PL in the 2017 application had a chemical composition of 2.7, 0.7, and 1.1 % N, P, and K, respectively, and had a pH of 6.1. The PL in the 2018 application had a chemical composition of 2.0, 0.6, and 1.0 % N, P, and K, respectively, and had a pH of 6.2. The PL in the 2019 application had a chemical composition of 2.5, 0.7, and 0.9 % N, P, and K, respectively, and had a pH of 5.2. Afterward fertilization each year, heifers (*Bos taurus* L.) grazed the study site at a density of 1.9 animal units (AU) ha^{-1} from May to June 2017, 2.2 AU ha^{-1} from May to July 2018, and 2.4 AU ha^{-1} from May to July 2019 [25,29,30]. On 30 March 2020 and 31 March 2021, urea (46-0-0) was applied to all alleys at a rate of 67.3 kg N ha^{-1} with a fertilizer spreader (Willmar S500;. Duluth, GA).

Survey Equipment

A Trimble R2 global positioning system (GPS) unit (Trimble Inc., Westminster, CO) and a DUALEM-1S sensor (DUAL□geometry Electro□Magnetic; Dualem Inc., Milton, ON, Canada) were used to collect the EMI-EC$_a$ measurements. The DUALEM-1S has a 3000 mS m^{-1} conductivity range and a 9-kHz transmitter with two receivers that have different orientations

[9,31]. The first receiver and the transmitter have a 1-m separation and both use vertical dipoles in horizontal coplanar geometry (HCP) [9,31]. The second receiver and the transmitter have a 1.1-m separation and use a vertical and horizontal dipole in the perpendicular geometry (PRP) [9,31]. The depths of exploration (DOE), which is defined as the depth to which an array accumulates 70% of its total sensitivity, were ~ 0.5 and 1.6 m for the PRP and HCP, respectively. Thus, the PRP measures the bulk EC_a of the 0 to 0.5-m depth the HCP measures the bulk EC_a of the 0 to 1.6-m depth [9,31]. Furthermore, a Can-Am Side-by-Side (Defender, BRP US, Inc., Sturtevant, WI) was used to power the DUALEM-1S through a 12-V, direct current (DC) battery and pull the DUALEM-1S on a sled during each survey. The DUALEM-1S's EMI-EC_a measurements were transmitted serially through a 9-socket, DB-9 connector port, and were obtained simultaneously with the GPS data though a hand-held geoinformation system program (HGIS; HGIS version 10.90, StarPal Inc., Fort Collins, CO) on a Trimble Yuma 2 rugged tablet computer (Trimble Inc., Westminster, CO) [9,31].

Survey Procedures EC_a Data Processing

Between August 2020 and July 2021, 12, mid-monthly EC_a-surveys were conducted at the AF site. To minimize temperature drift effects on the DUALEM-1S signal during surveying, the DUALEM-1S was powered on 30 minutes before each survey began to allow the DUALEM-1S to reach ambient temperature, and the EC_a surveys were conducted in the early morning. The DUALEM-1S was suspended in a plastic sled, 12.7 cm above the sled bottom, and the center of the DUALEM-1S was located 4.15 m behind the Trimble R2 GPS unit, where the front of the DUALEM-1S was located 2.1 m behind the side-by-side. For each survey, the DUALEM-1S was pulled at a rate of 4.8 to 8.0 km hr^{-1} in a looping pattern over two alleys at a time until four

parallel drive paths, 2 to 5 m apart, per alley had been completed. The DUALEM-1S was kept >

1 m away from any metal objects and unnecessary stops were avoided while each survey was

being conducted. Once each survey had been completed, a temperature-drift calibration line was

driven over all subsequent survey drive paths so that any measurement drift that occurred during

the survey period due to increases in internal temperature could be assessed and accounted for.

The temperature-drift calibration line was conducted in a sideways "V" shape, where the

calibration line began in the northwest corner and ended in the southwest corner of the site, with

the midpoint being around the eastern edge of Row 8 or 9 (Figure 1). After each EC_a survey was

conducted, the PRP and HCP EC_a of each survey underwent data cleaning, GPS-coordinate

adjustment, outlier removal, temperature-drift calibration, temperature standardization to 25°C,

averaging of coincidental points, experimental semi-variogram modeling, and universally-

kriging to a 5-m resolution. A 5-m resolution was chosen to be consistent with the resolution of

previous studies at the AF's site [18]. Specific details of the EC_a survey data processing

procedures were previously described [22]. The PRP and HCP EC_a of the 12, mid-monthly

surveys conducted were averaged to produce a single EC_a data file per configuration for the

analyses. Hereafter, the mean PRP and HCP EC_a of the 12 universally kriged surveys are

referred to as PRP and HCP EC_a, respectively.

Tree and Forage Data Collection

On 9 December 2020, the diameter at breast height (DBH) of the trees were measured at

137 cm above the soil surface [18,32]. Additionally, a hand-held clinometer (SS011096010;

Suunto; Vantaa, Finland) was used 12.2 m from each tree trunk to measure the angle to the

highest point on each tree on 15 March 2021. The angle's tangent was then used to calculate the vertical tree height (TH), with the clinometer operator's eye height added to Equation (1):

$$Tree\ height = (\tan(clinometer\ angle) \times distance\ from\ trunk) +$$

$$eye\ height\ of\ clinometer\ operator \tag{1}$$

During Summer 2018 and 2019, 4-m^2 cattle exclosures, three for each forage species-fertility treatment combination, were placed in alley centers to exclude forage areas from cattle grazing (Figure 2) [18,29,32]. Two, 0.25-m^2 forage total biomass subsamples were collected from each cattle exclosure on multiple occasions in 2018 and 2019 [18,29,32]. In 2018, forage biomass samples were collected on 25 May and 4, 15, and 29 June. In 2019, forage biomass samples were collected on 4 and 20 June and 3 July (n = 54 per timepoint). Forage samples were obtained by hand clipping aboveground biomass 6 cm above the soil surface [18,29,32]. Afterward, forage samples were geo-referenced, weighed, oven-dried at 70°C for 48 hr, and reweighed for moisture content and dry matter determinations [18,29,32].

Terrain Attribute and Soil Management Zone Data Collection

Terrain attribute data for the study site was obtained from a bare-earth digital elevation model (DEM) that was originally derived from Light Detection and Ranging (LiDAR) imagery [33]. The DEM had a 5-m resolution and was obtained from the United States Department of Agriculture's Natural Resources Conservation Service (USDA-NRCS) Geospatial Data Gateway [34], where the DEM was used to extract 14 terrain attributes within in System for Automated Geoscientific Analysis (SAGA GIS; SAGA GIS version 7.9.0) [35] and ArcGIS platforms (ArcGISmap version 10.6.1, Esri, Redlands, CA) [33]. The 14 terrain attributes and their

abbreviations, definitions, and summary statistics are presented in Table 1 and their spatial

pattern across the AF site can be visualized in Figure 3.

Furthermore, recently created EC_a-derived SMZs [22] were used for this study. The same

12 EC_a surveys used for the current study were used to create three precision SMZs at the AF

site [22] using the k-means clustering algorithm [36] by overlaying and grouping HCP and PRP

EC_a surveys [22]. Only the SMZs created by the HCP EC_a were used, as the SMZs created by the

PRP EC_a were less cohesive and presented less manageable SMZs as the HCP EC_a SMZs. Of the

three SMZs, SMZ 1 generally had the smallest mean EC_a and EC_a variability and was

characterized as an area of shallower depth to bedrock, increased coarse fragment abundance,

and an area of erosion rather deposition (Figure 2) [22]. Additionally, SMZ 2 generally had the

largest mean EC_a and EC_a variability of the three SMZs and contained the local drainageway and

areas of potential subsurface water movement [22].

Statistical Analyses

Correlation analyses were conducted with the collected EC_a and tree, forage, and terrain

attribute measurements to identify potential linkages among variables within treatment

combinations. Specific correlations conducted in this study were among 1) PRP and HCP EC_a

and TH, DBH, and total forage yield within the whole AF site and each SMZ, 2) PRP and HCP

EC_a and TH, DBH, and total forage yield within tree/forage species and 2001-2007 PL/N-

fertilizer treatment combinations within the whole AF site and each SMZ, 3) correlations among

PRP and HCP EC_a and total forage yield within forage species and 2017-2019 PL/control

treatment combinations within the whole AF site, and 4) correlations among PRP and HCP EC_a

and the terrain attribute data within the whole AF site and each SMZ. Pearson correlations were

performed between EC_a and plant properties (i.e., total forage yield, TH, and DBH) because the

plant properties were generally normally distributed, while Spearman correlations were

conducted between terrain attributes and EC_a because both EC_a configurations were generally

non-normally distributed. Additionally, multi-linear regression (MLR) models were applied over

the PRP and HCP EC_a to identify terrain attributes that had an effect on PRP and HCP EC_a, and

to determine which terrain attributes contributed the most to overall PRP and HCP EC_a

variability using terrain attributes' percent of total sum of squares within the MLR model.

Significance in the MLR models were judged at $P \leq 0.05$ and all statistical analyses were

conducted in R Studio (version 4.05, R Core Team, Boston, MA).

Results and Discussion

PRP and HCP EC_a

Correlations ($P < 0.05$) were identified between measured EC_a and tree growth (i.e., DBH

and TH), forage yield, and terrain attributes for both configurations (HCP and PRP; Figure 4).

The PRP EC_a ranged from 1.8 to 18.0 mS m^{-1} and averaged 5.9 mS m^{-1}, while the HCP EC_a

ranged from 3.1 to 25.8 mS m^{-1} and averaged 9.9 mS m^{-1} (Figure 4). For both the PRP and HCP

EC_a, maximum EC_a occurred within the local drainageway or areas of potential groundwater

movement [22], which was characterized by the trail of elevated EC_a that started in the northwest

corner, peaks in the center (Rows 5 to 7) and extends eastward, and dissipates towards bottom

middle of the AF site (Figures 1 and 4). The minimum EC_a for both the PRP and HCP occurred

within the areas of shallower depth to bedrock, increased coarse fragment abundance, and areas

of erosion rather than deposition [22], which were characterized by reduced EC_a occurring in the

western/southwestern portion of the AF site (Figure 4). Additional information regarding the

experimental semi-variogram parameters, models, summary statistics, and spatial pattern of the 12, universally kriged PRP and HCP EC_a that were averaged and used to create PRP and HCP EC_a maps are available in Ylagan et al. [22].

Correlations Among EC_a and Forage and Tree Data

Whole-site Correlations

Within the whole AF site, total forage yield did not have the same relationship to EC_a as the tree data (Table 2). The forage yields ranged from 284 (OG, 15 June 2018) to 6,387 kg ha^{-1} (NG mix, 3 July 2019), tree DBH ranged from 0.50 (pine) to 45.7 cm (oak), and TH ranged from 0.9 (pine) to 22.7 m (cottonwood). Forage yield was unrelated ($P > 0.05$) with either the PRP or HCP EC_a (Table 2). However, both DBH ($r = 0.34$ and 0.21) and TH ($r = 0.54$ and 0.42) were moderately, positively ($P < 0.05$) related with both the PRP and HCP EC_a, respectively, where the PRP EC_a had stronger relationships with tree properties than the HCP EC_a (averaged across DBH and TH, $r = 0.44$ and 0.32, respectively; Table 2). The positive relationship between the EC_a and tree properties at the whole-site level were likely the result of factors that increase EC_a and plant productivity (Table 2). Specifically, some of the largest measured EC_a values occurred within the local drainage way of the AF site [22] and were likely the result of the accumulation of transported water, nutrients/salinity, OM, and sediment from overland flow over time [10]. Increases in the SWC, nutrients, and OM also have the potential to increase plant productivity. Thus, increases in soil properties, such as SWC, nutrients, and OM, likely resulted in the positive relationship between the EC_a and DBH and TH for both EC_a configurations (Table 2).

Correlations were also conducted among EC_a and tree/forage data for the tree/forage species and 2001-2007 fertility treatment combinations, where only 10 of 72 total combinations

had a significant relationship (Tables 3 and 4). Tree height was moderately, negatively ($P < 0.05$) correlated with the PRP and HCP EC_a within the oaks treated with the 2001-2007 fertilizer-N applications ($r = -0.53$ and -0.46, respectively) and was also moderately, negatively ($P < 0.05$) within the oaks treated with 2001-2007 PL applications ($r = -0.53$ and -0.46, respectively; Tables 3 and 4). Within the pecans with 2001-2007 fertilizer-N applications, DBH was moderately, positively ($P < 0.05$) correlated with PRP and HCP EC_a ($r = 0.59$ and 0.56, respectively) and TH was also moderately, positively ($P < 0.05$) correlating the PRP and HCP EC_a ($r = 0.37$ and 0.36, respectively; Tables 3 and 4). Forage yield of the NG mix within the 2001-2007 fertilizer-N application areas was moderately, positively ($P < 0.05$) correlated with the PRP EC_a ($r = 0.48$; Tables 3). However, there was a moderate, negative ($P < 0.05$) correlation between forage yield of the OG within the 2001-2007 PL application areas and the HCP EC_a ($r = -0.44$; Tables 4). Additionally, there were no relationships between forage yield and EC_a for any of the eight EC_a configuration (PRP or HCP), forage species (NG mix or OG), and 2017-2019 fertility (PL or no fertilizer control) treatment combinations (Table 5).

The moderate, negative relationships between both the PRP and HCP EC_a and TH of the oaks that were within the 2001-2007 fertilizer-N and PL application areas were likely the result of soil properties that increase measured EC_a and decrease plant productivity (Tables 3 and 4). Jiang et al. [18] collected 51, 0-15-cm soil core samples from the tree-row alleys at the same AF site as used in the current study using a 3.3-cm-diameter soil core and used the Soil-Land Inference Model (SoLIM) to create interpolated maps of different soil properties across the AF site. The BD map that Jiang et al. [18] created displayed elevated BDs (1.45 to 1.70 g cm^3) across the oak area. Not only can increased BD cause increased measured EC_a through increased solid conductance pathways [10], but increased BD can also reduce plant growth, as increased

BD decreases soil water-holding capacity, air and water movement, microbial activity, and restricts root growth. Thus, elevated soil BD likely resulted in the negative relationship between the EC_a and the TH of the oaks that were within the 2001-2007 fertilizer-N and PL application areas (Tables 3 and 4).

It is unclear why there were moderate, positive relationships between the both the PRP and HCP EC_a and DBH and TH of the pecans within the 2001-2007 fertilizer-N application areas (Tables 3 and 4). However, perhaps because the pecans on the fertilizer-N side received less overall nutrient inputs than the PL side during the 2001-2007 period, pecan tree growth on the fertilizer-N side was more related to the inherent soil properties, including EC_a, than the pecan tree growth that occurred on the side that received PL (Tables 3 and 4). It is also unclear why there was a moderate, positive relationship between the PRP EC_a and forage yield of the NG mix in the 2001-2007 fertilizer-N application area, or why there was a moderate, negative relationship between the HCP EC_a and forage yield of the OG in the 2001-2007 PL application area (Tables 3 and 4). However, perhaps the relationships are dependent on other soil, terrain, or plant properties that were not assessed, rather than a lasting effect from the 2001-2007 fertilizer applications.

SMZ Correlations

Within a SMZ, relationships among EC_a and forage and tree data were generally similar between both EC_a configurations. Within SMZ 1, forage yield was unrelated ($P > 0.05$) to either PRP or HCP EC_a (Table 2). However, forage yield was moderately, positively ($P < 0.05$) correlated with both the PRP and HCP EC_a within SMZ 2 ($r = 0.52$ and 0.54, respectively; Table 2). Within SMZ 3, forage yield was moderately, negatively ($P < 0.05$) correlated with the HCP

EC$_a$ ($r = -0.51$), but was unrelated to the PRP EC$_a$ (Table 2). Within SMZ 1, both DBH and TH

were moderately, positively ($P < 0.05$) correlated with the PRP EC$_a$ ($r = 0.37$ and 0.35,

respectively), but was weakly, negatively ($P < 0.05$) correlated with the HCP EC$_a$ ($r = -0.20$ and

-0.22, respectively; Table 2). Of the tree and EC$_a$ data within SMZ 2, there was only a weak,

positive ($P < 0.05$) correlation between TH and PRP EC$_a$ ($r = 0.26$; Table 2). Only DBH was

weakly, negatively ($P < 0.05$) correlated with HCP EC$_a$ within SMZ 3 ($r = -0.22$; Table 2).

The weak to moderate, positive correlations between PRP EC$_a$ and DBH and TH in SMZ

1, the PRP EC$_a$ and the TH and forage yield in SMZ 2, and the HCP EC$_a$ and forage yield in

SMZ 2 were potentially the result of topographic features and soil properties that increase EC$_a$

and plant productivity (Table 2). Soil management zone 1 contains the greatest change in slope

(Figures 2 and 3) and SMZ 2 includes the local drainage way at the site. Overland flow causes

water and transported materials (i.e., sediment, nutrients, and OM) to be deposited downslope

and in depressional areas. Accumulation of transported material over time can result in increased

soil moisture, nutrient, clay, and OM contents, all of which can increase measured EC$_a$ and can

increase plant productivity [10]. Thus, the positive relationships between EC$_a$ and DBH, TH, and

forage yield in SMZ 1 and 2 were likely the result of transported materials increasing both EC$_a$

and plant growth (Table 2). Additionally, Ashworth et al. [25] observed cattle spent less time

grazing forages that were located within the drainage way at the AF site between 2017 and 2019.

Furthermore, it is unclear why there was a negative correlation between the HCP EC$_a$ and DBH

and TH within SMZ 1, as the PRP EC$_a$ and DBH and TH within SMZ 1 were positively

correlated (Table 2). Using the AF site's BD map created by Jiang et al. [18], SMZ 3 contains

more areas of elevated BD ($\sim$1.5 to 1.7 g cm^{-3}) than the other SMZs (Table 2; Figure 2). Elevated

BD can cause increased EC$_a$ measurements and can cause decreased plant productivity [10];

thus, the elevated BD within SMZ 3 likely resulted in the negative correlations between HCP EC_a and DBH and forage yield (Table 2).

Although tree growth properties and forage yield were not correlated to EC_a in all correlation groups evaluated (i.e., within the whole-site, SMZs, and species and fertility treatments), EC_a-tree and -forage correlations were established. Thus, the hypothesis that EMI-EC_a data will be correlated with forage yield and tree growth characteristics was confirmed within some, but not all correlation groups. Additionally, the EC_a-tree and -forage correlations demonstrated that relationships between EC_a and plant growth properties can vary from whole-site relationships and become explanatory (i.e., forage yield) when separated into SMZs (Table 2). As a result, using EC_a to describe plant growth variability in AF systems is potentially more effective within SMZs because more accurate EC_a-plant relationships can be established within sub-regions at a site that contain specific landscape features, soil properties, or EC_a ranges. However, the relationship strength (i.e., $|r|$) of the whole-site, EC_a-tree-property relationships, averaged across tree property (DBH and TH) and EC_a configuration, $r = 0.38$, was stronger than the relationship strength of SMZ EC_a-tree-property relationships, averaged across tree property, EC_a configuration, and SMZ, $r = 0.27$ (Table 2). Thus, the hypothesis that correlations among EMI-EC_a and total forage yield and tree growth data can be improved with EC_a-derived SMZs was confirmed for forage yield in some SMZs, but not for tree growth in any SMZ.

Correlations Among EC_a and Terrain Attributes

Whole-site Correlations

Most terrain attributes had correlations ($P < 0.05$) with EC_a; however, there were a few differences in the terrain attributes' relationships with both EC_a configurations. Specifically, both

NormHt and TPI identify areas of higher or lower relative elevation, and SlopeHt and VDistChn identify areas of increased height of above modeled drainage accumulation or channel network, respectively (Table 1) [37]. Additionally, LS-factor, which incorporates SlopePer, identifies areas of increased erosion potential, FlowAccum identifies where runoff accumulates, MRVBF identifies depositional areas, and SAGAWI identifies areas in valley floors with an increased potential of water accumulation (Table 1) [37]. Soil constituents (i.e., sediment, OM, nutrients, and water), which greatly contribute to EC_a [10], are eroded and/or transported from upslope positions and are deposited downslope in valley, depressional, and flow accumulation areas over time. The accumulation of soil constituents downslope and in depressional areas often results in these areas having greater EC_a than higher elevation areas and/or areas with increased erosion [22,38]. Thus, the negative relationships that NormHt, TPI, and SlopeHt had with the PRP EC_a; the negative relationships that LS-Factor, SlopePer, and VDistChn had with the PRP and HCP EC_a; and the positive relationships that FlowAccum, MRVBF, and SAGAWI had with the PRP and HCP EC_a within the whole AF site were likely the result of the terrain attributes identifying areas where increased soil erosion and deposition/accumulation occur, which decreased and increased EC_a measurements, respectively (Tables 1 and 6).

Other explanations for the relationships between terrain attributes and EC_a were not as obvious. Specifically, the weak, positive correlations between Aspect and both PRP and HCP EC_a were unexpected, as the mean and median slope aspect of the AF site were 185 and 189°, respectively, making the AF site primarily south facing (Tables 1 and 6). Additionally, it is unclear why there were weak, positive correlations between Elevation, NormHt, and SlopeHt and HCP EC_a, and a weak, negative correlation between ValleyDep and HCP EC_a (Tables 1 and 6). Specifically, it can be expected that EC_a will likely decrease with increasing elevation and

distance from valleys and drainage ways, as there would be decreasing EC_a-contributing soil

properties (i.e., clay, OM, nutrients, and water content, soil water-holding capacity, and soil

depth) from erosional forces removing and depositing soil constituents downslope and in

depositional areas [22,38]. However, the weak, positive correlations between Aspect and both

the PRP and HCP EC_a and between Elevation and HCP EC_a within the whole AF site (Table 6)

were similar to the result of Kitchen et al. [19]. Kitchen et al. [19] conducted an EC_a survey on a

13-ha field in Boone County, Missouri that had been previously planted with corn (*Zea mays* L.)

and soybean (*Glycine max* L.) and was mapped as Mexico (Aeric Vertic Epiaqualfs) and Adco

(Vertic Albaqualfs) soil series. The shallow EC_a (0-30 cm) had a positive relationship with

aspect ($r = 0.41$), while the deep EC_a (0-100 cm) had a positive relationship with aspect and

elevation ($r = 0.26$ and 0.37, respectively) [19].

The terrain attribute MidSlope identifies the mid-slope position between the greatest and

lowest elevation in the defined landscape (Table 1). The weak, negative correlation between the

MidSlope and both PRP and HCP EC_a was an indication that EC_a decreased with increasing

distance from the mid-slope position, vertically up- or down (Tables 1 and 6). However, the

negative relationship between the MidSlope and EC_a was likely a result of some of the largest

EC_a values at the AF site occurring within the local depressional area in the drainage way, which

was located within or just around the mid-slope position of study site (Figures 3 and 4; Table 6).

SMZ Correlations

Correlations between EC_a and terrain attributes within the SMZs differed from the whole-

site results and varied between SMZs and EC_a configuration (Table 6). Specifically, no terrain

attribute had a consistent relationship with the HCP EC_a across all three SMZs, whereas eight

terrain attributes had consistent relationships with PRP EC_a across all three SMZs (i.e., Elevation, LS-Factor, MRVBF, NormHt, SlopeHt, SlopePer, TPI, and ValleyDep; Tables 1 and 6). The PRP EC_a had 4 to 10 more significant correlations to the terrain attributes than the HCP EC_a in each of the SMZs (Tables 1 and 6). Additionally, all 15 correlations between terrain attributes and HCP EC_a within SMZs were weak ($|r| < 0.30$), whereas the 75% of the 36 significant correlations between the terrain attributes and the PRP EC_a within the SMZs were moderate ($|r| \geq 0.30$; Tables 1 and 6). In all instances where both the PRP and HCP EC_a had a significant relationship with the same terrain attribute within the SMZs, the absolute value of the correlation coefficient was numerically greater from the PRP than the HCP EC_a (Tables 1 and 6). The increased quantity and strength of correlations between the terrain attributes and PRP EC_a, compared to HCP EC_a, was likely a result of the 0-0.5 m soil depth and its properties being more associated with the surface terrain attributes and the landscape-level process that they influence (i.e., overland flow, erosion, deposition, accumulation, and sunlight exposure) than the 0-1.6 m soil depth. The differences between the terrain attributes' relationships with the PRP and/or HCP EC_a across SMZs, and between the SMZs and whole site, were likely a result of different terrain attributes affecting the soil and its properties, including EC_a, to different degrees and depths within the configuration boundaries.

Because terrain-attribute-EC_a correlations were established within both the whole-site and SMZs, the hypothesis that EMI-EC_a data will be correlated with terrain attributes was confirmed. Additionally, when terrain attributes had a relationship with PRP EC_a for the whole-site and all SMZs (i.e., LS-Factor, MRVBF, NormHt, SlopeHt, SlopePer, and TPI), the strength of the relationships between the terrain attributes and the PRP EC_a were 9 to 205% greater for

the SMZs than for the whole-site (Table 6). Thus, the hypothesis that correlations among EMI-EC$_a$ and terrain attribute data can be improved with EC$_a$-derived SMZs was confirmed.

Terrain Attribute MLR Model on EC$_a$

Whole-site MLR Models

The relationships among the terrain attributes and EC$_a$ in the MLR models varied between EC$_a$ configurations and among the whole-site and SMZs (Tables 1 and 7). Within the whole-site, all terrain attributes were significant ($P < 0.05$) in the models for both the PRP and HCP EC$_a$; however, the degree to which the terrain attributes influenced (i.e., percent of total sum of squares) the whole-site PRP and HCP EC$_a$ variability varied (Table 7). Thus, the hypothesis that different terrain attributes would contribute to the EC$_a$ variability to different degrees within the AF site was confirmed. The terrain attributes LS-Factor, MidSlope, and ValleyDep had the greatest influence (i.e., largest percent of total sum of squares) on the PRP EC$_a$ variability (10.5, 9.4, and 7.2 %, respectively), with MRVBF and SAGAWI following closely behind (7.1 and 6.1 %, respectively; Tables 1 and 7). Alternatively, ValleyDep, SAGWAI, and MidSlope and the greatest influence on the HCP EC$_a$ variability (15.3, 11.9, and 11.2 %, respectfully; Tables 1 and 7).

With exception of MidSlope, the terrain attributes that had the greatest influence on the EC$_a$ variability across the whole AF site were likely due to the effect of topography and climate and the properties the terrain attributes describe (Table 7). As previously mentioned, the effect of MidSlope on EC$_a$ was more likely due to some of the largest EC$_a$ values at the AF site occurring within the local depressional area in the drainage way, which is located within or just around the mid-slope position of study site (Figures 3 and 4; Tables 1 and 7). The study site has variable

126

topography (8-m elevation change and < 9.1 % slope gradient) and is located in the humid

subtropics, where the AF site receives a large amount of precipitation annually [1156 mm, 30-yr

means (1981 to 2010)] [26]. As a result of the AF site's elevation change and level of

precipitation, it can be expected that some of the largest contributors to the development of soils

and their properties, including EC_a, to be dominated by alluvial- and colluvial-related processes

(i.e., erosion upslope and translocation and deposition downslope) within the local scale. Thus,

because LS-Factor depicts erosional areas and MRVBF, SAGAWI, and ValleyDep depict

depositional and water accumulation areas, it was expected that LS-Factor, MRVBF, SAGAWI,

and ValleyDep be large contributors to the EC_a variability at this AF site (Tables 1 and 7).

SMZ MLR Models

Unlike the whole-site MLR models, neither EC_a configuration was influenced ($P < 0.05$)

by all terrain attributes in any of the three SMZs (Tables 1 and 7). Within SMZ 1, Aspect,

Elevation, FlowAccum, LS-Factor, MRVBF, SAGAWI, SlopeHt, ValleyDep, and VDistChn

were significant in the model for PRP EC_a, where MRVBF, LS-Factor, and SlopeHt had the

greatest influence on the PRP EC_a variability (19.8, 18.2, and 3.0 %, respectively; Tables 1 and

7). Alternatively, except for VDistChn, all other terrain attributes were significant in the model

for HCP EC_a in the SMZ 1, where MRVBF, NormHt, and LS-Factor had the greatest influence

on the HCP EC_a variability (9.0, 5.5, and 5.4 %, respectively; Tables 1 and 7). Furthermore,

within SMZ 2, except for SAGAWI, ValleyDep, and VDistChn, all other terrain attributes were

significant in the model for PRP EC_a, where Aspect, SlopePer, and MidSlope had the greatest

influence on the PRP EC_a variability (13.1, 8.8, and 7.1 %, respectively; Tables 1 and 7). Except

for LS-Factor, SAGAWI, and SlopeHt VD, all other terrain attributes in SMZ 2 were significant

in the model for HCP EC$_a$, where SlopePer, TPI, and NormHt had the greatest influence on the HCP EC$_a$ variability (7.8, 5.5, and 5.3 %, respectively; Tables 1 and 7). Additionally, within SMZ 3, Elevation, FlowAccum, LS-Factor, MRRTF, MRVBF, NormHt, SAGAWI, SlopeHt, and SlopePer were significant in the model for PRP EC$_a$, where LS-Factor, FlowAccum, and MRRTF had the greatest influence on the PRP EC$_a$ variability (13.8, 8.9, and 3.6 % respectively; Tables 1 and 7). Alternatively, Elevation, FlowAccum, LS-Factor, MidSlope, SAGAWI, SlopeHt, SlopePer, ValleyDep, and VDistChn were significant in the model for HCP EC$_a$ within SMZ 3, where MidSlope, SAGAWI, and ValleyDep had the greatest influence on the HCP EC$_a$ variability (7.6, 4.4, and 3.7 %, respectively; Tables 1 and 7).

Similar to the terrain attribute-EC$_a$ correlations within the SMZs (Table 6), the terrain attributes that had a significant influence on the EC$_a$ variability varied across the SMZs and between the EC$_a$ configurations (Tables 1 and 7). Thus, the hypothesis that different terrain attributes would contribute to the EC$_a$ variability to different degrees across the SMZs was confirmed. The terrain attributes that had no or minimal influence on the PRP or HCP EC$_a$ variability within the SMZs were likely the result of those terrain attributes having minimal variability within the SMZs, or terrain attributes other than the ones evaluated being the dominant factor(s) influencing EC$_a$ within SMZs (Tables 1 and 7). Furthermore, Elevation, FlowAccum, LS-Factor, MRVBF, and SlopeHt had a consistent influence on the PRP EC$_a$ variability across the SMZs, whereas Elevation, FlowAccum, MidSlope, SlopePer, and ValleyDep had a consistent, significant influence on the HCP EC$_a$ variability across the SMZs (Tables 1 and 7). Additionally, unlike the whole-site MLR models, the terrain attributes that had a significant effect on the EC$_a$s in the SMZ MLR models were able to describe 10.2 to 17.9% more of the PRP variability than the HCP variability (Tables 1 and 7). Alternatively, in the

whole-site MLR models, the terrain attributes were able to describe 10.3% more of the HCP EC_a variability than the PRP EC_a variability (Tables 1 and 6).

Because this study site was relatively small (4.25 ha), the factors that likely influenced the overall study site's soil, and thus EC_a, variability also likely contributed to the SMZs' EC_a variability. Additionally, many of the terrain attributes that were the greatest contributors to PRP and HCP EC_a variability in the SMZs were, or were similar to, the terrain attributes (i.e., LS-Factor, MRVBF, SAGAWI, and ValleyDep) that had the greatest contribution to the EC_a variability across the whole site. The terrain attributes that were the largest contributors to the EC_a variability in the SMZs included ones that identified areas of higher and/or lower elevation (NormHt, TPI, and SlopeHt), depositional/accumulation (MRVBF, FlowAccum, SAGAWI, and ValleyDep), and increased erosion potential (LS-Factor and SlopePer; Tables 1 and 7).

Although the correlations and MLR models between the terrain attributes and EC_a were slightly different methods, both provided similar, useful information on what terrain attributes were related and significant influencers on the site's EC_a. The correlations between the terrain attributes and EC_a assessed whether there was an individual relationship between the terrain attributes and EC_a, whereas the MLR models evaluated which terrain attributes had the largest impact on EC_a. Additionally, the MLR models demonstrated that, even though terrain attributes may have an individual relationship with EC_a, the terrain attributes may not be contributors to the overall EC_a variability when evaluating all terrain attributes together. The MLR models also demonstrated that the largest contributors to the overall EC_a variability can vary when assessed at different soil depths or when separated into SMZs with potentially specific EC_a ranges, landscape features, or soil properties.

129

Evaluating the relationships between EC_a and plant responses in limited EC_a-investigated systems (i.e., AF) is essential for determining if, when, and what agronomic systems EMI-EC_a sensing is a useful tool for assessing plant property variations. Additionally, quantifying plant-soil-terrain relationships is necessary for efficient management and maximization of AF systems' potential [33]. Terrain attributes control soil formation by dictating water and energy flow across landscapes and have the potential to have a greater influence on tree growth than soil properties [18,33]. Understanding the relationships between terrain attributes and EC_a allows for better contextualization of spatial EC_a measurements. Furthermore, assessing field variability within SMZs, whether its soil property, EC_a, or terrain attribute variability, potentially allows for a better understanding of the causes of yield variability, allowing managers to adjust practices for each SMZ to improve yields while efficiently managing resources.

The relationships between the terrain attributes and plant properties were not assessed in this study because of previous work already completed. Jiang et al. [18] assessed the absolute growth rate (AGR) of the different tree species at the AF site compared to seven of the same terrain attributes used in this study (i.e., SlopePer, Aspect, FlowAccum, SAGAWI, MRRTF, MRVBF, and VDistChn). Excluding the pines, the AGR was calculated using the 2019 DBH for all tree species and the DBH in 2004 for pecans, BDH in 2005 for oaks, and DBH in 2016 for cottonwoods and sycamores [18]. Jiang et al. [18] reported positive correlations ($P < 0.05$) between MRRTF and the AGR for the oaks and pecans, between SAGAWAI and the AGR for the pecans and cottonwoods, between MRVBF and the AGR for the cottonwoods, and between VDistChn and the AGR for the oaks. Jiang et al. [18] also concluded that the terrain attributes had a greater effect on tree growth variability than soil properties within each tree species. In addition, Ashworth et al. [32] assessed the relationships between the same terrain attributes used

in the current study at 1-m resolution and the same forage samples used in the current study and annual DBH and TH measurements made between 2017 and 2019. Ashworth et al. [32] reported no correlation ($P > 0.05$) between any of the terrain attributes and either total forage yield or biomass accumulation. However, Ashworth et al. [32] reported moderate, negative correlations between SlopeHt and TH and DBH ($r = -0.44$ and -0.40, respectively) and a moderate, positive correlation between Aspect and DBH ($r = 0.40$).

Although not in AF systems, Kitchen et al. [19] conducted a study that assessed the relationship between EC_a, terrain attributes, and grain yield in three different soil-crop agroecosystems using correlations, forward stepwise regression, nonlinear neural network (NNs), and boundary-line analyses. A Veris model 3100 (Veris 3100 Division of Geoprobe Systems, Salina, KS) was used to collect EC_a measurements from the 0-30- and 0-100-cm soil depths and yield measurements were obtained between 1997 and 1999 from three different fields: Colorado (Ustic Haplargids), Missouri (Cumuic Haplustoll), and Kansas (Aeric Vertic Epiaqualfs) [19]. The crops produced at these fields during the study period were corn, soybean, grain sorghum [*Sorghum bicolor* (L.) Moench], and winter wheat (*Triticum aestivum* L.) and the terrain attributes used in the analyses were slope, curvature, and aspect [19]. Although many of the correlations between the yield data and the EC_a and terrain attributes were significant, it was concluded that the correlations were not that useful in describing yield variability [19]. Apparent EC alone better described yield variability than the terrain attributes in the regression (averaged over sites and years, $R^2 = 0.21$) and NNs analyses (averaged over sites and years, $R^2 = 0.17$) and the R^2 was generally increased when EC_a was combined with terrain attributes (averaged over sites and years, $R^2 = 0.32$) [19]. However, more information on additional terrain-attribute-EC_a relationships within AF and uninvestigated agroecosystems is necessary to further enhance

spatial EC_a characterization, field variability (i.e., soil and plant) prediction, and to improve EC_a-derived SMZs in precision agriculture.

Practical Implications

The EC_a-tree and -terrain-attribute correlations and MLR models provided useful information on using EMI-EC_a to describe and contextualize field variability in AF systems. Specifically, the stronger relationships between the PRP EC_a and tree properties at the whole-site level, compared to the HCP EC_a, are a potential indication that AF managers could describe the relationship between EC_a and tree growth variability to a greater extent using the PRP rather than the HCP EC_a. Additionally, the increased number and strength of significant terrain-attribute-PRP-EC_a relationships suggest that the EC_a variability, thus soil variability, in the 0-0.5-m soil depth can be better described by terrain attributes in AF systems with variable topography than in the 0-1.6-m soil depth. Furthermore, because the terrain attributes significantly related to the PRP EC_a generally had stronger relationships in the SMZs than the whole-site, AF managers can potentially better describe 0-0.5-m EC_a and soil variability with terrain attributes using EC_a-derived SMZs.

Conclusions

Electromagnetic induction-EC_a surveys and terrain attribute data have been used to assess field variability within a variety of land management systems and ecosystems across the world. However, no research has been conducted exploring relationships between EMI-EC_a and pasture forage yield, tree growth, and terrain attributes or whether the relationships could be improved with EC_a-derived SMZs within an AF system within an environment similar to the Ozark

Highlands. Due to this lack of information, the objectives of this study were to: i) identify correlations between EMI-EC_a and forage yield, tree growth, and terrain attribute data within the whole site and three EC_a-derived SMZs, ii) identify correlations between EC_a and total forage yield and tree growth data within forage/tree species and fertility treatment combinations, and iii) identify terrain attributes that contribute to EMI-EC_a variations at a 20-year AF system in the Ozark Highlands of northwest Arkansas. Results partially supported the hypothesis that EMI-EC_a data would be correlated with total forage yield and tree growth characteristics and supported the hypothesis that EMI-EC_a data would be correlated with terrain attributes. However, results did not support the hypothesis that correlations among EMI-EC_a and tree growth data can be improved with EC_a-derived SMZs. Results supported the hypothesis that correlations among EMI-EC_a and total forage yield and terrain attribute data can be improved with EC_a-derived SMZs. Results also supported the hypothesis that different terrain attributes would contribute to the EC_a variability to different degrees within the AF site and across the SMZs.

Results demonstrated that EC_a-tree, -forage, and -terrain attribute relationships can be established in AF systems in the Ozark Highlands and can vary with soil depth and when separated into EC_a-derived SMZs and management history (species and fertility treatments). Results also demonstrated that the largest contributors of EC_a/soil variability (i.e., terrain attributes) can vary with soil depth and when separated into EC_a-derived SMZs. Additionally, results demonstrated that the PRP EC_a can potentially have stronger and additional relationships with tree, forage properties, and/or terrain properties in AF systems than the HCP EC_a. Results also demonstrated that terrain attributes that identify areas of higher and/or lower elevation, deposition/accumulation, and increased erosion potential are potentially necessary to include

when developing yield-soil-terrain variability models in AF systems with variable topography and increased precipitation. Results provided further support and information on the potential versatility, applicability, and usefulness of EMI-EC$_a$ surveys for assessing and contextualizing in-field variability in a variety of ecosystems with different land management systems.

References

1. Johnson, C.K.; Mortensen, D.A.; Wienhold, B.J.; Shanahan, J.F.; Doran, J.W. Site-Specific Management Zones Based on Soil Electrical Conductivity in a Semiarid Cropping System. *Agron. J.* **2003**, *95*, 303–315.

2. Cicore, P.L.; Franco, M.C.; Peralta, N.R.; Marques da Silva, J.R.; Costa, J L. Relationship between Soil Apparent Electrical Conductivity and Forage Yield in Temperate Pastures According to Nitrogen Availability and Growing Season. *Crop Pasture Sci.* **2019**, *70*, 908–916.

3. Allered, B.J.; Adamchuck, V.I.; Viscarra Rossel, R.A.; Doolittle, J.; Freeland, R.S.; Grote, K.R.; Corwin, D.L. Geophysical Methods. *Encycl. Soil Sci.* **2016**, *3*, 1–8.

4. Soil Science Division Staff. Tools for Proximal Soil Sensing. In *USDA Handbook 18: Soil survey manual*; Ditzler, C., Scheffe, K., Monger, H.C., Eds.; Government Printing Office: Washington, D.C, 2017; pp 355–394.

5. Serrano, J.; Shahidian, S.; Silva, J. Spatial and Temporal Patterns of Apparent Electrical Conductivity: DUALEM vs. Veris Sensors for Monitoring Soil Properties. *Sensors* **2014**, *14*, 1–19.

6. Corwin, D.L.; Lesch, S.M. Apparent Soil Electrical Conductivity Measurements in agriculture. Comput. Electron. Agric. **2005**, *46*, 11–43.

7. Corwin, D.L.; Lesch, S.M. Characterizing Soil Spatial Variability with Apparent Soil Electrical Conductivity – Survey Protocols. Comput. Electron. Agric. **2005**, *46*, 103–133.

8. Garcia-Tomillo, A.; Miras-Avalos, J.; Dafonte-Dafonte, J.; Paz-Gonzalez, A. Mapping Soil Texture Using Geostatistical Interpolation Combined with Electromagnetic Induction Measurements. Soil Sci. **2017**, *182*, 278–284.

9. Abdu, H.; Robinson, D.A.; Boettinger, J.; Jones, S.B. Electromagnetic Induction Mapping at Varied Soil Moisture Reveals Field-Scale Soil Textural Patterns and Gravel Lenses. Front. Agric. Sci. Eng. **2017**, *4*, 135–145.

10. Corwin, D.L.; Scudiero, E. Field-Scale Apparent Soil Electrical Conductivity. In *Methods of soil analysis*; Logsdon, S., Ed.; Soil Science Society of America: Madison, WI, US, 2017; Volume 1*, pp 1–29.

11. Heil, K.; Schmidhalter, U. The Application of EM38: Determination of Soil Parameters, Selection of Soil Sampling Points and Use in Agriculture and Archaeology. *Sensors* **2017**, *17*, 1–44.

12. Johnson, C.K.; Doran, J.W.; Duke, H.R.; Wienhold, B.J.; Eskridge, K.M.; Shanahan, J.F. Field□scale Electrical Conductivity Mapping for Delineating Soil Condition. *Soil Sci. Soc. Am. J.* **2001**, *65*, 1829–1837.

13. Singh, G.; Williard, K.; Schoonover, J. Spatial Relation of Apparent Soil Electrical Conductivity with Crop Yields and Soil Properties at Different Topographic Positions in a Small Agricultural Watershed. *Agronomy* **2016**, *6*, 1–22.

14. Corwin, D.L.; Lesch, S.M.; Shouse, P.J.; Soppe, R.; Ayars, J.E. Identifying Soil Properties That Influence Cotton Yield Using Soil Sampling Directed by Apparent Soil Electrical Conductivity. *Agron. J.* **2003**, *95*, 352–364.

15. Altdorff, D.; Dietrich, P. Delineation of Areas with Different Temporal Behavior of Soil Properties at a Landslide Affected Alpine Hillside Using Time-Lapse Electromagnetic Data. *Environ. Earth Sci.* **2014**, *72*, 1357–1366.

16. Beucher, A.; Koganti, T.; Iversen, B.V.; Greve, M.H. Mapping of Peat Thickness Using a Multi-Receiver Electromagnetic Induction Instrument. *Remote Sens.* **2020**, *12*, 1–21.

17. Pedrera-Parrilla, A.; Martínez, G.; Espejo-Pérez, A.J.; Gómez, J. A.; Giráldez, J.V.; Vanderlinden, K. Mapping Impaired Olive Tree Development Using Electromagnetic Induction Surveys. *Plant Soil* **2014**, *384*, 381–400.

18. Jiang, Z.-D.; Owens, P.R.; Ashworth, A.J.; Ponce, B.F.; Thomas, A.L.; Sauer, T. Evaluating Tree Growth Factors into Species-Specific Functional Soil Maps for Improved Agroforestry System Efficiency. *Agrofor. Syst.* **2021**, *96*, 479–490.

19. Kitchen, N.R.; Drummond, S.T.; Lund, E.D.; Sudduth, K.A.; Buchleiter, G.W. Soil Electrical Conductivity and Topography Related to Yield for Three Contrasting Soil–Crop Systems. *Agron. J.* **2003**, *95*, 483–495.

20. Robinson, D.A.; Lebron, I.; Querejeta, J.I. Determining Soil-Tree-Grass Relationships in a California Oak Savanna Using Eco-Geophysics. *Vadose Zone J.* **2010**, *9*, 528–536.

21. Taghizadeh-Mehrjardi, R.; Minasny, B.; Sarmadian, F.; Malone, B.P. Digital Mapping of Soil Salinity in Ardakan Region, Central Iran. *Geoderma* **2014**, *213*, 15–28.

22. Ylagan, S.; Brye, K.R.; Ashworth, A.J.; Owens, P.R.; Smith, H.; Poncet, A. Using Apparent Electrical Conductivity to Delineate Field Variation in an Agroforestry System in the Ozark Highlands. *Remote Sens.* **2022**. Manuscript in Review.

23. Major Land Resource Areas. Available online: https://data.nal.usda.gov/dataset/major-land-resource-areas-mlra (accessed 29 June 2022).

24. Web Soil Survey. https://websoilsurvey.sc.egov.usda.gov/App/WebSoilSurvey.aspx (accessed 29 June 2022).

25. Ashworth, A.J.; Adams, T.C.; Kharel, T.; Philip, D.; Owens, P.R.; Sauer, T. Root Decomposition in Silvopastures Is Influenced by Grazing, Fertility, and Grass Species. *Agrosystems Geosci. Environ.* **2021**, *4*, 1–15.

26. Data Tools: 1981-2010 Normals. Fayetteville Experimental Station, AR US. Available online: https://www.ncei.noaa.gov/access/us-climate-normals/#dataset=normals-monthly&timeframe=81 (accessed 23 June 2022).

27.   Sauer, T.J.; Coblentz, W.K.; Thomas, A.L.; Brye, K.R.; Brauer, D.K.; Skinner, J.V.; Brahana, J.V.; DeFauw, S.L.; Hays, P.D.; Moffit, D.C.; Robinson, J.L.; James, T.A.; Hickie, K.A. Nutrient Cycling in an Agroforestry Alley Cropping System Receiving Poultry Litter or Nitrogen Fertilizer. *Nutr. Cycl. Agroecosystems* **2014**, *101*, 167–179.

28.   Ylagan, S.; Amorim, H.C.S.; Ashworth, A.J.; Sauer, T.; Wienhold, B.J.; Owens, P.R.; Zinn, Y.L.; Brye, K.R. Soil Quality Assessment of an Agroforestry System Following Long-Term Management in the Ozark Highlands. *Agrosystems Geosci. Environ.* **2021**, *4*, 1–15.

29.   Niyigena, V.; Ashworth, A.J.; Nieman, C.; Acharya, M.; Coffey, K.P.; Philipp, D.; Meadors, L.; Sauer, T.J. Factors Affecting Sugar Accumulation and Fluxes in Warm- and Cool-Season Forages Grown in a Silvopastoral System. *Agronomy* **2021**, *11*, 1–14.

30.   Gurmessa, B.; Ashworth, A.J.; Yang, Y.; Adhikari, K.; Savin, M.; Owens, P.R.; Sauer, T.J.; Pedretti, E.F.; Cocco, S.; Corti, G. Soil Bacterial Diversity Based on Management and Topography in a Silvopastoral System. *Appl. Soil Ecol.* **2021**, *163*, 1–10.

31.   Abdu, H.; Robinson, D.; Jones, S. Comparing Bulk Soil Electrical Conductivity Determination Using the DUALEM□1S and EM38□DD Electromagnetic Induction Instruments. *Soil Sci. Soc. Am. J.* **2007**, *71*, 189–196.

32.   Ashworth, A.J.; Kharel, T.; Sauer, T.; Adams, T.C.; Philip, D.; Thomas, A.L.; Owens, P.R. Spatial Monitoring Technologies for Coupling the Soil Plant Water Animal Nexus. *Sci. Rep.* **2022**, *12*, 1–14.

33.   Adhikari, K.; Owens, P.R.; Ashworth, A.J.; Sauer, T.J.; Libohova, Z.; Miller, D.M. Topographic Controls on Soil Nutrient Variations in a Silvopasture System. *Agrosystems Geosci. Environ.* **2018**, *1*, 1–15.

34.   Geospatial Data Gateway. Available online: https://datagateway.nrcs.usda.gov/ (accessed 23 June 2022).

35.   Conrad, O.; Bechtel, B.; Bock, M.; Dietrich, H.; Fischer, E.; Gerlitz, L.; Wehberg, J.; Wichmann, V.; Boehner, J. System for Automated Geoscientific Analyses (SAGA) v. 2.1.4. *Geosci. Model Dev.* **2015**, *8*, 1991–2007.

36.   Hartigan, J.A. *Clustering Algorithms*; John Wiley & Sons: Hoboken, NJ, US, 1975; pp 1–351.

37.   Spatial Data for Soil Mapping. Available online: https://www.nrcs.usda.gov/wps/PA_NRCSConsumption/download?cid=nrcseprd1079006&ext=pdf (accessed 26 July 2022).

38.   Zhu, Q.; Lin, H.; Doolittle, J. Repeated Electromagnetic Induction Surveys for Determining Subsurface Hydrologic Dynamics in an Agricultural Landscape. *Soil Sci. Soc. Am. J.* **2010**, *74*, 1750–1762.

Tables and Figures

Table 1. Summary of the abbreviations, definitions, units, and summary statistics [i.e., minimum (Min), maximum (Max), mean] for 14 terrain attributes describing an agroforestry site in the Ozark Highlands northwest Arkansas.

Terrain Attribute	Abbreviation	Definition	Unit	Min	Max	Mean
Aspect	Aspect	Direction of the steepest slope from the north	°	5.3	357.1	185.0
Elevation	Elevation	Height above sea level	m	379	387	382
Flow Accumulation	FlowAccum	Quantity of upland cells draining to a given cell	n[†]	25	21538	653
Slope-length Factor	LS-Factor	Calculates the slope length as used in the Universal Soil Loss Equation	m	< 0.01	0.74	0.22
Mid-slope Position	MidSlope	Classifies the slope position in both crest and valley directions	index	< 0.01	0.85	0.41
Multi-resolution Ridge Top Flatness Index	MRRTF	Identifies high flat regions at a range of scales	index	< 0.01	4.86	1.34
Multi-resolution Valley Bottom Flatness Index	MRVBF	Identifies zones of deposited material in flat valley bottoms	index	< 0.01	5.77	2.24
Normalized Height	NormHt	Assigns a value of 1 and 0 to the highest and lowest elevation, respectively	index	0.14	0.92	0.44
System for Automated Geoscientific Analysis Wetness Index	SAGAWI	A specific catchment area and slope-based wetness index	index	4.5	10.5	7.2
Slope Height	SlopeHt	Relative height difference to the immediate adjacent crest lines	m	0.35	4.67	1.46
Slope Percent	SlopePer	Maximum rate of change between a cell and its neighboring cells	%	0.02	9.10	3.02
Topographic Position Index	TPI	+ and - values identify cells that are higher and lower than their surroundings, respectively	index	-1.27	2.39	0.04
Valley Depth	ValleyDep	Relative height difference to the immediate adjacent channel lines	m	0.00	3.23	1.18
Altitude Above Channel Network	VDistChn	Difference between channel base and surface elevation	m	0.00	2.28	0.21

[†] Degrees from true north (°), Number of pixels (n).

Table 2. Summary of the number of observations (n) and resulting correlation coefficients (r) from Pearson linear correlations evaluating the relationship between the perpendicular (PRP) and horizontal coplanar geometry (HCP) apparent electrical conductivity (EC$_a$) and tree diameter at breast height (DBH), tree height, and total forage yield across multiple sampling dates in 2018 and 2019, within the whole-site and three EC$_a$-derived soil management zones (SMZs) [22], at an agroforestry site in the Ozark Highlands of northwest Arkansas. The location of the trees, forages, yield samples, and SMZs are presented on Figure 1 and 2.

| | | Tree Data[†] | | | | Forage Data[††] | |
| | | DBH | | Tree Height | | Total Yield | |
EC$_a$	Area	n	r	n	r	n	r
PRP	Whole-Site	417	0.34*	421	0.54*	84	0.01
	SMZ 1	188	0.37*	191	0.35*	39	-0.02
	SMZ 2	82	0.15	81	0.26*	17	0.52*
	SMZ 3	147	-0.13	149	0.16	28	-0.26
HCP	Whole-Site	417	0.21*	421	0.42*	84	-0.04
	SMZ 1	188	-0.20*	191	-0.22*	39	0.07
	SMZ 2	82	0.11	81	0.12	17	0.54*
	SMZ 3	147	-0.22*	149	0.05	28	-0.51*

[†] DBH and tree height measurements were collected on 9 December 2020 and 15 March 2021, respectively.
[††] Forage total yield measurements were collected on 25 May and 5, 15, 29 June 2018, and 4 and 20 June and 3 July 2019.
* Significant correlation at $P < 0.05$.

Table 3. Summary of the number of observations (n) and resulting correlation coefficients (r) from Pearson linear correlations evaluating the relationship between the perpendicular geometry (PRP) apparent electrical conductivity (EC$_a$) and tree diameter at breast height (DBH), tree height, and total forage yield across multiple sampling dates in 2018 and 2019, within six tree/forage species and 2001-2007 fertility treatments [i.e., inorganic-N fertilizer (NF) and poultry litter applications (PL)] at an agroforestry site in the Ozark Highlands of northwest Arkansas. The location of the trees, forages, yield samples, and fertility treatments are presented on Figure 1 and 2.

Treatment Combinations		Tree Data[†]				Forage Data[††]	
		DBH		Tree Height		Total Yield	
Species	2001-2007 Fertility	n	r	n	r	n	r
Cottonwood	NF	27	0.27	27	0.31	-	-
	PL	23	0.24	23	0.24	-	-
Oak	NF	32	-0.25	32	-0.53*	-	-
	PL	32	-0.25	32	-0.53*	-	-
Pecan	NF	52	0.59*	53	0.37*	-	-
	PL	48	-0.08	48	-0.06	-	-
Pine	NF	127	0.15	131	0.09	-	-
Sycamore	PL	57	0.08	56	0.20	-	-
Native grass mix	NF	-	-	-	-	21	0.48*
	PL	-	-	-	-	21	0.30
Orchardgrass	NF	-	-	-	-	21	-0.14
	PL	-	-	-	-	21	-0.13

[†] DBH and tree height measurements were collected on 9 December 2020 and 15 March 2021, respectively.
[††] Forage total yield measurements were collected on 25 May and 5, 15, 29 June 2018, and 4 and 20 June and 3 July 2019.
* Significant correlation at $P < 0.05$.

Table 4. Summary of the number of observations (n) and resulting correlation coefficients (r) from Pearson linear correlations evaluating the relationship between the horizontal coplanar geometry (HCP) apparent electrical conductivity (EC_a) and tree diameter at breast height (DBH), tree height, and total forage yield across multiple sampling dates in 2018 and 2019, within six tree/forage species and 2001-2007 fertility treatments [i.e., inorganic-N fertilizer (NF) and poultry litter applications (PL)] at an agroforestry site in the Ozark Highlands of northwest Arkansas. The location of the trees, forages, yield samples, and fertility treatments are presented on Figure 1 and 2.

Treatment Combinations		Tree Data[†]				Forage Data[††]	
		DBH		Tree Height		Total Yield	
Species	2001-2007 Fertility	n	r	n	r	n	r
Cottonwood	NF	27	0.29	27	0.34	-	-
	PL	23	0.13	23	0.12	-	-
Oak	NF	32	-0.31	32	-0.46*	-	-
	PL	32	-0.31	32	-0.46*	-	-
Pecan	NF	52	0.56*	53	0.36*	-	-
	PL	48	-0.08	48	-0.14	-	-
Pine	NF	127	0.10	131	0.02	-	-
Sycamore	PL	57	0.21	56	0.07	-	-
Native grass mix	NF	-	-	-	-	21	0.40
	PL	-	-	-	-	21	0.26
Orchardgrass	NF	-	-	-	-	21	-0.10
	PL	-	-	-	-	21	-0.44*

[†] DBH and tree height measurements were collected on 9 December 2020 and 15 March 2021, respectively.

[††] Forage total yield measurements were collected on 25 May and 5, 15, 29 June 2018, and 4 and 20 June and 3 July 2019.

* Significant correlation at $P < 0.05$.

Table 5. Summary of the number of observations (n) and resulting correlation coefficients (r) from Pearson linear correlations evaluating the relationship between the perpendicular (PRP) and horizontal coplanar geometry (HCP) apparent electrical conductivity (EC_a) and the total forage yield across multiple sampling dates in 2018 and 2019, within four forage species and 2017-2019 fertility treatments [i.e., no fertilizer control (Control) and poultry litter applications (PL)] at an agroforestry site in the Ozark Highlands of northwest Arkansas.

EC_a	Species	2017-2019 Fertility	Total Yield[†] n	r
PRP	Native grass mix	Control	21	0.39
		PL	21	-0.37
	Orchardgrass	Control	21	0.26
		PL	21	0.00
HCP	Native grass mix	Control	21	0.37
		PL	21	-0.34
	Orchardgrass	Control	21	-0.23
		PL	21	0.02

[†] Forage total yield measurements were collected on 25 May and 5, 15, 29 June 2018, and 4 and 20 June and 3 July 2019.

Table 6. Summary of the number of observations (n) and resulting correlation coefficients (r) from Pearson linear correlations evaluating the relationship between the perpendicular (PRP) and horizontal coplanar geometry (HCP) apparent electrical conductivity (EC$_a$) and 14 terrain attributes, within the whole-site and three EC$_a$-derived soil management zones (SMZs) [22], at an agroforestry site in the Ozark Highlands of northwest Arkansas. The non-abbreviated terrain attribute names and their definitions are presented on Table 1.

| Terrain Attribute | | Whole-site | | | Soil Management Zones | | | | | | | | |
| | | | | | 1 | | | 2 | | | 3 | |
	n	PRP	HCP	n	PRP	HCP	n	PRP	HCP	n	PRP	HCP
		—— r ——			—— r ——			—— r ——			—— r ——	
Aspect	1836	0.22*	0.23*	691	0.17*	-0.11*	344	-0.38*	-0.17*	801	-0.04	-0.01
Elevation	1836	< -0.01	0.27*	691	-0.31*	0.09	344	-0.22*	0.18*	801	-0.49*	0.02
FlowAccum	1836	0.14*	0.07*	691	0.12*	-0.05	344	0.12	0.10	801	0.19*	0.12*
LS-Factor	1836	-0.38*	-0.20*	691	-0.45*	-0.24*	344	-0.41*	-0.08	801	-0.38*	0.07
MidSlope	1836	-0.09*	-0.21*	691	0.07	0.17*	344	-0.30*	0.11	801	0.26*	-0.22*
MRRTF	1836	0.01	0.14*	691	-0.05*	0.02	344	0.07	0.02	801	-0.37*	-0.07
MRVBF	1836	0.33*	0.10*	691	0.44*	0.17*	344	0.45*	0.05	801	0.49*	< -0.01
NormHt	1836	-0.20*	0.06*	691	-0.41*	-0.04	344	-0.24*	0.15*	801	-0.53*	-0.01
SAGAWI	1836	0.36*	0.16*	691	0.47*	0.20*	344	0.08	-0.12	801	0.50*	0.05
SlopeHt	1836	-0.13*	0.11*	691	-0.40*	< -0.01	344	-0.38*	0.20*	801	-0.41*	0.05
SlopePer	1836	-0.43*	-0.23*	691	-0.44*	-0.21*	344	-0.56*	-0.16*	801	-0.50*	0.03
TPI	1836	-0.21*	0.02	691	-0.35*	0.01	344	-0.33*	0.02	801	-0.51*	-0.04
ValleyDep	1836	-0.02	-0.25*	691	0.33*	-0.08	344	0.24*	-0.16*	801	0.50*	-0.03
VDistChn	1836	-0.33*	-0.22*	691	-0.30*	0.05	344	-0.15	-0.02	801	-0.29*	-0.12*

* Significant correlation at $P < 0.05$.

Table 7. Summary of the percent of total sum of squares of each terrain attribute that was used in a multiple linear regression model evaluating the effect of 14 terrain attributes on the perpendicular (PRP) and horizontal coplanar geometry (HCP) apparent electrical conductivity (EC_a), within the whole-site and three EC_a-derived soil management zones (SMZs) [22], at an agroforestry site in the Ozark Highlands of northwest Arkansas. The non-abbreviated terrain attribute names and their definitions are presented on Table 1.

	Percent of Total Sum of Squares							
			Soil Management Zone					
	Whole-site		1		2		3	
Terrain Attribute	PRP	HCP	PRP	HCP	PRP	HCP	PRP	HCP
	%							
Aspect	1.3*	1.7*	2.2*	1.0*	13.1*	2.8*	< 0.1	< 0.1
Elevation	0.9*	0.8*	0.4*	2.0*	2.3*	2.6*	0.5*	2.3*
FlowAccum	4.2*	1.6*	0.7*	1.3*	0.7*	1.7*	8.9*	0.7*
LS-Factor	10.5*	1.8*	18.2*	5.4*	6.7*	0.2	13.8*	0.7*
MidSlope	9.4*	11.2*	0.1	1.4*	7.1*	2.7*	< 0.1	7.6*
MRRTF	3.6*	6.0*	0.3	1.0*	5.7*	1.0*	3.6*	0.3
MRVBF	7.1*	1.2*	19.8*	9.0*	6.8*	0.7*	3.0*	< 0.1
NormHt	1.4*	5.3*	0.1	5.5*	1.0*	5.3*	1.8*	0.2
SAGAWI	6.1*	11.9*	0.4*	3.7*	0.1	0.1	1.2*	4.4*
SlopeHt	0.7*	1.6*	3.0*	2.5*	2.2*	< 0.1	1.6*	3.3*
SlopePer	5.0*	5.7*	0.3	2.0*	8.8*	7.8*	1.2*	1.1*
TPI	1.7*	4.5*	< 0.1	0.5*	1.2*	5.5*	0.0	0.2
ValleyDep	7.2*	15.3*	1.1*	4.5*	0.2	4.0*	0.3	3.7*
VDistChn	0.2*	0.8*	1.0*	0.1	< 0.1	3.5*	0.2	1.6*

* Terrain attribute was significant ($P < 0.05$) in the multiple regression model to explain EC_a variations.

Figure 1. The agroforestry (AF) site in the Ozark Highlands of northwest Arkansas is organized into 16 rows, where Row 1 starts at the northern most row. Rows 1-5 consists of the northern red oak; the western, central, and eastern portion of Rows 6-10 consists of the pitch/loblolly pine, cottonwood, and American Sycamore; and Rows 11-16 consist of pecan. The soils at the AF site include Captina silt loam (CaB), Pickwick silt loam (PsC2), Nixa cherty silt loam (NaC), Johnsburg silt loam (Js), and Cleora fine sandy loam (Cr; Soil Survey Staff, 2019b) and the alleys between the tree rows consist of either orchardgrass or a native grass mix forages (big bluestem, little bluestem, and Indiangrass). The forage total yield samples were collected from within cattle exclosures on 25 May and 5, 15, 29 June 2018 (X), and 4 and 20 June and 3 July 2019 (•). Maps were created in ArcGIS (ArcGISmap version 10.6.1, Esri, Redlands, CA).
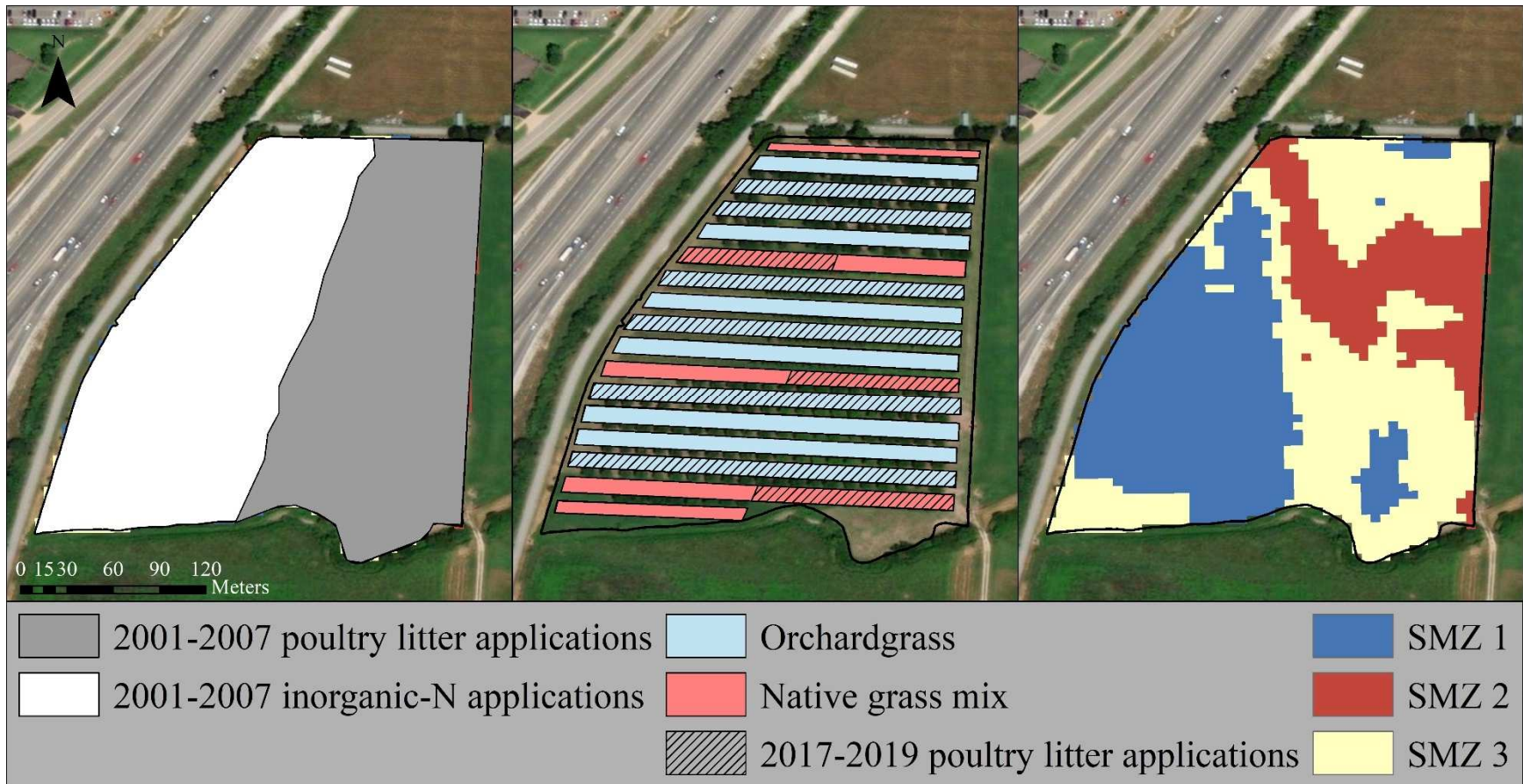
Figure 2. The agroforestry (AF) site in the Ozark Highlands of northwest Arkansas had poultry litter or inorganic-nitrogen (N) applications across the whole site between 2001 and 2007 based on fertility treatment. The alleys between the tree rows consist of either orchardgrass or a native grass mix (big bluestem, little bluestem, and Indiangrass), where fertility treatments were fertilized with poultry litter in 2017, 2018, and 2019. Three precision soil management zones (SMZs) at the AF site were created by Ylagan et al. [22] using 12 horizontal coplanar geometry (HCP) apparent electrical conductivity (EC$_a$) surveys. Maps were created in ArcGIS (ArcGISmap version 10.6.1, Esri, Redlands, CA).
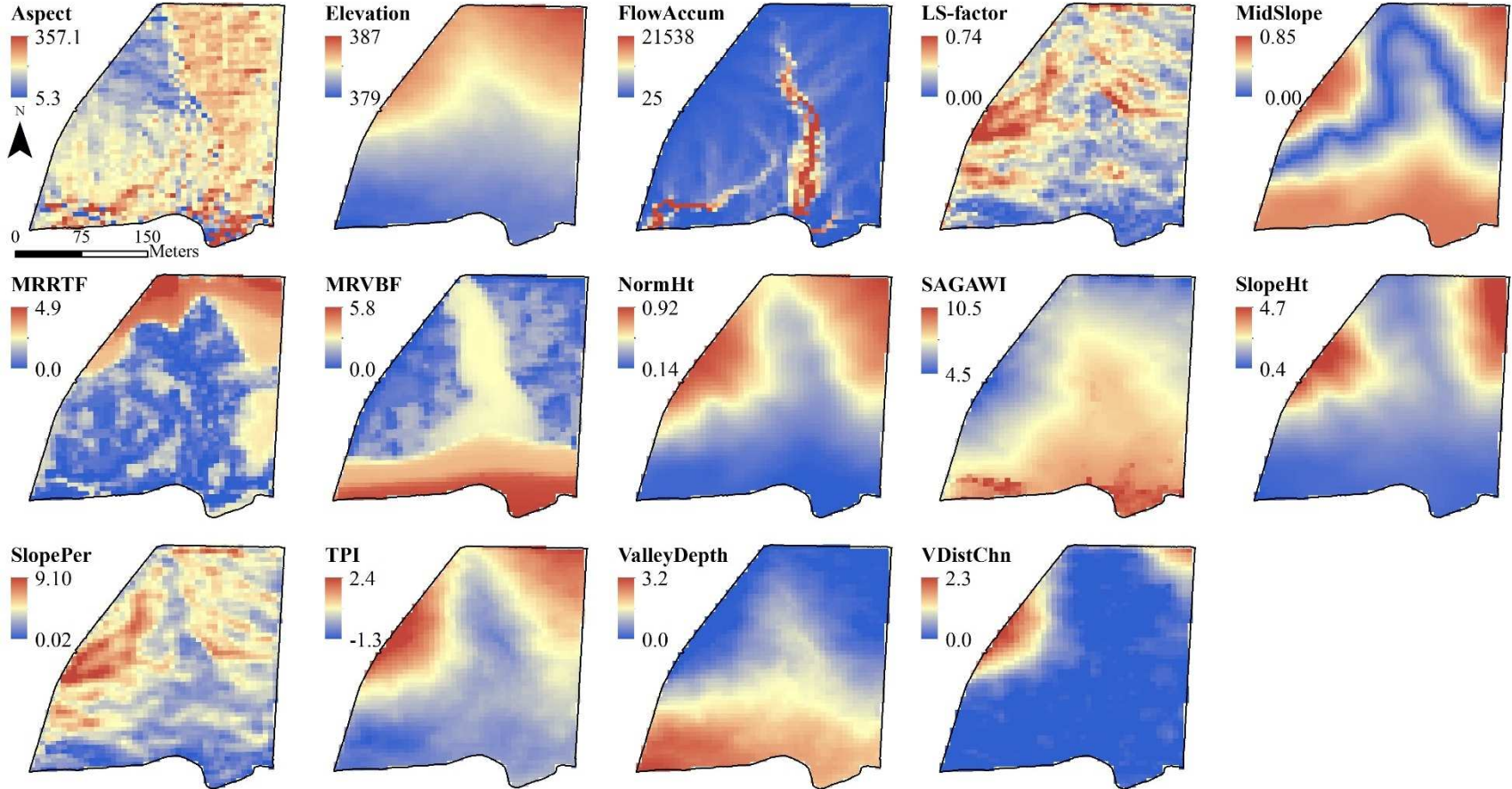
Figure 3. The spatial pattern of the terrain attributes of the agroforestry site the Ozark Highlands of northwest Arkansas. Terrain attribute data were obtained from the USDA-NRCS Geospatial Data Gateway [34] and are derived from a Light Detection and Ranging (LiDAR)-based, 5-m bare earth digital elevation model (DEM). The non-abbreviated terrain attribute names, definitions, units, and summary statistics are presented on Table 1. Maps were created in ArcGIS (ArcGISmap version 10.6.1, Esri, Redlands, CA).
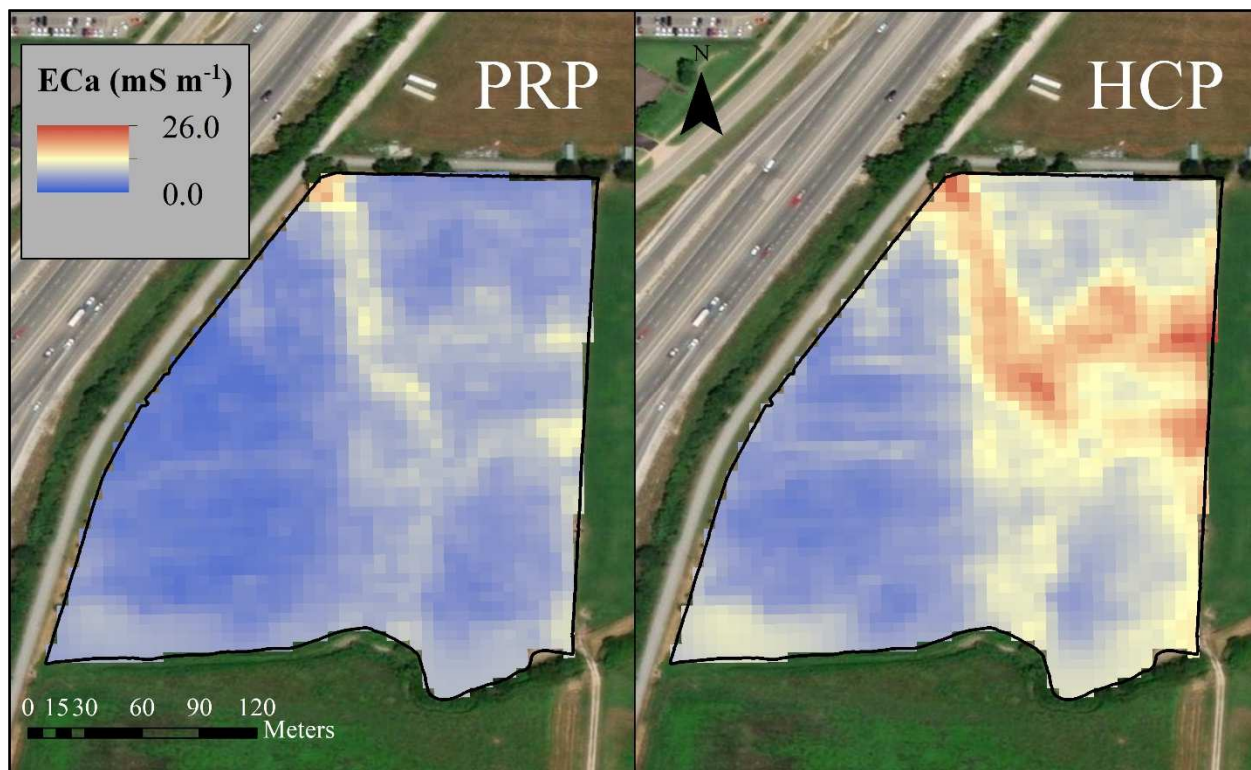
Figure 4. The overall mean of 12 perpendicular (PRP) and horizontal coplanar geometry (HCP) apparent electrical conductivity (EC$_a$) surveys after universal kriging at the agroforestry site in the Ozark Highlands of northwest Arkansas. Maps were created in ArcGIS (ArcGISmap version 10.6.1, Esri, Redlands, CA).

Overall Conclusions

Electromagnetic induction-EC_a surveys have been widely used to assess field variability within different ecosystems and land management systems across the world. However, little to no work has been conducted using repeated EMI-EC_a surveys to assess spatiotemporal field variability and create SMZs in AF systems within similar regions to the Ozark Highlands. As a result, objectives were to identify i) spatiotemporal EC_a variability; ii) EC_a-derived SMZs; iii) correlations among EMI-EC_a and *in-situ*, sentential-site soil properties; iv) whether fewer, EMI-EC_a surveys could be conducted to capture similar EC_a variance as mid-monthly EMI-EC_a surveys; v) correlations between EC_a and forage yield, tree growth, and terrain attributes based on plant (forage and tree) species, and fertility treatments, and EC_a-derived SMZs, and vi); and terrain attributes that have the largest contribution to EC_a variability at a 20-year-old, 4.25-ha, AF system in the Ozark Highlands of northwest Arkansas.

In Chapter 2, results partially supported the hypothesis that there would be a change in the mean EC_a and EC_a variability (i.e., SD and CV) across time and the weather seasons. However, results of did not support the hypothesis that there would be differences between the EC_a mean, SD, and CV of surveys that were conducted in different weather seasons and in the tree growing/non-growing season at a 20-year AF system within the Ozark Highlands. Results also supported the hypothesis that monthly EMI-EC_a surveys at a 20-year-old AF system within the Ozark Highlands can be grouped into similar functional populations and be made into zones for precision soil management. Results of this study partially supported the hypothesis that monthly EMI-EC_a survey data are correlated with soil-sensor-based VWC and EC_a and soil-sample-based EC, GWC, and pH. Results of this study also partially supported the hypothesis that fewer, strategically timed, and evenly spaced EC_a surveys could be conducted to capture the same amount of overall EC_a variance at the AF site as the 12 monthly EC_a surveys conducted.

In Chapter 3, results partially supported the hypothesis that EMI-EC$_a$ data would be correlated with total forage yield and tree growth characteristics and supported the hypothesis that EMI-EC$_a$ data would be correlated with terrain attributes. However, results did not support the hypothesis that correlations among EMI-EC$_a$ and tree growth data can be improved with EC$_a$-derived SMZs. Results supported the hypothesis that correlations among EMI-EC$_a$ and total forage yield and terrain attribute data can be improved with EC$_a$-derived SMZs. Results also supported the hypothesis that different terrain attributes would contribute to the EC$_a$ variability to different degrees within the AF site and across the SMZs.

Results from these studies provide beneficial and valuable insight on the spatiotemporal variability of measured EMI-EC$_a$ over time, not only in an AF system, but also an AF system that is located within a unique environment like the Ozark Highlands. Results of this study demonstrated that a variety of different methods can be used to assess spatial and temporal changes in measured EMI-EC$_a$, and that the effects of pedogenic and anthropogenic factors on measured EMI-EC$_a$ can be observed in AF systems. Additionally, results also demonstrated that measured EMI-EC$_a$ can be used to create precision SMZs in an AF system within the Ozark Highlands. Results demonstrated that EC$_a$-tree, -forage, and -terrain attribute relationships can be established in AF systems in the Ozark Highlands and can vary with soil depth and when separated into EC$_a$-derived SMZs and management history (species and fertility treatments). Results also demonstrated that the PRP EC$_a$ can potentially have stronger and additional relationships with tree, forage properties, and/or terrain properties in AF systems than the HCP EC$_a$. Results of these studies provide further evidence on the potential versatility and ability of EMI-EC$_a$ surveys to help delineate and contextualize in-field variability in a variety of ecosystems with different land management systems.

Appendix

<p style="text-align:center">EMI-EC$_a$ Survey Instructions</p>

General Information

- For most surveying, DUALEM-1S should always be >1 m distance from the substantial metal area of the all-terrain vehicle (ATV) and at low clearance above the ground.
- It should be held in a sled securely to prevent rotation about its axis during surveying.
- It's always preferred to align the instrument with the direction of travel and with transmitter closest to the ATV.
- A Trimble GPS Unit is provided to position the data and a Field Computer for user input, data recording and to guide navigation.
- Both units should be securely mounted in the ATV.
- During the survey, the sensor and position data are synchronously logged to a field computer with HGIS software and can be downloaded using USB ports.
- Usually, the power to the sensor is provided by the ATV but external power could also be used if needed.

Survey Instructions

Note: Read the entire Survey Instruction section before conducting a survey.

Equipment Set Up

1. To begin with the survey, first bring all equipment's [ATV, DUALEM-1S sensor, Field Computer (Yuma 2), GPS Unit, cables, extension cords etc.] together, preferably in an open space.
2. Dualem set up options
   a. Mounted to the side-by-side with GPS above the dualem
      i. Securely mount the Dualem > 1 m away from the side-by-side as close to the ground as possible
      ii. Securely mount the Field Computer and GPS Unit above the DUALEM-1S Sensor
      iii. Skip to step 3.
   b. Sled set up
      i. Securely mount the Field Computer and GPS Unit in the ATV.
      ii. Take the DUALEM-1S sensor (Boom) out of its housing and place it in the sled, make sure the black mark on either end of the sensor is facing upward, and the transmitter (boom end with LED lights) closest to the ATV.
      iii. The front of the DUALEM-1S in the sled should be 2.1 m behind the side-by-side and the center of the DUALEM-1S should be 4.15 m behind the Trimble R2 GPS unit.
      iv. Duct tape the DUALEM securely to the sled.
      v. Tie up the sled to the back of the ATV.

3. It is recommended to cover the DUALEM-1S with a non-metallic relative cover or a thin, white cloth to reduce increases in the DUALEM-1S's internal temperatures due to sunlight.
4. Connect the DUALEM-1S and GPS Unit to the Field Computer using the cables provided.
5. Plug in the power outlet to the ATV.
6. Plug in the DUALEM-1S and the Field Computer's charger to the power outlet.
7. Make sure all cables are out of the way and will not get snapped during the survey.
    a. You may need to use an extension cord to connect everything and to make sure things are out of the way.
8. It is recommended that the DUALEM-1S is powered on ~**30 minutes** before conducting a survey.
9. Make sure the LED light labeled P located at front of DUALEM-1S is steady green.

Preparing the Dualem for the Survey

10. Turn the GPS Unit on and log into the Field Computer.
11. To find what comm port the DUALEM-1S is connected to go to **Device Manager** in the control panel and click **Ports**.
12. The comm port for the DUALEM-1S should be "**Prolific USB-to-Serial Comm Port (COM#)**," and remember the comm port within the parentheses.
13. Open and run **Termite**.
14. In Termite, go to **Settings** and click the drop-down arrow for **Port.**
15. Select the comm port for the DUALEM-1S that you remembered from **Step 12**.
16. Make sure the baud rate is **38400,** then click **ok.**
17. Make sure $PDLM1 and $PDLMA data are continuously appearing, if so, close Termite.
18. Open **HGIS**.
19. Click **Start GPS** in the pop-up window and click **ok**.
20. Name the file appropriately **AND YOU MUST PUT ".txt" AT THE END OF THE FILE NAME,** if not, it will not save the file as a .txt file and cannot be assessed after the survey.
21. A GPS port pop-up window will appear, if you do not know the appropriate comm port for the GPS, click **Find**, and then click **ok** when it has found one.
22. A pop-up window will appear to confirm to Auto Start GPS, click **ok**.
23. Make sure that there are at **least four (4) satellites** in the GPS summary pop-up window, if so, close the pop-up window.
24. A cross-mark should be blinking in the middle of the screen now.
25. Click the **File** button at the top left of the screen, then click **PRO**, followed by clicking **Device Setup**.
26. A SensorTrack pop-up window should appear, click the drop-down arrow and select the comm port for the DUALEM-1S that you used in **Step 12** and **15**.
27. Click the next **drop-down arrow** and select **Dualem EC meter**.
28. Make sure the baud rate is **38400.**

29. Click the check box for **Connect Device.**
30. Then click **View Data**, make sure $PDLM data is popping up.
31. Then click **Manual**.
32. In the new pop-up window, check both boxes for **Add to map** and **Log to File**, then click **Sensor + GPS**.
33. Click **New Layer** in the new pop-up window and then select the **PRO template.**
34. Name and date the layer appropriately, and then click **ok.**
35. Click **Point** in the new pop-up window and then click **Done.**
36. In the new pop-up window, name the start value appropriately, then check the box for **Label**, then click **ok.**
37. Close all the remaining small pop-up windows.
38. Click the **drop-down arrow** (to the right of the **Help** Menu) and select **GPS draw**.
39. Click the **Point** button at the top of the screen and then click the **Auto** button.
40. In the **GPS Auto Collect** pop-up window, make the necessary edits to the Auto Collect measurement values so that the DUALEM-1S and the GPS will take measurements within your desired measurement interval, then click **ok.**
    a. If you would like to alter the measurement interval to something other than every 1 s, <u>you will need to abort this current survey, go into Termite, and follow the instructions in the DUALEM-1S manual, in section **4x20 Operation,**</u> on how to edit the measurement interval for the DUALEMS-1S using the ROOT menu.
        i. After editing the measurement interval, <u>unplug and re-plug in</u> the DUALEMS-1S to the power outlet.

Starting the Survey

41. In order to start the scan, click the **User Pause** button in the top right of the screen, it will then say "**Run.**" It is now collecting data and you can now <u>begin your scan</u>.
42. You can click the **Run** button during surveying to pause the scan.
43. Survey the field in a <u>serpentine pattern</u>, where the drive paths are <u>parallel</u> and **2-5 m** apart from each other and make sure the sensor stays **> 1 m** away from any metal objects.
44. While surveying, <u>avoid unnecessary stops</u> and stays at a drive speed of **3 to 5 mi hr⁻¹.**
    a. You can increase or decrease the drive speed of your survey by increasing or decreasing your sampling/measurement interval.
        i. This can be done <u>before the survey</u> in the **GPS Auto Collect** pop-up window and in the DUALEM-1S ROOT menu in Termite, as mentioned back in **Step 40.**

Calibration Line

45. Once you completed the survey, conduct the calibration line.

46. To conduct the calibration line, start in one corner of the field and drive in a zig-zag pattern across the field, going across all of your previous survey drive paths, and ending at the opposite corner of the field.
   a. It should look something like this.
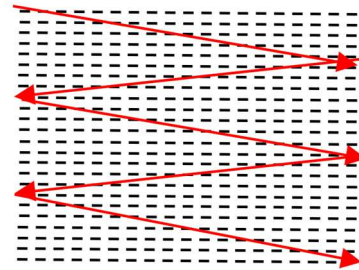
47. Once you completed the survey and calibration line, click the **Run** button to stop measurements.

After the Survey

48. Click the **File** button at the top left of the screen, click the **>>** button, and then click **Save Project As.**
49. Name the entire project file appropriately and then click **Save**.
50. You can now exit HGIS.
51. The txt file of the data will be in **Computer > OS Disk (C:) > My HGIS Documents > Logs.**
52. To export the data, plug in an external memory device (i.e., flash drive), **Copy and paste/drag** the file to the flash drive, and then **Eject and remove** the flash drive.

Temperature Measurements

1. Soil temperature measurements need to be taken in order to temperature-adjust the recorded EC_a values later in the data post-processing procedures.
   a. During the survey, record the soil temperature at the 15-cm (for the PRP EC_a) and 75-cm soil depth (for the HCP EC_a) at multiple locations across the field.

Note: If you are surveying multiple large fields, you will need to conduct a survey with a calibration line, and collected additional temperature measurements, for every field you are surveying in same manner.

Viewing the Data on the Computer

1. To access the data in organized columns, you will have to insert the flash drive into a compatible device and open a **new blank excel file.**
2. Click **Import** in the **File** tab.

3. In the pop-up window, click the **.CSV** check box, then select the file.
4. Select the check box for **delimited** and then click **Next**.
5. <u>Unselect</u> the check box for **Tab** and <u>select</u> the check box for **Comma,** then click **Next.**
6. Click the check box for **General** and then click **Finish**.
7. For more detail, refer to **Dualem Termite**, **DUALEM-1S**, and **HGIS** manual provided separately.

Survey Data Post Processing

Note: Post-processing of data can be done different ways. The following is how Shane Ylagan in 2021 processed his data

Note: For each step in the following data handling procedures, read the entire bullet point, and its sub-bullet points, before executing the instructions that are given at each step

Data-cleaning, GPS-shift, and Survey and Calibration Line Separation

1. Change column names to (left to right in the following order):
   a. DATE, GPS_TIME, GPS_FIX, Longitude, Latitude, Altitude, Height_Above_Ellipsoid, Speed_(KPH), STATION_ID, REMARK, $PDLM1, EC_Time, HCP_Conductivity_(mS/m), HCP_Inphase_(ppt), PRP_Conductivity_(mS/m), PRP_Inphase_(ppt), $PDLMA, Voltage, Internal_sensor_temp_(C), Pitch_(deg), Roll_(deg).
   b. The first 11 columns are a part of the GPS output.
   c. The second 11 columns are a part of the DUALEM-1S output.
2. Delete any row which contains "com"# in the REMARK column and shift up the cells upward (usually just one row).
3. Insert a blank column to the right of the DATE with and title it as "Seconds".
4. Adjusting for the GPS and DUALEM-1S location difference.
   a. If you mounted the DUALEM-1S with the GPS unit above the DUALEM-1S.
      i. Delete one row of cells above the DUALEM-1S data (columns $PDLM1 and on), so that the DUALEM-1S and GPS data are on the same rows, shift the cells upward, and then skip to Step 5.
      ii. It should look like this
         1. Before

	A DATE	B Seconds	C GPS_TIME	D GPS_FIX	E Longitude	F Latitude	G Altitude	H Height Ab	I Speed (KP	J STATION_	K REMARK	L $PDLM1	M EC Time	N HCP Cond	O HCP Inpha	P PRP Cond	Q PRP Inpha	R $PDL
1	DATE	Seconds	GPS_TIME	GPS_FIX	Longitude	Latitude	Altitude	Height Ab	Speed (KP	STATION_	REMARK	$PDLM1	EC Time	HCP Cond	HCP Inpha	PRP Cond	PRP Inpha	$PDL
9	2E+07		134155									$PDLM1	113028	10.7	0.05	8.5	-0.47	
10	2E+07		134155									$PDLMA	12.15	31.1	-1.6	3.2		
11	2E+07		134156									$PDLM1	113029	10.8	0.05	8.8	-0.47	
12	2E+07		134156									$PDLMA	12.12	31.1	-1.6	3.2		
13	2E+07		134156	20810	-94.1892	36.0905	390.4	362.4	0.1	0	gps							
14	2E+07		134157									$PDLM1	113030	11	0.05	8.6	-0.47	
15	2E+07		134157									$PDLMA	12.15	31.1	-1.6	3.2		
16	2E+07		134157	20810	-94.1892	36.0905	390	362	0.1	0	gps							
17	2E+07		134158									$PDLM1	113031	10.9	0.05	8.7	-0.47	
18	2E+07		134158									$PDLMA	12.12	31.2	-1.6	3.2		
19	2E+07		134158	20810	-94.1892	36.0905	389.8	361.8	0	0	gps							
20	2E+07		134159									$PDLM1	113032	10.8	0.05	8.5	-0.48	
21	2E+07		134159									$PDLMA	12.15	31.2	-1.6	3.2		
22	2E+07		134159	20810	-94.1892	36.0905	389.6	361.6	0	0	gps							
23	2E+07		134160									$PDLM1	113033	11.1	0.05	8.6	-0.47	
24	2E+07		134160									$PDLMA	12.12	31.2	-1.6	3.2		

Tester (T12)

2. After

	A DATE	B Seconds	C GPS_TIME	D GPS_FIX	E Longitude	F Latitude	G Altitude	H Height Ab	I Speed (KP	J STATION_	K REMARK	L $PDLM1	M EC Time	N HCP Cond	O HCP Inpha	P PRP Cond	Q PRP Inpha	R $PDL
1	DATE	Seconds	GPS_TIME	GPS_FIX	Longitude	Latitude	Altitude	Height Ab	Speed (KP	STATION_	REMARK	$PDLM1	EC Time	HCP Cond	HCP Inpha	PRP Cond	PRP Inpha	$PD
8												$PDLM1	113028	10.7	0.05	8.5	-0.47	
9	2E+07		134155									$PDLMA	12.15	31.1	-1.6	3.2		
10	2E+07		134155									$PDLM1	113029	10.8	0.05	8.8	-0.47	
11	2E+07		134156									$PDLMA	12.12	31.1	-1.6	3.2		
12	2E+07		134156															
13	2E+07		134156	20810	-94.1892	36.0905	390.4	362.4	0.1	0	gps	$PDLM1	113030	11	0.05	8.6	-0.47	
14	2E+07		134157									$PDLMA	12.15	31.1	-1.6	3.2		
15	2E+07		134157															
16	2E+07		134157	20810	-94.1892	36.0905	390	362	0.1	0	gps	$PDLM1	113031	10.9	0.05	8.7	-0.47	
17	2E+07		134158									$PDLMA	12.12	31.2	-1.6	3.2		
18	2E+07		134158															
19	2E+07		134158	20810	-94.1892	36.0905	389.8	361.8	0	0	gps	$PDLM1	113032	10.8	0.05	8.5	-0.48	
20	2E+07		134159									$PDLMA	12.15	31.2	-1.6	3.2		
21	2E+07		134159															
22	2E+07		134159	20810	-94.1892	36.0905	389.6	361.6	0	0	gps	$PDLM1	113033	11.1	0.05	8.6	-0.47	
23	2E+07		134160									$PDLMA	12.12	31.2	-1.6	3.2		
24	2E+07		134160															

Tester (T12)

b. If you mounted the DUALEM-1S on the sled with its center being 4.15 m behind the GPS unit, traveled 3-5 mph during the survey, and had a sampling interval of every 3 m or 1 s.

    i. Bring the DUALEM-1S data (columns $PDLM1 and on) back 2.32 s to closest GPS point (usually 7 rows), and align the GPS data with the DUALEM-1S $PDLM1 data row, and then skip to Step 5.

    ii. It should look like something below

        1. Before

Before

Row	DATE	Seconds	GPS_TIME	GPS_FIX	Longitude	Latitude	Altitude	Height Ab	Speed (KP	STATION_	REMARK	$PDLM1	EC Time	HCP Cond	HCP Inpha	PRP Cond	PRP Inpha	$P
1	DATE	Seconds	GPS_TIME	GPS_FIX	Longitude	Latitude	Altitude	Height Ab	Speed (KP	STATION_	REMARK	$PDLM1	EC Time	HCP Cond	HCP Inpha	PRP Cond	PRP Inpha	$P
9	2E+07		134155									$PDLM1	113028	10.7	0.05	8.5	-0.47	
10	2E+07		134155									$PDLMA	12.15	31.1	-1.6	3.2		
11	2E+07		134156									$PDLM1	113029	10.8	0.05	8.8	-0.47	
12	2E+07		134156									$PDLMA	12.12	31.1	-1.6	3.2		
13	2E+07		134156	20810	-94.1892	36.0905	390.4	362.4	0.1	0	gps							
14	2E+07		134157									$PDLM1	113030	11	0.05	8.6	-0.47	
15	2E+07		134157									$PDLMA	12.15	31.1	-1.6	3.2		
16	2E+07		134157	20810	-94.1892	36.0905	390	362	0.1	0	gps							
17	2E+07		134158									$PDLM1	113031	10.9	0.05	8.7	-0.47	
18	2E+07		134158									$PDLMA	12.12	31.2	-1.6	3.2		
19	2E+07		134158	20810	-94.1892	36.0905	389.8	361.8	0	0	gps							
20	2E+07		134159									$PDLM1	113032	10.8	0.05	8.5	-0.48	
21	2E+07		134159									$PDLMA	12.15	31.2	-1.6	3.2		
22	2E+07		134159	20810	-94.1892	36.0905	389.6	361.6	0	0	gps							
23	2E+07		134160									$PDLM1	113033	11.1	0.05	8.6	-0.47	
24	2E+07		134160									$PDLMA	12.12	31.2	-1.6	3.2		

Tester (T12)

2. After

Row	DATE	Seconds	GPS_TIME	GPS_FIX	Longitude	Latitude	Altitude	Height Ab	Speed (KP	STATION_	REMARK	$PDLM1	EC Time	HCP Cond	HCP Inpha	PRP Cond	PRP Inpha	$P
1	DATE	Seconds	GPS_TIME	GPS_FIX	Longitude	Latitude	Altitude	Height Ab	Speed (KP	STATION_	REMARK	$PDLM1	EC Time	HCP Cond	HCP Inpha	PRP Cond	PRP Inpha	$P
2												$PDLM1	113028	10.7	0.05	8.5	-0.47	
3												$PDLMA	12.15	31.1	-1.6	3.2		
4												$PDLM1	113029	10.8	0.05	8.8	-0.47	
5												$PDLMA	12.12	31.1	-1.6	3.2		
6																		
7												$PDLM1	113030	11	0.05	8.6	-0.47	
8												$PDLMA	12.15	31.1	-1.6	3.2		
9	2E+07		134155															
10	2E+07		134155									$PDLM1	113031	10.9	0.05	8.7	-0.47	
11	2E+07		134156									$PDLMA	12.12	31.2	-1.6	3.2		
12	2E+07		134156															
13	2E+07		134156	20810	-94.1892	36.0905	390.4	362.4	0.1	0	gps	$PDLM1	113032	10.8	0.05	8.5	-0.48	
14	2E+07		134157									$PDLMA	12.15	31.2	-1.6	3.2		
15	2E+07		134157															
16	2E+07		134157	20810	-94.1892	36.0905	390	362	0.1	0	gps	$PDLM1	113033	11.1	0.05	8.6	-0.47	
17	2E+07		134158									$PDLMA	12.12	31.2	-1.6	3.2		
18	2E+07		134158															
19	2E+07		134158	20810	-94.1892	36.0905	389.8	361.8	0	0	gps	$PDLM1	113034	10.6	0.05	8.6	-0.47	
20	2E+07		134159									$PDLMA	12.15	31.2	-1.6	3.2		
21	2E+07		134159															
22	2E+07		134159	20810	-94.1892	36.0905	389.6	361.6	0	0	gps	$PDLM1	113035	10.7	0.04	8.6	-0.47	
23	2E+07		134160									$PDLMA	12.12	31.2	-1.6	3.2		
24	2E+07		134160															

c. If you mounted the DUALEM-1S on the sled with its center being 4.15 m behind the GPS unit, **<u>BUT</u>** traveled at a speed **other** than 3-5 mph during the survey, and had a sampling interval of something **other** than every 1 s.

  i. You will need to find the time it took you to travel 4.15 m using the average speed you traveled during the survey.

  ii. Using the value you just found, bring the DUALEM-1S data (columns $PDLM1 and on) back that amount to closest GPS point, and align the GPS data with the DUALEM-1S $PDLM1 data row.

  1. Similar to the procedure done in Step 4bi.

  iii. It should look like something below

  1. Before

5. Delete the rows above the first GPS + DUALEM-1S data point, and also the rows after the last GPS + DUALEM-1S data point.

  a. Above

	A	B	C	D	E	F	G	H	I	J	K	L	M	N	O	P	Q	R
1	DATE	Seconds	GPS_TIME	GPS_FIX	Longitude	Latitude	Altitude	Height Ab	Speed (KP	STATION_	REMARK	$PDLM1	EC Time	HCP Cond	HCP Inpha	PRP Cond	PRP Inpha	$PDLMA
2												$PDLM1	113028	10.7	0.05	8.5	-0.47	
3												$PDLMA	12.15	31.1	-1.6	3.2		
4												$PDLM1	113029	10.8	0.05	8.8	-0.47	
5												$PDLMA	12.12	31.1	-1.6	3.2		
6																		
7												$PDLM1	113030	11	0.05	8.6	-0.47	
8												$PDLMA	12.15	31.1	-1.6	3.2		
9	2E+07		134155															
10	2E+07		134155									$PDLM1	113031	10.9	0.05	8.7	-0.47	
11	2E+07		134156									$PDLMA	12.12	31.2	-1.6	3.2		
12	2E+07		134156															
13	2E+07		134156	20810	-94.1892	36.0905	390.4	362.4	0.1		0 gps	$PDLM1	113032	10.8	0.05	8.5	-0.48	
14	2E+07		134157									$PDLMA	12.15	31.2	-1.6	3.2		
15	2E+07		134157															
16	2E+07		134157	20810	-94.1892	36.0905	390	362	0.1		0 gps	$PDLM1	113033	11.1	0.05	8.6	-0.47	
17	2E+07		134158									$PDLMA	12.12	31.2	-1.6	3.2		
18	2E+07		134158															
19	2E+07		134158	20810	-94.1892	36.0905	389.8	361.8	0		0 gps	$PDLM1	113034	10.6	0.05	8.6	-0.47	
20	2E+07		134159									$PDLMA	12.15	31.2	-1.6	3.2		
21	2E+07		134159															
22	2E+07		134159	20810	-94.1892	36.0905	389.6	361.6	0		0 gps	$PDLM1	113035	10.7	0.04	8.6	-0.47	
23	2E+07		134160									$PDLMA	12.12	31.2	-1.6	3.2		
24	2E+07		134160															

Tester (T12)

a. Below

	A	B	C	D	E	F	G	H	I	J	K	L	M	N	O	P	Q	R
22368	2E+07		154608															
22369	2E+07		154608	21109	-94.1912	36.0904	382.9	354.9	0.1		0 gps	$PDLM1	133444	10.5	0.21	10	0.01	
22370	2E+07		154609									$PDLMA	12.1	33.4	-3.8	2.8		
22371	2E+07		154609															
22372	2E+07		154609	21109	-94.1912	36.0904	382.9	354.9	0.1		0 gps	$PDLM1	133445	10.6	0.2	9.8	0.01	
22373	2E+07		154610									$PDLMA	12.05	33.4	-3.8	2.8		
22374	2E+07		154610															
22375	2E+07		154610	21109	-94.1912	36.0904	382.9	354.9	0		0 gps	$PDLM1	133446	10.4	0.21	9.6	0	
22376	2E+07		154611									$PDLMA	12.09	33.4	-3.8	2.8		
22377	2E+07		154611															
22378	2E+07		154611	21209	-94.1912	36.0904	382.9	354.9	0.1		0 gps	$PDLM1	133447	10.4	0.2	9.6	0.01	
22379	2E+07		154612									$PDLMA	12.06	33.4	-3.8	2.9		
22380	2E+07		154612															
22381	2E+07		154612	21109	-94.1912	36.0904	382.9	354.9	0.2		0 gps							
22382	2E+07		154613															
22383	2E+07		154613															
22384	2E+07		154613	21109	-94.1912	36.0904	382.8	354.8	0.2		0 gps							
22385	2E+07		154614															
22386	2E+07		154614															
22387	2E+07		154614	21109	-94.1912	36.0904	382.8	354.8	0.2		0 gps							
22388																		
22389																		
22390																		
22391																		

2. Sort by remark then GPS time.
3. Number the rows by starting at 1 and increasing by 1 in the Seconds column.
4. Sort by $PDLM1 then GPS time.
5. Delete the extra rows at the bottom below the last row with $PDLMA data in it.

	A	B	C	D	E	F	G	H	I	J	K	L	M	N	O	P	Q
14901	2E+07	22343	154560									$PDLMA	12.08	33.4	-3.8	2.8	
14902	2E+07	22345	154601									$PDLMA	12.05	33.4	-3.8	2.8	
14903	2E+07	22347	154602									$PDLMA	12.09	33.4	-3.8	2.8	
14904	2E+07	22349	154603									$PDLMA	12.05	33.4	-3.8	2.8	
14905	2E+07	22351	154604									$PDLMA	12.09	33.4	-3.8	2.8	
14906	2E+07	22353	154605									$PDLMA	12.07	33.4	-3.8	2.8	
14907	2E+07	22355	154606									$PDLMA	12.1	33.4	-3.8	2.8	
14908	2E+07	22357	154607									$PDLMA	12.05	33.4	-3.8	2.8	
14909	2E+07	22359	154608									$PDLMA	12.06	33.4	-3.8	2.8	
14910	2E+07	22361	154609									$PDLMA	12.1	33.4	-3.8	2.8	
14911	2E+07	22363	154610									$PDLMA	12.05	33.4	-3.8	2.8	
14912	2E+07	22365	154611									$PDLMA	12.09	33.4	-3.8	2.8	
14913	2E+07	22367	154612									$PDLMA	12.06	33.4	-3.8	2.9	
14914	2E+07	7458	134157														
14915	2E+07	7460	134158														
14916	2E+07	7462	134159														
14917	2E+07	7464	134160														
14918	2E+07	7466	134201														
14919	2E+07	7468	134202														
14920	2E+07	7470	134203														
14921	2E+07	7472	134204														
14922	2E+07	7474	134205														
14923	2E+07	7476	134206														
14924	2E+07	7478	134207														

Tester (T12)

6. Move $PDLMA data rows next to $PDLM1 rows.

    a. Before

	A	B	C	D	E	F	G	H	I	J	K	L	M	N	O	P	Q
7451	2E+07	7450	154605	21109	-94.1912	36.0904	382.8	354.8	0.1	0	gps	$PDLM1	133441	10.7	0.21	10.1	0
7452	2E+07	7451	154606	21109	-94.1912	36.0904	382.9	354.9	0.2	0	gps	$PDLM1	133442	10.3	0.21	9.8	0.01
7453	2E+07	7452	154607	21109	-94.1912	36.0904	382.9	354.9	0.1	0	gps	$PDLM1	133443	10.6	0.2	9.4	0.01
7454	2E+07	7453	154608	21109	-94.1912	36.0904	382.9	354.9	0.1	0	gps	$PDLM1	133444	10.5	0.21	10	0.01
7455	2E+07	7454	154609	21109	-94.1912	36.0904	382.9	354.9	0.1	0	gps	$PDLM1	133445	10.6	0.2	9.8	0.01
7456	2E+07	7455	154610	21109	-94.1912	36.0904	382.9	354.9	0	0	gps	$PDLM1	133446	10.4	0.21	9.6	0
7457	2E+07	7456	154611	21209	-94.1912	36.0904	382.9	354.9	0.1	0	gps	$PDLM1	133447	10.4	0.2	9.6	0.01
7458	2E+07	7457	134157									$PDLMA	12.15	31.2	-1.6	3.2	
7459	2E+07	7459	134158									$PDLMA	12.12	31.2	-1.6	3.2	
7460	2E+07	7461	134159									$PDLMA	12.15	31.2	-1.6	3.2	
7461	2E+07	7463	134160									$PDLMA	12.12	31.2	-1.6	3.2	
7462	2E+07	7465	134201									$PDLMA	12.13	31.2	-1.6	3.2	
7463	2E+07	7467	134202									$PDLMA	12.15	31.2	-1.6	3.2	
7464	2E+07	7469	134203									$PDLMA	12.12	31.2	-1.6	3.2	
7465	2E+07	7471	134204									$PDLMA	12.15	31.2	-1.6	3.2	
7466	2E+07	7473	134205									$PDLMA	12.12	31.2	-1.6	3.2	
7467	2E+07	7475	134206									$PDLMA	12.15	31.2	-1.6	3.2	
7468	2E+07	7477	134207									$PDLMA	12.13	31.2	-1.6	3.2	
7469	2E+07	7479	134208									$PDLMA	12.16	31.2	-1.6	3.2	
7470	2E+07	7481	134209									$PDLMA	12.16	31.2	-1.6	3.2	
7471	2E+07	7483	134210									$PDLMA	12.13	31.2	-1.6	3.2	
7472	2E+07	7485	134211									$PDLMA	12.16	31.2	-1.6	3.2	
7473	2E+07	7487	134212									$PDLMA	12.13	31.2	-1.6	3.2	
7474	2E+07	7489	134213									$PDLMA	12.16	31.2	-1.6	3.2	

Tester (T12)

    b. After

	C	D	E	F	G	H	I	J	K	L	M	N	O	P	Q	R	S	T	U	V
1	GPS_TIME	GPS_FIX	Longitude	Latitude	Altitude	Height Ab	Speed (KP	STATION_	REMARK	$PDLM1	EC Time	HCP Cond	HCP Inpha	PRP Cond	PRP Inpha	$PDLMA	Voltage	Internal s	Pitch (deg	Roll (de
2	134156	20810	-94.1892	36.0905	390.4	362.4	0.1	0	gps	$PDLM1	113032	10.8	0.05	8.5	-0.48	$PDLMA	12.15	31.2	-1.6	
3	134157	20810	-94.1892	36.0905	390	362	0.1	0	gps	$PDLM1	113033	11.1	0.05	8.6	-0.47	$PDLMA	12.12	31.2	-1.6	
4	134158	20810	-94.1892	36.0905	389.8	361.8	0	0	gps	$PDLM1	113034	10.6	0.05	8.6	-0.47	$PDLMA	12.15	31.2	-1.6	
5	134159	20810	-94.1892	36.0905	389.6	361.6	0	0	gps	$PDLM1	113035	10.7	0.04	8.6	-0.47	$PDLMA	12.12	31.2	-1.6	
6	134200	20810	-94.1892	36.0905	389.4	361.4	0	0	gps	$PDLM1	113036	11	0.05	8.7	-0.47	$PDLMA	12.13	31.2	-1.6	
7	134201	20910	-94.1892	36.0905	389.3	361.3	0.2	0	gps	$PDLM1	113037	10.9	0.05	8.7	-0.47	$PDLMA	12.15	31.2	-1.6	
8	134202	20910	-94.1892	36.0905	389.3	361.3	0.3	0	gps	$PDLM1	113038	10.8	0.05	8.8	-0.47	$PDLMA	12.12	31.2	-1.6	
9	134203	20910	-94.1892	36.0905	389.4	361.4	0.4	0	gps	$PDLM1	113039	10.7	0.05	8.8	-0.47	$PDLMA	12.15	31.2	-1.6	
10	134204	20910	-94.1892	36.0905	389.4	361.4	0.5	0	gps	$PDLM1	113040	10.6	0.05	8.9	-0.47	$PDLMA	12.12	31.2	-1.6	
11	134205	20910	-94.1892	36.0905	389.6	361.6	0.6	0	gps	$PDLM1	113041	10.7	0.05	8.7	-0.47	$PDLMA	12.15	31.2	-1.6	
12	134206	20910	-94.1892	36.0905	389.7	361.7	0.5	0	gps	$PDLM1	113042	10.6	0.05	8.6	-0.47	$PDLMA	12.13	31.2	-1.6	
13	134207	20910	-94.1892	36.0905	389.8	361.8	0.6	0	gps	$PDLM1	113043	10.8	0.05	8.5	-0.47	$PDLMA	12.16	31.2	-1.6	
14	134208	20910	-94.1892	36.0905	390	362	0.6	0	gps	$PDLM1	113044	10.8	0.05	8.6	-0.47	$PDLMA	12.16	31.2	-1.6	
15	134209	20910	-94.1892	36.0905	390.2	362.2	0.6	0	gps	$PDLM1	113045	10.6	0.05	8.6	-0.47	$PDLMA	12.13	31.2	-1.6	
16	134210	20910	-94.1892	36.0905	390.2	362.2	0.4	0	gps	$PDLM1	113046	10.9	0.05	8.5	-0.47	$PDLMA	12.16	31.2	-1.6	
17	134211	20910	-94.1892	36.0905	390.3	362.3	0.3	0	gps	$PDLM1	113047	10.9	0.05	8.3	-0.46	$PDLMA	12.13	31.2	-1.6	
18	134212	20910	-94.1892	36.0905	390.5	362.5	0.3	0	gps	$PDLM1	113048	10.8	0.05	8.8	-0.47	$PDLMA	12.16	31.2	-1.6	
19	134213	20910	-94.1892	36.0905	390.5	362.5	0.2	0	gps	$PDLM1	113049	11	0.05	8.7	-0.47	$PDLMA	12.13	31.2	-1.6	
20	134214	20910	-94.1892	36.0905	390.7	362.7	0.2	0	gps	$PDLM1	113050	10.9	0.05	8.7	-0.47	$PDLMA	12.16	31.2	-1.6	
21	134215	20910	-94.1892	36.0905	391	363	0.2	0	gps	$PDLM1	113051	10.8	0.05	8.7	-0.47	$PDLMA	12.13	31.2	-1.6	
22	134216	20910	-94.1892	36.0905	391	363	0.2	0	gps	$PDLM1	113052	10.9	0.05	8.8	-0.47	$PDLMA	12.14	31.2	-1.6	
23	134217	20910	-94.1892	36.0905	391.1	363.1	0.1	0	gps	$PDLM1	113053	10.7	0.05	8.6	-0.47	$PDLMA	12.16	31.2	-1.6	
24	134218	20910	-94.1892	36.0905	391	363	0.1	0	gps	$PDLM1	113054	10.7	0.05	8.7	-0.47	$PDLMA	12.13	31.2	-1.6	

Tester (T12)

7. Delete remaining extra rows at the bottom columns and shift over.

	A	B	C	D	E	F	G	H	I	J	K	L	M	N	O	P	Q	R	S	T
7448	2E+07	7447	154602	21209	-94.1912	36.0904	382.7	354.7	0.2	0 gps	$PDLM1	133438	10	0.21	9.7	0.01	$PDLMA	12.05	
7449	2E+07	7448	154603	21209	-94.1912	36.0904	382.7	354.7	0	0 gps	$PDLM1	133439	10.5	0.22	10.1	0.01	$PDLMA	12.09	
7450	2E+07	7449	154604	21109	-94.1912	36.0904	382.7	354.7	0	0 gps	$PDLM1	133440	10.8	0.21	10.2	0	$PDLMA	12.07	
7451	2E+07	7450	154605	21109	-94.1912	36.0904	382.8	354.8	0.1	0 gps	$PDLM1	133441	10.7	0.21	10.1	0	$PDLMA	12.1	
7452	2E+07	7451	154606	21109	-94.1912	36.0904	382.9	354.9	0.2	0 gps	$PDLM1	133442	10.3	0.21	9.8	0.01	$PDLMA	12.05	
7453	2E+07	7452	154607	21109	-94.1912	36.0904	382.9	354.9	0.1	0 gps	$PDLM1	133443	10.6	0.2	9.4	0.01	$PDLMA	12.06	
7454	2E+07	7453	154608	21109	-94.1912	36.0904	382.9	354.9	0.1	0 gps	$PDLM1	133444	10.5	0.21	10	0.01	$PDLMA	12.1	
7455	2E+07	7454	154609	21109	-94.1912	36.0904	382.9	354.9	0.1	0 gps	$PDLM1	133445	10.6	0.2	9.8	0.01	$PDLMA	12.05	
7456	2E+07	7455	154610	21109	-94.1912	36.0904	382.9	354.9	0	0 gps	$PDLM1	133446	10.4	0.21	9.6	0	$PDLMA	12.09	
7457	2E+07	7456	154611	21209	-94.1912	36.0904	382.9	354.9	0.1	0 gps	$PDLM1	133447	10.4	0.2	9.6	0.01	$PDLMA	12.06	
7458	2E+07	7457	134157																
7459	2E+07	7459	134158																
7460	2E+07	7461	134159																
7461	2E+07	7463	134160																
7462	2E+07	7465	134201																
7463	2E+07	7467	134202																
7464	2E+07	7469	134203																
7465	2E+07	7471	134204																
7466	2E+07	7473	134205																
7467	2E+07	7475	134206																
7468	2E+07	7477	134207																
7469	2E+07	7479	134208																
7470	2E+07	7481	134209																
7471	2E+07	7483	134210																

Tester (T12)

8. The DUALEM-1S starts collecting measurements when it is turned on, thus during the 30 min it was turned on before the survey started and when the dualem stopped moving at the end of the survey, it was collecting measurements. Remove the points which occurred before the survey started and afterward.
   a. You can do this by either bring the file into GIS program and looking at when DUALEM-1S started moving, or by looking when the recorded speed began to increase/slowdown in the Speed_(KPH) column. For instructions on how to bring the data in ArcMap, go to Page 18.
      i. Before survey

	A	B	C	D	E	F	G	H	I	J	K	L	M	N	O	P	Q	R	S	T
191	2E+07	190	134505	21207	-94.1892	36.0906	380.3	352.3	0.1	0 gps	$PDLM1	113341	10.8	0.06	8.8	-0.48	$PDLMA	12.13	3
192	2E+07	191	134506	21207	-94.1892	36.0906	380.4	352.4	0.2	0 gps	$PDLM1	113342	10.9	0.05	8.7	-0.48	$PDLMA	12.16	3
193	2E+07	192	134507	21207	-94.1892	36.0906	380.4	352.4	0.2	0 gps	$PDLM1	113343	10.9	0.05	8.7	-0.48	$PDLMA	12.13	3
194	2E+07	193	134508	21208	-94.1892	36.0906	380.6	352.6	0.1	0 gps	$PDLM1	113344	10.9	0.05	8.5	-0.48	$PDLMA	12.16	3
195	2E+07	194	134509	21208	-94.1892	36.0906	380.9	352.9	0.1	0 gps	$PDLM1	113345	10.6	0.05	8.6	-0.48	$PDLMA	12.13	3
196	2E+07	195	134510	21208	-94.1892	36.0906	381	353	0.2	0 gps	$PDLM1	113346	10.9	0.06	8.5	-0.48	$PDLMA	12.16	3
197	2E+07	196	134511	21208	-94.1892	36.0906	381	353	0.2	0 gps	$PDLM1	113347	10.7	0.05	8.5	-0.48	$PDLMA	12.13	3
198	2E+07	197	134512	21208	-94.1892	36.0906	381.1	353.1	0.2	0 gps	$PDLM1	113348	10.6	0.05	9	-0.48	$PDLMA	12.13	3
199	2E+07	198	134513	21208	-94.1892	36.0906	381.5	353.5	0.2	0 gps	$PDLM1	113349	10.7	0.05	8.7	-0.48	$PDLMA	12.16	3
200	2E+07	199	134514	21207	-94.1892	36.0906	381.5	353.5	0.2	0 gps	$PDLM1	113350	11	0.05	8.6	-0.49	$PDLMA	12.13	3
201	2E+07	200	134515	21208	-94.1892	36.0906	381.2	353.2	0.2	0 gps	$PDLM1	113351	10.9	0.06	8.7	-0.48	$PDLMA	12.16	3
202	2E+07	201	134516	21208	-94.1892	36.0906	381.2	353.2	0.1	0 gps	$PDLM1	113352	11.1	0.06	8.9	-0.48	$PDLMA	12.13	3
203	2E+07	202	134517	21207	-94.1892	36.0906	381.2	353.2	0.1	0 gps	$PDLM1	113353	10.9	0.04	8.5	-0.49	$PDLMA	12.16	3
204	2E+07	203	134518	21208	-94.1892	36.0906	381.1	353.1	0.3	0 gps	$PDLM1	113354	10.2	0.01	8.2	-0.52	$PDLMA	12.13	3
205	2E+07	204	134519	21208	-94.1893	36.0906	381.3	353.3	1.2	0 gps	$PDLM1	113355	9.2	0.04	7.8	-0.57	$PDLMA	12.16	3
206	2E+07	205	134520	21208	-94.1893	36.0906	381	353	2.2	0 gps	$PDLM1	113356	8.8	0.01	6.7	-0.57	$PDLMA	12.16	3
207	2E+07	206	134521	21208	-94.1893	36.0906	380.8	352.8	3	0 gps	$PDLM1	113357	8.1	-0.02	5.9	-0.59	$PDLMA	12.13	3
208	2E+07	207	134522	21207	-94.1893	36.0906	380.5	352.5	3.2	0 gps	$PDLM1	113358	7.9	-0.04	5.5	-0.6	$PDLMA	12.16	3
209	2E+07	208	134523	21207	-94.1893	36.0906	380.5	352.5	3.7	0 gps	$PDLM1	113359	7.8	-0.03	5.6	-0.62	$PDLMA	12.13	3
210	2E+07	209	134524	21207	-94.1893	36.0906	380.4	352.4	4.3	0 gps	$PDLM1	113400	8.1	-0.04	6	-0.6	$PDLMA	12.16	3
211	2E+07	210	134525	21207	-94.1893	36.0906	380.4	352.4	4.8	0 gps	$PDLM1	113401	8.4	-0.04	6.5	-0.61	$PDLMA	12.13	3
212	2E+07	211	134526	21207	-94.1894	36.0906	380.3	352.3	5.5	0 gps	$PDLM1	113402	8.7	-0.06	6.5	-0.61	$PDLMA	12.15	3
213	2E+07	212	134527	21207	-94.1894	36.0906	380	352	5.8	0 gps	$PDLM1	113403	8.5	-0.06	6.5	-0.6	$PDLMA	12.12	3
214	2E+07	213	134528	21207	-94.1894	36.0906	379.3	351.3	5.9	0 gps	$PDLM1	113404	8.5	-0.1	5.9	-0.53	$PDLMA	12.13	3

   i. After survey

	A	B	C	D	E	F	G	H	I	J	K	L	M	N	O	P	Q	R	S	T
7126	2E+07	7328	154403	21208	-94.1913	36.0904	378	350	3.9	0	gps	$PDLM1	133239	8.5	0.12	7	-0.16	$PDLMA	12.07	
7127	2E+07	7329	154404	21208	-94.1913	36.0904	378.4	350.4	4.4	0	gps	$PDLM1	133240	9	0.15	7.5	-0.2	$PDLMA	12.1	
7128	2E+07	7330	154405	21208	-94.1913	36.0904	378.3	350.3	4.9	0	gps	$PDLM1	133241	8.8	0.17	7.3	-0.21	$PDLMA	12.07	
7129	2E+07	7331	154406	21209	-94.1913	36.0904	378.3	350.3	4.9	0	gps	$PDLM1	133242	9.6	0.17	8.1	-0.24	$PDLMA	12.11	
7130	2E+07	7332	154407	21209	-94.1913	36.0904	378.3	350.3	4.9	0	gps	$PDLM1	133243	10	0.2	8.8	-0.23	$PDLMA	12.1	
7131	2E+07	7333	154408	21209	-94.1913	36.0904	378.4	350.4	4.9	0	gps	$PDLM1	133244	10.2	0.22	9.5	-0.22	$PDLMA	12.07	
7132	2E+07	7334	154409	21209	-94.1913	36.0904	378.4	350.4	4.2	0	gps	$PDLM1	133245	10.3	0.23	9.7	-0.21	$PDLMA	12.1	
7133	2E+07	7335	154410	21209	-94.1913	36.0904	378.2	350.2	2.9	0	gps	$PDLM1	133246	10.4	0.23	9.7	-0.21	$PDLMA	12.07	
7134	2E+07	7336	154411	21208	-94.1913	36.0904	378.2	350.2	1.7	0	gps	$PDLM1	133247	10.4	0.24	9.7	-0.21	$PDLMA	12.1	
7135	2E+07	7337	154412	21209	-94.1913	36.0904	377.9	349.9	1	0	gps	$PDLM1	133248	10.4	0.24	9.5	-0.21	$PDLMA	12.07	
7136	2E+07	7338	154413	11209	-94.1913	36.0904	377.8	349.8	0.7	0	gps	$PDLM1	133249	10.4	0.23	9.8	-0.21	$PDLMA	12.1	
7137	2E+07	7339	154414	11209	-94.1913	36.0904	377.5	349.5	0.4	0	gps	$PDLM1	133250	10.3	0.23	9.9	-0.2	$PDLMA	12.07	
7138	2E+07	7340	154415	11209	-94.1913	36.0904	377.4	349.4	0.1	0	gps	$PDLM1	133251	9.9	0.24	9.8	-0.21	$PDLMA	12.07	
7139	2E+07	7341	154416	11109	-94.1913	36.0904	377.1	349.1	0.1	0	gps	$PDLM1	133252	10.5	0.24	9.8	-0.21	$PDLMA	12.1	
7140	2E+07	7342	154417	11209	-94.1913	36.0904	377.1	349.1	0.4	0	gps	$PDLM1	133253	10.5	0.23	9.7	-0.21	$PDLMA	12.07	
7141	2E+07	7343	154418	11208	-94.1913	36.0904	377.1	349.1	0.3	0	gps	$PDLM1	133254	10.2	0.23	9.8	-0.21	$PDLMA	12.1	
7142	2E+07	7344	154419	11208	-94.1913	36.0904	377.2	349.2	0.1	0	gps	$PDLM1	133255	10.6	0.23	9.7	-0.21	$PDLMA	12.07	
7143	2E+07	7345	154420	11208	-94.1913	36.0904	377.2	349.2	0	0	gps	$PDLM1	133256	10.3	0.23	9.6	-0.21	$PDLMA	12.1	
7144	2E+07	7346	154421	11208	-94.1913	36.0904	377.3	349.3	0.1	0	gps	$PDLM1	133257	10.3	0.23	9.7	-0.21	$PDLMA	12.07	
7145	2E+07	7347	154422	11208	-94.1913	36.0904	377.3	349.3	0.1	0	gps	$PDLM1	133258	10.4	0.23	9.6	-0.21	$PDLMA	12.1	
7146	2E+07	7348	154423	11208	-94.1913	36.0904	377.4	349.4	0.1	0	gps	$PDLM1	133259	10.5	0.23	9.6	-0.2	$PDLMA	12.09	
7147	2E+07	7349	154424	11208	-94.1913	36.0904	377.5	349.5	0.2	0	gps	$PDLM1	133300	10.2	0.23	9.7	-0.2	$PDLMA	12.07	
7148	2E+07	7350	154425	11208	-94.1913	36.0904	377.5	349.5	0.2	0	gps	$PDLM1	133301	10.2	0.23	9.7	-0.2	$PDLMA	12.1	
7149	2E+07	7351	154426	11208	-94.1913	36.0904	377.6	349.6	0.2	0	gps	$PDLM1	133302	10.4	0.23	9.6	-0.21	$PDLMA	12.07	

9. Renumber the cells in the Seconds column (starting at 1 and increasing by 1).
10. If any major stops occurred during the survey, delete those points as well.
    a. This can also be found by bringing the file to a GIS program and visually looking for where the stops occurred and deleting those points or
        i. A potential quick and dirty method is to delete and points with a speed of less than 1 kph.
11. Now calibration line must be separated from the survey. Find where the calibration line begins by bringing the file to a GIS program and visually looking for where the calibration began, and the survey ended.
12. Select all of the calibration line points and move them to a new file. Now you have a file for the calibration line and one for the survey.
13. If your calibration line occurred in reverse direction that you did your survey (i.e., Survey: South to north, Calibration line: North to south), renumber the calibration line's Seconds column in reverse order (i.e., bottom to top), starting at 1 and increasing by 1, and then resort.
14. If your calibration line went in the same direction as your survey (i.e., Survey: South to north, Calibration line: South to north). Renumber the calibration line's Seconds column from top to bottom, starting at 1 and increasing by 1.
15. Now you have your base survey and calibration line file.

Column Information

1. Columns (most important columns are underlined)
    a. DATE: Date of the survey (Year-month-day)
    b. Seconds: Was created to number and index the measurement points
    c. GPS_TIME: Measurement time recorded by the GPS
        i. **Do not trust**
    d. GPS_FIX: unknown meaning
    e. Longitude: WGS84 (°)
    f. Latitude: WGS84 (°)

162

g. Altitude: WGS84 (m)
h. Height_Above_Ellipsoid: WGS84 (m)
i. Speed_(KPH): Speed that the GPS was moving at time of measurement (KPH)
    i. **Do not trust**
j. STATION_ID: unknown meaning
k. REMARK: unknown meaning
l. $PDLM1: Start of the DUALEM-1S output columns
m. EC_Time: Measurement time recorded by the DUALEM-1S
    i. **Do not trust**
n. HCP_Conductivity_(mS/m): The horizontal co-planar geometry which measures the bulk EC_a of the ~ 0-1.6 m depth (mS/m)
o. HCP_Inphase_(ppt): HCP inphase (ppt)
p. PRP_Conductivity_(mS/m): The perpendicular geometry which measures the bulk EC_a of the ~ 0-0.5 m depth (mS/m)
q. PRP_Inphase_(ppt): PRP inphase (ppt)
r. $PDLMA: Start of information of the DUALEM-1S sensor during measurement
s. Voltage: The voltage produced in the DUALEM-1S to create the electromagnetic field (V)
t. Internal_sensor_temp_(C): The temperature inside the DUALEM-1S during measurement
u. Pitch_(deg): The degree of rotation front-to-back (i.e., long ways) of the DUALEM-1S during measurement (°)
v. Roll_(deg): The degree of rotation side-to-side (i.e., short ways) of the DUALEM-1S during measurement (°)

The following steps are best conducted in R

Outlier Removal

1. If there are soil sensors at the site, **delete any points that occurred within 2.0-m of the soil sensor network** (including the sensor head and their cables) in the survey and calibration line data sets to remove any points that were potentially altered due to magnetic components of the sensors. (Finding these points can be conducted in a GIS program).
    a. **Create a new data frame with the removed points** to be combined with outliers found later.
2. **Delete entire measurement points (i.e., rows) that have an HCP** [column HCP_Conductivity_(mS/m)] **and/or PRP EC_a** [column PRP_Conductivity_(mS/m)] **of less than 0.1 mS/m** in both the survey and calibration line data sets.
    a. Combined the removed points with the points that were removed in Step 1.

3. In the Survey data set, create a column titled "index" and index the rows by starting at 1.
4. In the Calibration Line data set, create a column titled "calindex" and index the rows by starting at 1.
5. Hampel filter (optional)
    a. **Apply a Hampel filter** with a 10-point half-width (K= 10), (i.e., 21 point moving data window), and a threshold of t=3, according to the 3σ edit rule of Pearson, 1999 on to the:
        i. ≥ 0.1 mS/m Survey
            1. HCP EC$_a$ [column HCP_Conductivity_(mS/m)]
            2. PRP EC$_a$ [column PRP_Conductivity_(mS/m)]
        ii. ≥ 0.1 mS/m Calibration line
            1. HCP EC$_a$ [column HCP_Conductivity_(mS/m)]
            2. PRP EC$_a$ [column PRP_Conductivity_(mS/m)]
    b. The Hampel filter replaces the point it deemed as an outlier with the median. **Instead of replacing the outlier, remove the values that the Hampel filter deemed to be an outlier**
        i. The Hampel filter applied to the PRP and HCP EC$_a$ will most likely determine different observations/measurement points as outliers.
        ii. Because of that and to be consistent with earlier procedures, **remove the entire observation/measurement points (i.e., row)** from the survey or calibration line data sets wherever the Hampel filter determines there to be an outlier (i.e., in the HCP or PRP EC$_a$)
6. Combine the outliers from the Hampel filter, the measurement points that were removed because they had an HCP and PRP EC$_a$ values of < 0.1 mS/m, and the measurement that removed because they occurred within 2.0-m of the soil sensor network
7. **The four data sets** you should have are:
    a. The outlier-removed
        i. Survey data set
        ii. Calibration Line data set
    b. All the removed outliers and values of the
        i. Survey data set
        ii. Calibration Line data set

Calibration

1. Using the outlier-removed survey and calibration line data set, **find Survey points that occurred within 1.5 m of the Calibration Line points,** and identify them with the calindex of the Calibration Line point that were within 1.5 m.
2. **Average the HCP and PRP EC$_a$ and time (i.e., Seconds)** of the Survey's measurement points that occurred within 1.5 m of the Calibration Line points, and **group them by calindex.**

3. Create a data frame of the HCP and PRP EC$_a$ of the Calibration Line points, and the average time, HCP, and PRP of the survey point that occurred with in 1.5 m of the calibration line points.
    a. It should something like this

|	callndex	avg_time_ECpoints	avg_HCP_ECpoints	avg_PRP_ECpoints	CL_HCP_Con	CL_PRP_Con
1	9	847.000	10.400000	8.900000	10.0	10.6
2	10	847.500	10.000000	8.950000	8.8	9.4
3	11	848.000	9.600000	9.000000	7.6	8.6
4	13	622.000	6.200000	5.800000	6.2	7.0
5	14	622.500	6.100000	5.800000	6.1	7.2
6	15	623.000	6.000000	5.800000	6.3	7.6
7	18	394.000	6.200000	7.200000	6.0	7.3
8	19	395.000	5.900000	6.600000	5.2	6.6
9	20	396.000	5.400000	5.800000	4.8	5.5
10	21	397.000	5.400000	5.400000	4.9	5.1
11	23	155.000	5.100000	4.500000	4.5	5.2
12	24	156.000	5.400000	4.300000	4.7	4.6
13	25	157.000	5.500000	4.700000	4.4	3.9

4. Subtract the Calibration line's HCP from the average HCP of the survey points, and the Calibration line's PRP from the average PRP of the survey points, and add the values to the data frame.
    a. It should look something like this

	callndex	avg_time_ECpoints	avg_HCP_ECpoints	avg_PRP_ECpoints	CL_HCP_Con	CL_PRP_Con	Index	HCP_Diff	PRP_Diff
1	9	847.000	10.400000	8.900000	10.0	10.6	9	0.4000000	-1.7000000
2	10	847.500	10.000000	8.950000	8.8	9.4	10	1.2000000	-0.4500000
3	11	848.000	9.600000	9.000000	7.6	8.6	11	2.0000000	0.4000000
4	13	622.000	6.200000	5.800000	6.2	7.0	13	0.0000000	-1.2000000
5	14	622.500	6.100000	5.800000	6.1	7.2	14	0.0000000	-1.4000000
6	15	623.000	6.000000	5.800000	6.3	7.6	15	-0.3000000	-1.8000000
7	18	394.000	6.200000	7.200000	6.0	7.3	18	0.2000000	-0.1000000
8	19	395.000	5.900000	6.600000	5.2	6.6	19	0.7000000	0.0000000
9	20	396.000	5.400000	5.800000	4.8	5.5	20	0.6000000	0.3000000
10	21	397.000	5.400000	5.400000	4.9	5.1	21	0.5000000	0.3000000
11	23	155.000	5.100000	4.500000	4.5	5.2	23	0.6000000	-0.7000000
12	24	156.000	5.400000	4.300000	4.7	4.6	24	0.7000000	-0.3000000
13	25	157.000	5.500000	4.700000	4.4	3.9	25	1.1000000	0.8000000

5. Plot both the difference between the Survey and Calibration Line's HCP and PRP across the average time of Survey points that occurred within 1.5 m of the Calibration Line points.
   a. It should look like this
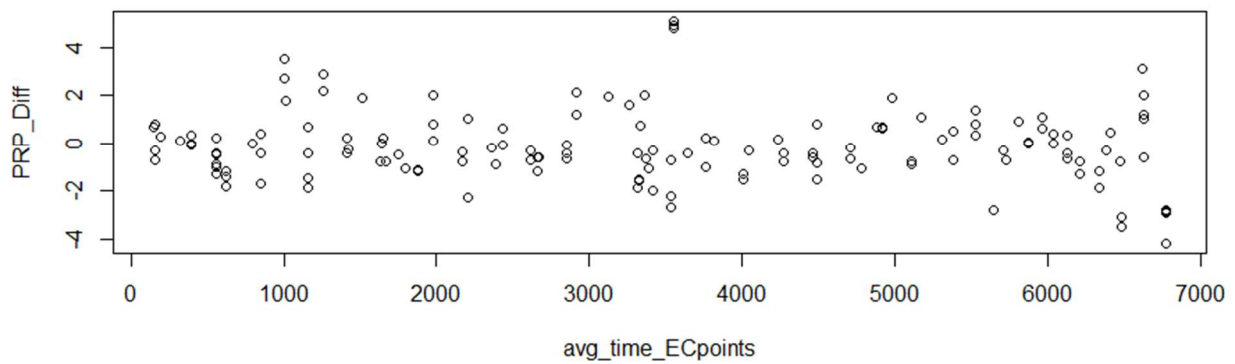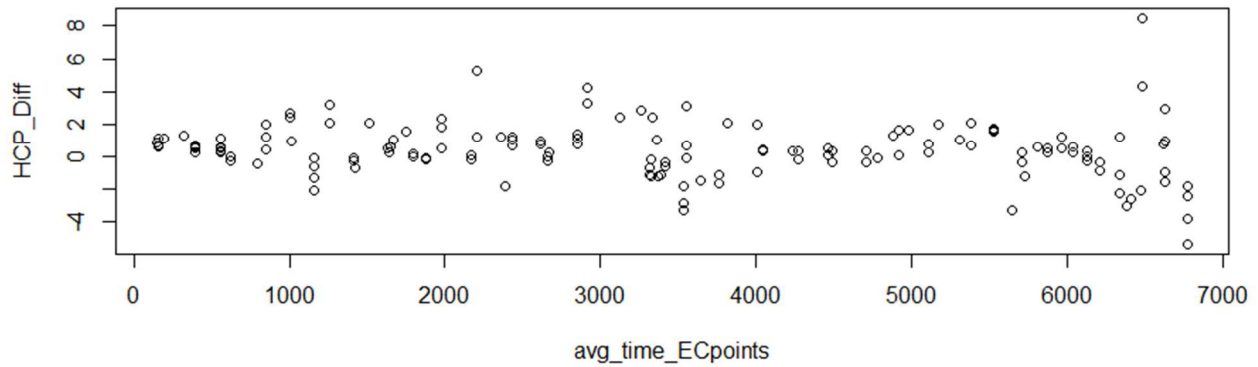
6. Create a linear regression model over difference between the Survey and Calibration Line's HCP and PRP across the average time of Survey points that occurred within 1.5 m of the Calibration Line points

```
HCP_model <- lm(data_All$HCP_Diff  ~ data_All$avg_time_ECpoints)
PRP_model<- lm(data_All$PRP_Diff  ~ data_All$avg_time_ECpoints)
```

Diff between the Cal point and the avg of the survey points HCP within 1.5m of each Cal point after the Hampel Filter was applied For Scan 12

Diff between the Cal point and the avg of the survey points PRP within 1.5m of each Cal point after the Hampel Filter was applied for Scan 12
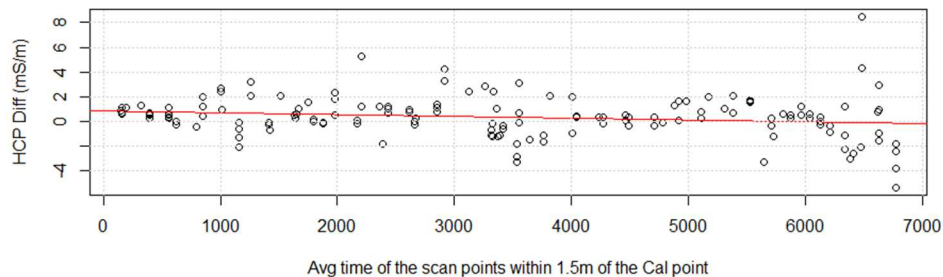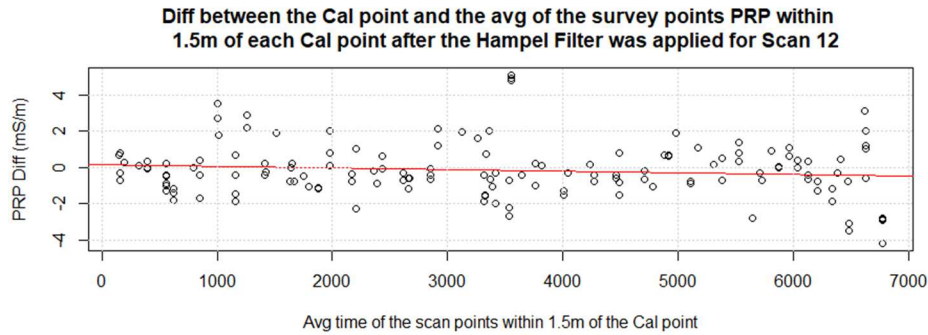
7. Apply both linear regression models to the Seconds of the full, outlier-removed Survey data set, and add the values to the Survey data frame.

```
cleaned_survey <- mutate(cleaned_survey, HCP_lm_predict_diff=(Seconds*HCP_model$coefficients[2]) + HCP_model$coefficients[1])
```

```
cleaned_survey <- mutate(cleaned_survey, PRP_lm_predict_diff=(Seconds*PRP_model$coefficients[2]) + PRP_model$coefficients[1])
```

8. Subtract the Survey data frame's actual HCP and PRP from the projected difference created from the model and add those values to the Survey data frame.

```
cleaned_survey<- mutate(cleaned_survey, Cal_HCP_Con=(HCP_Con-HCP_lm_predict_diff))

Cal_survey_df<- mutate(cleaned_survey, Cal_PRP_Con=(PRP_Con-PRP_lm_predict_diff))
```

HCP_lm_predict_diff	PRP_lm_predict_diff	Cal_HCP_Con	Cal_PRP_Con
0.8609889	0.1280159	8.339011	7.671984
0.8608430	0.1279307	7.939157	6.572069
0.8606970	0.1278455	7.239303	5.772155
0.8605511	0.1277602	7.039449	5.372240
0.8604051	0.1276750	6.939595	5.472325
0.8602592	0.1275898	7.239741	5.872410
0.8601132	0.1275046	7.539887	6.372495
0.8599673	0.1274193	7.840033	6.372581
0.8598214	0.1273341	7.640179	6.372666

9. Now you have a calibrated Survey.

Temperature adjustment of the EC_a

1. Using the outlier-removed, calibrated Survey data set, the HCP EC_a will be adjusted using the temperature recorded at the 75-cm depth, and the PRP EC_a will be adjusted using the temperature recorded at the 15-cm depth.
2. Apply the following equation to both the HCP and PRP EC_a of the outlier-removed, calibrated Survey data set and add them to the Survey data frame

$$EC_{25} = EC_T \times \left(0.447 + 1.4034^{-T/26.8615}\right)$$

   a. EC_{25}: The EC_a standardized to 25°C (mS m^{-1})
   b. EC_T: The EC_a at a particular soil temperature
   c. T: Soil temperature (°C)

```
Cal_survey_df<- mutate(Cal_survey_df, Temp_Cal_HCP_Con=(Cal_HCP_Con*(0.447+1.4034^(-L_MSen_temp/26.815))))
Cal_survey_df<- mutate(Cal_survey_df, Temp_Cal_PRP_Con=(Cal_PRP_Con*(0.447+1.4034^(-U_MSen_temp/26.815))))
```

Temp. adjusted and calibrated HCP ECa (RED) and just calibrated HCP ECa (black) Scan 12
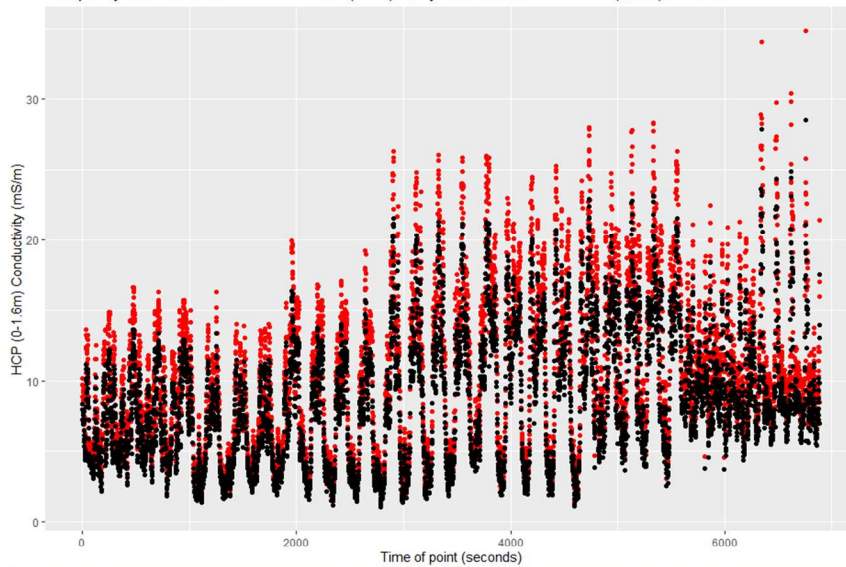
Temp. adjusted and calibrated PRP ECa (RED) and just calibrated PRP ECa (black) Scan 12
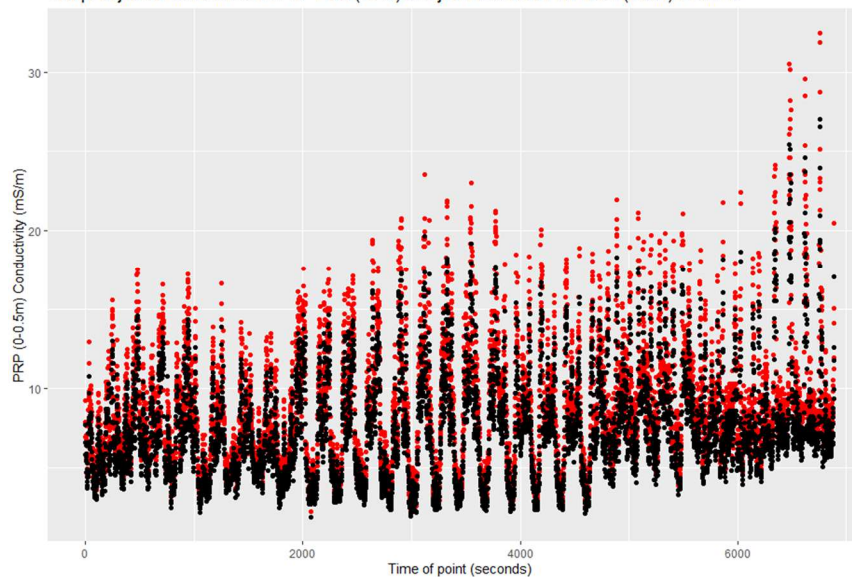
3. This is the outlier-removed, calibrated, temperature-adjusted data set which can be used for analysis.

Interpolation Through Kriging

1. Average any points that coincidentally occurred in the same GPS location.
2. Using the outlier-removed, calibrated, temperature-adjusted Survey data set, randomly select 20 % of the Survey data. This will be used for model validation.
3. Using the remaining 80 % of the data, calculate an experimental semi-variogram for the HCP and PRP EC$_a$ and fit semi-variogram with a nugget and exponential, spherical, Gaussian, Matern, circular, and linear models.

168

4. Select the best model which minimized the sum of square of error for the HCP and PRP EC_a
    a. They can have different models,
5. Use the selected model to preform universal kriging to a 5-m resolution (or to a dimension of your choosing) and within the boundaries of the site for both the HCP and PRP EC_a.
6. Now you have interpolated images of site's HCP and PRP EC_a.